POROUS CARBON CARRIERS FOR AMORPHOUS DRUG DELIVERY

Nikhila Miriyala

Doctor of Philosophy

ASTON UNIVERSITY

June 2017

Aston University

Porous carbon carriers for amorphous drug delivery

Nikhila Miriyala

Doctor of Philosophy

2017

Thesis summary

Given the great potential of porous carrier based drug delivery for stabilising the amorphous form of drugs and enhancing dissolution profiles, this thesis centred on investigations into the application of activated carbon (AC) and carbon onion (OLC) as porous carriers for oral delivery, using paracetamol (PA) and ibuprofen (IBU) as model drugs.

Initial work was focussed on the toxicity studies of AC followed by preparation and characterisation of drug/AC complex. Results showed that AC is a promising drug carrier with low toxicity, high loading capacity and ability to stabilise amorphous drug. However, loading efficiency and solid state characteristics were different for PA and IBU, whilst the drug release from AC was incomplete in the absence of surfactant.

To investigate the factors affecting drug loading, three different loading methods were compared, with solution adsorption followed by centrifugation found to be the optimum method to achieve maximum loading with least crystallinity. Initial drug concentration in the loading solution was also found to influence the loading, where the optimum concentration to achieve maximum loading without any crystallinity differed depending on the chemical nature of the drug. Further, the surface chemistry of AC was modified in order to achieve complete drug release, and results showed that drug release increased with an increase in the surface oxygen content of AC. Also, drug release was found to increase with a decrease in the micropore volume fraction.

The second part of the work was focussed on the synthesis and characterisation of OLC, followed by drug loading studies. Results showed that annealing of nano-diamonds (ND) at 1100 ℃ produced OLC with a diamond core, which is non-toxic. Drug loading studies revealed that loadings achieved were lower than those seen with AC, regardless of drug solubility.

Of the both carriers investigated, AC was less expensive and found to be a promising carrier with higher loading capacity and lower toxicity.

Keywords: dissolution; loading; factors; release; adsorption; activated carbon; carbon onion

Acknowledgements

Dedication

To my husband, who has always stayed by my side and supported me on this journey. When I am weak, it's you who makes me stronger.

To my mom who has shown me nothing but affection.

To my dad who has inspired me and instigated my love for science.

Publications

Miriyala, N., Ouyang, D., Perrie, Y., Lowry, D., Kirby, D (2017), "Activated carbon as a carrier for amorphous drug delivery: Effect of drug characteristics and carrier wettability" *European Journal of Pharmaceutics and Biopharmaceutics*, 115, pp.197–205.

Miriyala, N., Kirby, D., Pazaras, I., Bo, Y., Ouyang, D., Ye, H (2017), "Synthesis and application of carbon onion for drug delivery" *(in preparation)*

Conference Abstracts

Miriyala, N., Ye, H., Perrie, Y., Ouyang, D (2014), "Development of a novel oral drug delivery system using carbon onion as drug carrier" *Postgraduate Research day, Aston University, Birmingham, UK*

Miriyala, N., Ye, H., Perrie, Y., Ouyang, D (2014), "Development of carbon onion based novel oral drug delivery systems" *APS PharmSci conference, Hatfield, UK.*

Miriyala, N., Ouyang, D., Ye, H., Lowry, D., Kirby, D (2015), "Application of carbon onion as a porous carrier for amorphous drug delivery" *UKICRS conference, Nottingham, UK.*

Miriyala, N., Ouyang, D., Lowry, D., Kirby, D (2015), "Application of activated carbon as a porous carrier for amorphous drug delivery" *Postgraduate Research day, Aston University, Birmingham, UK*

Miriyala, N., Ouyang, D., Lowry, D., Kirby, D (2015), "Carbon onion as a porous carrier for amorphous drug delivery" *CRS conference, Edinburgh, July 2015.*

Miriyala, N., Ye, H., Ouyang, D., Lowry, D., Kirby, D (2016), "Synthesis of carbon onion at low annealing temperatures for drug delivery applications" *NDNC conference, Xi'an, China, May 2016.*

Miriyala, N., Ouyang, D., Lowry, D., Kirby, D (2016), "Activated carbon as a porous carrier for amorphous drug delivery: Effect of porosity and surface characteristics on drug loading and release" *Postgraduate Research day, Aston University, Birmingham, UK*

Table of Contents

List of Figures

11

13

List of Tables

Abbreviations

AC	Activated carbon
API	Active pharmaceutical ingredient
BCS	Biopharmaceutical classification system
Caco-2	Colorectal adenocarcinoma
CNT	Carbon nanotubes
OLC	Carbon onion/ onion like carbon
DMEM	Dulbecco's modified eagles medium
DMSO	Dimethyl sulfoxide
DSC	Differential scanning calorimetry
EDX	Energy dispersive X-ray
FTIR	Fourier transform infrared
HPCM	Hierarchical porous carbon monolith
MCM	Mobil composition of matter
MTT	3-(4,5-dimethylthiazol-2-yl)-2,5-diphenyltetrazolium bromide
MWCNT	Multi walled carbon nanotubes
ND	Nano diamond
OMC	Ordered mesoporous carbon
PA	Paracetamol
PBS	Phosphate buffered saline
PEG	Polyethylene glycol
SBA	Santa Barbara amorphous
SEM	Scanning electron microscopy
SWCNT	Single walled carbon nanotubes

Chapter 1 – **Introduction**

1.1. Importance of solubility and dissolution profile of drugs

About 80% of globally marketed drug dosage forms are oral delivery systems, due to low manufacturing costs and high patient compliance (Morishita & Peppas 2012). However, more than 90% of the active pharmaceutical ingredients (API) are reported to have oral bioavailability limitations (Fasinu et al. 2011).

The effectiveness of an oral dosage form depends on the bioavailability of the drug, which in turn depends on the solubility and dissolution rate of the drug; according to the Biopharmaceutical Classification System (BCS), a drug is classified as highly soluble, when the highest dose (mg) is soluble in $\leq$ 250 mL of water at 37 ^{o}C over the pH range 1-7.5, and is classified as highly permeable when the fraction of dose absorbed is more than 90% (Lindenberg, Kopp et al. 2004).

Of the 133 orally administered drugs in the WHO essential drug list, 40% were reported to have solubility and dissolution problems and fall under Class II (low solubility and high permeability) or class IV (low solubility and low permeability) of BCS (Dahan et al. 2013; Douroumis & Fahrenkamp 2012).

Poor solubility and dissolution of drugs have necessitated the formulation of drugs with more than the required dose, leading to economic wastage and an increased risk of toxicity. Hence, it is very important for pharmaceutical scientists to develop effective techniques to improve the solubility and dissolution behaviour of poorly water-soluble drugs.

1.2. Drug delivery strategies to improve solubility and dissolution

Solubility is the maximum amount of drug/solute that can be dissolved in the solvent, whereas dissolution is the rate at which this solute dissolves in the solvent. According to the Nernst and Brunner equation (Equation 1), dissolution of the drug in a medium is affected by various factors, such as solubility, the surface area of the drug, sink conditions of the dissolution medium and wettability of the drug (Banker et al. 2002).

$$\frac{dm}{dt} = \frac{DA(C_s-C)}{h}$$
(Equation 1)

Where dm/dt is the dissolution rate of the drug (m is the mass of the dissolved drug and t is the time); D is the diffusion coefficient of the drug, which depends on several factors, such as the viscosity of the dissolution medium; A is the surface area of the drug, which in turn depends on the particle size of the drug; Cs is the saturation solubility of the drug in the dissolution medium, which depends on many factors, such as intermolecular attractions and polarity; C is the concentration of the drug in the medium, which depends on the gastric permeability of the compound and volume of the dissolution media; h is the thickness of the diffusion layer surrounding the drug particle (Leuner & Dressman 2000; Limnell et al. 2007; Smith 2016).

Numerous formulation technologies have been developed to modify the aforementioned factors to enhance the solubility and dissolution rate of poorly water-soluble drugs (Table 1-1); however, such strategies are often associated with limitations with regards to low drug loading and poor stability. One of the many solubility enhancing techniques includes conversion of crystalline drug to an amorphous state, since the dissolution rate of the amorphous form is markedly better than the crystalline form, especially in drugs with high crystal energy (Hancock & Zografi 1997; Salonen et al. 2008).

24

Table 1-1: Drug delivery strategies for poorly water-soluble drugs to enhance their oral bioavailability

Strategies	Advantages	Limitations	Reference
Physical modification			
Particle size reduction	Simple and cost effective.	Potential degradation of the drug due to physical or thermal stress and potential particle aggregation.	(Khadka et al. 2014; Pouton 2006)
Self-emulsifying drug delivery systems	Rapid absorption	Drug precipitation upon dilution and potential toxicity of surfactant.	(He et al. 2010; Wang & Zhang 2013)
Polymeric micelles-drugs incorporated into the hydrophobic core	Low critical micellar concentration compared to low molecular weight surfactants	Poor stability and low solubilisation capacity.	(Pouton 2006; Douroumis & Fahrenkamp 2012; Biswas et al. 2013)
Inclusion complex	Can enhance stability of drugs	Difficult large scale production of cyclodextrin and low drug loading efficiency.	(Loftsson & Brewster 2013)
Solid lipid nanoparticles	Biocompatible, Controlled release	Low drug loading and potential lipid aggregation	(Sonja & Bunjes 2013; Luo et al. 2015)
Amorphous drugs	Better compression characteristics compared to crystalline drugs	Poor stability; converts into crystalline form	(Yu 2001)
Chemical modification			
Salt formation	Absence of excipients	Poor stability; difficulty in the identification of the salt form.	(Serajuddin 2007)
Prodrugs	Simple and cost effective	Reduced drug permeability, Poor chemical stability	(Stella & Nti-Addae 2007)

1.3. Amorphous drugs: Preparation methods and stabilising strategies

Amorphous forms of drugs lack three-dimensional molecular order, resulting in higher solubility, unlike crystalline forms that have a long range molecular order (Figure 1-1 :). Molecules in an amorphous form are randomly positioned relative to each other and possess high free energy, which allows greater motion of molecules, thereby resulting in higher solubility compared to crystalline forms (Hancock & Parks 2000).
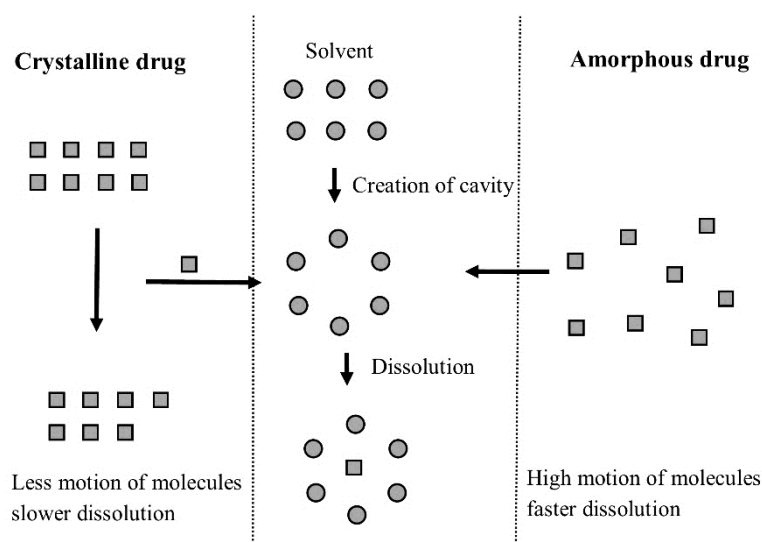
Figure 1-1 :Schematic diagram of the stages of drug dissolution in amorphous and crystalline drugs [Adapted from (Smith 2016)].

Solubility ratio of the amorphous and crystalline forms of a drug is directly proportional to the difference in the Gibbs free energy (Equation 2):

$$\Delta G_T = RT \ln \left(\frac{\text{Solubility}_a}{\text{Solubility}_c} \right) \qquad \text{(Equation 2)}$$

Where ΔG is the difference in the Gibbs free energy, R is the gas constant and T is temperature, a is amorphous and c is crystalline.

The difference in the Gibbs free energy between amorphous and crystalline form is determined from the enthalpy and entropy of the solid forms (Equation-3).

$$\Delta G = \Delta H - (T\Delta S) \qquad \text{(Equation 3)}$$

Where ΔG is the difference in the Gibbs free energy, ΔH is the difference in the enthalpy, T is temperature and ΔS is the difference in the entropy.

Amorphous forms possess higher enthalpy and entropy due to their disordered structure compared to the crystalline form, resulting in higher Gibbs free energy; the higher the difference in the Gibbs free energy between amorphous and crystalline forms, the higher will be the solubility of amorphous form compared to its crystalline form (Hughey & Williams 2012; Hancock & Parks 2000; Singhal & Curatolo 2004).

The amorphous form of drugs can be prepared by various methods (Hancock & Zografi 1997; Löbmann et al. 2012; Craig et al. 1999):

1) Melt method, which involves melting the drug followed by rapid cooling using liquid nitrogen.

2) Rotary evaporation, where the drug is dissolved in an organic solvent and the solvent is rapidly removed under vacuum using a rotary evaporator.

3) Spray drying, where the drug is dissolved in a suitable solvent and is sprayed into a drying chamber

4) Cryo-milling, which involves milling the crystalline drug in a ball mill immersed in liquid nitrogen.

5) Freeze drying, which involves freezing the aqueous solution of the drug followed by sublimation under vacuum.

However, the amorphous form of drugs often have poor stability and tend to convert back to crystalline forms, and this tendency is a major drawback in formulations containing amorphous drug (Yu 2001). Several studies have been performed to develop stabilising strategies for amorphous form of drugs (Table 1-2) and, in recent years, adsorption of drugs onto porous materials/adsorbents, to produce stabilised amorphous drugs, has gained increasing interest (Laitinen et al. 2013).

Table 1-2: Techniques to stabilise amorphous drugs and their limitations

Stabilization strategies	Advantages	Limitations	References
Solid dispersion	Biocompatibility and optimum wettability.	High production costs and low drug loading efficiency. Carrier is hygroscopic in nature leading to poor stability.	(Kalia & Poddar 2011; Leuner & Dressman 2000)
Co-amorphous mixtures	Other excipients such as polymers are not required.	Poor stability, molecular interactions, and potential co-crystal formation.	(Laitinen et al. 2013)
Adsorption/Porous carrier based drug delivery	Controlled drug release.	Expensive carrier production, High Potential toxicity of carriers.	(Mamaeva et al. 2013; Preisig et al. 2014)

1.4. Porous carrier based amorphous drug delivery

Porous carrier based drug delivery involves adsorption of drugs on to the pores of a carrier and has shown great potential to produce and stabilise the amorphous form of drugs that

tend to convert into the crystalline state during storage. The interactions between the carrier and the adsorbed drug, in addition to the small pore size, restrict the crystallisation of the drug, resulting in a stable amorphous form. In addition to stabilisation, adsorption of drugs onto pores of a carrier increases the effective surface area of the drug that is in contact with the dissolution media, resulting in higher solubility (Salonen et al. 2008; Vallet-Regi et al. 2001).

1.4.1. Adsorption

Adsorption is a spontaneous process, where molecules (adsorbate) in a gaseous or liquid medium attach mainly to the surface of a solid (adsorbent), in order to partially restore the balance of excess forces on the surface of the adsorbent and to reduce the entropy of the adsorbate.

Adsorption is of two kinds, based on the phase of the solution: 1) Liquid phase adsorption; and 2) gas/vapour phase adsorption. Liquid phase adsorption is more complicated than gas phase adsorption, since in the former case, the driving force for adsorption could be both attraction of solute molecules by the adsorbent and also rejection by the solvent (Dąbrowski 2001). Adsorption in the liquid phase usually occurs in three stages: 1) Transport of solute through the liquid film or hydrodynamic boundary layer to the adsorbent surface; 2) Diffusion of solute within the pores of adsorbent; and 3) Adsorption of solute particles on to the internal surface of the pores of the adsorbent (Newcombe 2008).

Adsorption can be classified into two types based on the interactions between the adsorbent and adsorbate: 1) Physical adsorption (physisorption), which involves weak, non-specific, short ranged, van der Waals forces between the adsorbent and adsorbate;

and 2) Chemical adsorption (chemisorption) which involves chemical bonding between the drug and the carrier (Taylor et al. 2010; Dąbrowski 2001; Arce et al. 2008).

Physisorption is the most favourable mechanism of drug loading for amorphous drug delivery where immediate drug release is desired, since the drug can readily desorb from the carrier and get released into the dissolution medium. The driving force for physical adsorption can be electrostatic or non-electrostatic interactions, whereby electrostatic interactions are due to the charge densities of the adsorbent and adsorbate and can be repulsive or attractive. Aromatic or pi-pi interactions are also a special type of electrostatic interactions which only exist between aromatic compounds due to the partial positive charge around the periphery or on the edges of an aromatic ring and partial negative energy above both aromatic faces (Martinez & Iverson 2012). Non-electrostatic interactions include hydrophobic interactions and van der Waals forces, which are interactions between neutral atoms/molecules at short distances and are always attractive (Radke & Prausnitz 1972; Kaplan 2006).

Chemisorption is advantageous when controlled drug release is required, since the release of the chemically adsorbed drug will depend on the dissolution rate of the carrier. However, high drug loading cannot be achieved with chemisorption, since only a monolayer of the drug can be adsorbed, thereby limiting the drug loading capacity (Wu et al. 2008; Douroumis & Fahrenkamp 2012).

1.4.2. Porosity of the carrier

Porosity is the measure of voids/pores in a material and these pores can be closed or open (accessible to the exterior of the material). Porous materials may contain pores of uniform size or variable size in their structure and can be arranged in a disordered or ordered manner (Figure 1-2). These pores can be slit-shaped, which can be seen with micropores of activated carbon that originate from spaces between the multiple graphite sheets, or can be cylindrical shaped, which can be seen in ordered mesoporous silica.
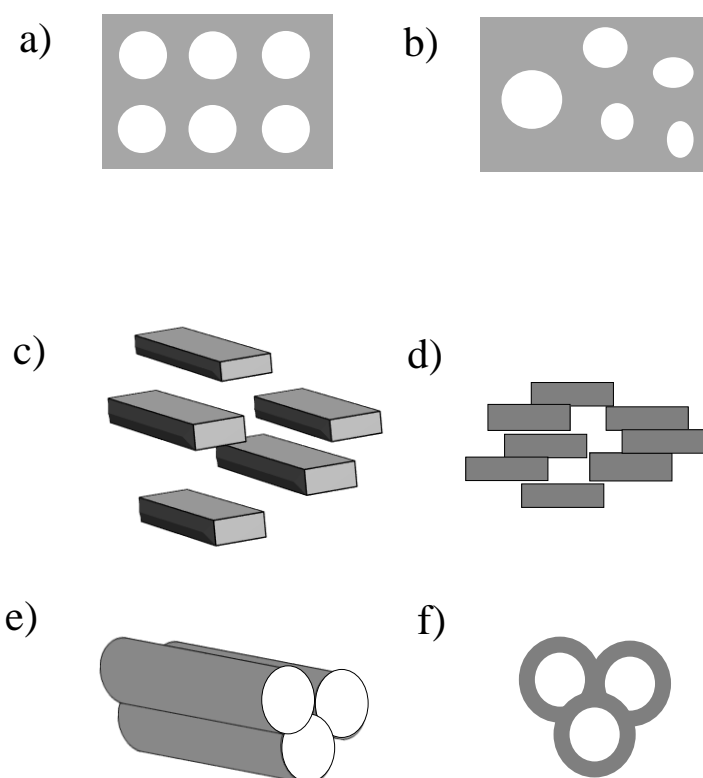
Figure 1-2 :Illustration showing different types of porosity: (a) Uniform ordered porosity (b) non-uniform disordered porosity (c) Slit-shaped pores-side view (d) slit-shaped pores-front view (e) cylindrical pores-side view (f) cylindrical pores- front view

Pores are classified into three types based on their width: 1) micropores with a diameter less than 2 nm; 2) mesopores with a diameter in the range of 2 and 50 nm; and 3)

macropores with a diameter more than 50 nm. Micropores have a width slightly greater than most drug molecules (spherical diameters of most small molecule drugs is less than 1 nm (Knappe et al. 2004; Ehrhardt & Kim 2007)), which can result in the interaction between all the atoms of the pore wall and all the atoms of the drug molecule, thereby leading to stronger adsorption and higher stability. In the case of mesopores, the pore width is a few times larger than the molecular size of the drug and can accommodate multilayer adsorption. Whereas, in macropores, the pore size is much larger and exhibit less specific surface area; since the adsorption can only occur on the pore wall, drug adsorption in macropores is negligible (Bruce et al. 2010; Dąbrowski 2001; Lawrence & Jiang 2017).

1.4.3. Drug loading methods and factors influencing the drug loading

Several loading methods (Table 1-3), such as solvent evaporation, supercritical CO_2, melting and solution adsorption have been studied to allow drugs to be successfully adsorbed onto carriers; however, the loaded drug often exists as a mixture of crystalline and amorphous drug. Solution adsorption, also called immersion, is the most widely used method for drug loading due to ease of reproducibility. Solution adsorption, solvent evaporation, and incipient wetness methods use the same principle of dissolving the drug in an organic solvent before adding the carrier, followed by removal of the solvent. However, these solvent based methods can be challenging when the drug is not soluble in any suitable organic solvent. The melt method can be employed in such cases, since it does not employ any organic solvents; however, most drugs undergo degradation before melting (Salonen, Paski, et al. 2005; Li-hong et al. 2013; Piotto & Bettotti 2017; Ahern et al. 2013).

Table 1-3: Methods of drug loading into porous carriers: Advantages and limitations

Loading Method	Conditions	Advantages	Limitations	Reference
Solution adsorption/ immersion	Carrier is added to a high-concentrated or saturated drug solution under sonication or continuous stirring.	Simple and reproducible	Solute–solvent interactions can reduce the drug uptake by the carrier; Residual solvent toxicity.	(X. Wang et al. 2011; Mellaerts et al. 2008)
Melting	The molten drug and carrier are mixed and maintained above the melting point of the drug for 24 hours.	High drug loading compared to solution adsorption	Not suitable for drugs that are unstable at high temperatures.	(Ahern et al. 2013)
Solvent evaporation	Carrier is added to the drug solution followed by removal of solvent using a rotary evaporator.	Simple and fast technique	Potential crystallisation of the drug at the surface	(Preisig et al. 2014)
Super critical fluid	Drug and carrier are mixed under constant temperature in a high-pressure reactor vessel filled with CO_2 until the final pressure reaches 25-30 MPa and is then depressurised by removing the CO_2.	High loading efficiency; Absence of residual solvents	Involves complicated procedures	(Li-hong et al. 2013; Ahern et al. 2013)
Incipient wetness/ impregnation	Concentrated drug solution is added to the carrier drop-wise and mixed intensively. The sample is then dried under vacuum.	Less wastage of drug; Loading can be determined in advance.	Non-uniform drug distribution; Drug crystallisation on the external surface cannot be controlled.	(Xu et al. 2013; Mellaerts et al. 2010; Lehto et al. 2013)

Significant research has been undertaken in loading drugs under different loading conditions (Table 1-4) and drug loading efficiency was found to depend on several factors, such as porosity and surface chemistry of the carrier (Lai et al. 2017; Jarvis et al. 2012; Li et al. 2002).

For the drug to exist in a stable amorphous form inside the carrier, the drug should be adsorbed on the pore wall of the carrier and adequate surface area should be available for adsorption; therefore, it can be deduced that with an increase in the surface area of the carrier, drug loading capacity increases. When it comes to pore width of carrier, it is a prerequisite that pore width should be slightly higher than the molecular size of the target drug, to be able to fit inside the pore without any steric hindrance. Also, when the pore width is sufficiently larger than the molecular size of the drug, multilayer adsorption is possible, resulting in higher drug loading. However, drug loading into pores that are too wide can lead to crystallisation of the drug, since there is enough space for the drug to rearrange into an ordered crystal; therefore, it is important to determine the optimum pore size that can result in the maximum drug loading without leading to crystallisation (Doadrio et al. 2015; Jarvis et al. 2012).

In addition to porosity, surface chemistry of the carrier was also found to play a significant role in affecting the drug loading capacity, especially when specific drug-carrier interactions, such as hydrophobic or electrostatic interactions, were involved in the adsorption of the drug or when the drug loading method involves use of a solvent (Solution adsorption method), where solvent-carrier interactions are possible. For example, application of a hydrophilic carrier for drug loading in an aqueous media can lead to reduced drug loading, due to the adsorption of water on the hydrophilic carrier inhibiting the adsorption of solute/drug (Limnell 2011; Taylor et al. 2010; Li et al. 2002).

Table 1-4: Factors affecting drug loading efficiency and solid state characteristics of the loaded drug

Property	Effect on drug loading and solid state characteristics	Drug	Carrier	Reference
Pore volume	Drug loading increased with increase in the pore volume, irrespective of the surface chemistry.	Ibuprofen	Porous silicon (pSi)	(Jarvis et al. 2012)
Surface area	Drug loading increased with increase in the surface area.	Ibuprofen	MIL-100, MIL-101, MCM-41, SBA-15	(Vallet-Regi- et al. 2007)
Pore width	The crystallinity of the loaded drug increased with increase in the pore width.	Ibuprofen	Porous silicon	(Jarvis et al. 2012)
	Microporous carriers exhibited lower drug loading compared to mesoporous carriers; however, no dependency on the pore size could be observed when two mesoporous materials were compared.	Ibuprofen	Mesoporous SBA-3 and microporous SBA-3	(Andersson et al. 2004)
Surface chemistry	Crystallinity of the loaded drug is lowest when stronger negative charge is used, due to stronger interactions between the drug and the carrier	Ibuprofen	Thermally carbonised pSi and unoxidised pSi	(Jarvis et al. 2012)
Loading method	Compared to solvent impregnation method and supercritical fluid method, melting method exhibited higher crystallinity in the loaded drug.	Fenofibrate	SBA-15	(Ahern et al. 2013)

1.4.4. Factors affecting drug release

Drug release or desorption from the carrier can be immediate or sustained, depending on various factors (Table 1-5), such as porosity of the carrier, surface chemistry of carrier, type of adsorption, drug characteristics, etc.

Drug release was found to decrease with a decrease in the pore size in the range of 2.5-3.6 nm due to spatially hindered diffusion (Ukmar et al. 2011; Wang 2009). Also, the particle size of the carrier was found to affect the drug release rate, with smaller particles exhibiting faster drug release due to shorter pore length and less steric diffusion hindrance (Y. Zhang, Che, et al. 2014; Zhang et al. 2010; Burguete et al. 2012).

Drug release in porous carriers, such as MCM-41 (Mobile crystalline material) and SBA-15 (Santa Barbara amorphous), with unidirectional pore channels was found to be slower when compared with MCM-48 and LP-*la3d* (Large pore with *la3d* space group), with three-dimensional cubic pore geometry, due to higher molecular accessibility and faster transport in the three-dimensional pore network (Wang 2009; Qu, G Zhu, et al. 2006).

In addition to porosity, surface chemistry of the carrier was also found to play a significant role in affecting drug release, where an increase in the population of hydrocarbon chains in the carrier decreased the wettability of the carrier, resulting in slower drug release (Izquierdo-Barba et al. 2005). In addition to changing the hydrophobicity, functionalisation of the carrier also results in the reduction of pore width, which could lead to slower drug release (Wang 2009).

Table 1-5: Factors affecting the drug release from porous carriers

Property	Effect on drug release rate	Drug	Carrier	Reference
Pore diameter	Drug release was faster when loaded into mesoporous carrier compared to microporous carrier	Ibuprofen	Microporous and mesoporous SBA-3	(Andersson & Rosenholm 2008)
Carrier particle shape/pore channel length	Spherical particles have faster drug release compared to fibre-like material due to increase in the pore channel length	Vancomycin	SBA-15	(Cauda et al. 2008)
		Captopril	MCM-41	(Qu, G Zhu, et al. 2006)
Pore arrangement	Faster for 3D interconnected pores than 2D cylindrical pores.	Ibuprofen	MCM-41 (unidirectional cylindrical pores) and MCM-48 (3D interconnected pores)	(Qu, Guangshan Zhu, et al. 2006)
		Valsartan	HPCM (3D interconnected pores) and OMC (unidirectional cylindrical pores)	(Y. Zhang, Che, et al. 2014)
Surface chemistry	Drug release decreased with increase in hydrophobicity of the carrier.	Erythromycin	LP-*Ia3d* functionalised with octyl hydrocarbon chain	(Izquierdo-Barba et al. 2005)

1.5. Porous materials for amorphous drug delivery

For the development of porous carrier based amorphous drug delivery system, an ideal carrier should exhibit the following properties (Liu et al. 2013; Zhu et al. 2012; Zhu et al. 2014; Kwon et al. 2013):

1) Biocompatibility- material that does not undergo dissolution in the gastro-intestinal environment can pose less risk of toxicity due to the less possibility of cellular internalisation.

2) Chemical inertness to prevent undesired drug-carrier interactions that could lead to loss of drug potency.

3) Low production costs.

4) Large surface area for high loading.

5) Chemical and thermal stability- carrier material should not undergo degradation during handling or storage.

6) Strong adsorption capacity- to prevent crystallisation or loss of drug during storage.

7) Tuneable pore size to control the rate of drug release.

8) Modifiable surface chemistry to control the rate of drug release.

Various porous materials have been studied as carriers for drug delivery, resulting in the intentional or unintentional conversion of crystalline to amorphous drugs (Figure 1-3), amongst which, silicon-based materials were most widely studied for intentional development of porous carrier based amorphous drug delivery system, due to their high surface area and ordered porous structure. Also, materials such as calcium carbonate, calcium silicate, magnesium alumino- metasilicate, titanium dioxide, porous ceramic and calcium phosphate have been studied as porous carriers for amorphous drug delivery

(Preisig, Haid et al. 2014). Recently, several carbon-based materials, namely mesoporous amorphous carbon, hierarchical porous carbon monolith etc., have gained attention, due to their chemical inertness, higher stability and stronger adsorption compared to silicon based materials (Zhang, Zhi, et al. 2013; Zhu et al. 2014).

Despite the extensive research on various types of carriers, several limitations are often associated, such as lack of reproducibility, toxicity, poor stability and high production costs (Table 1-6), which hinder the commercialisation of this technique. Hence, it is important to develop more efficient carriers that can address the aforementioned issues (Salonen, Laitinen, et al. 2005; Xu et al. 2013; Limnell 2011; Choudhari et al. 2014).
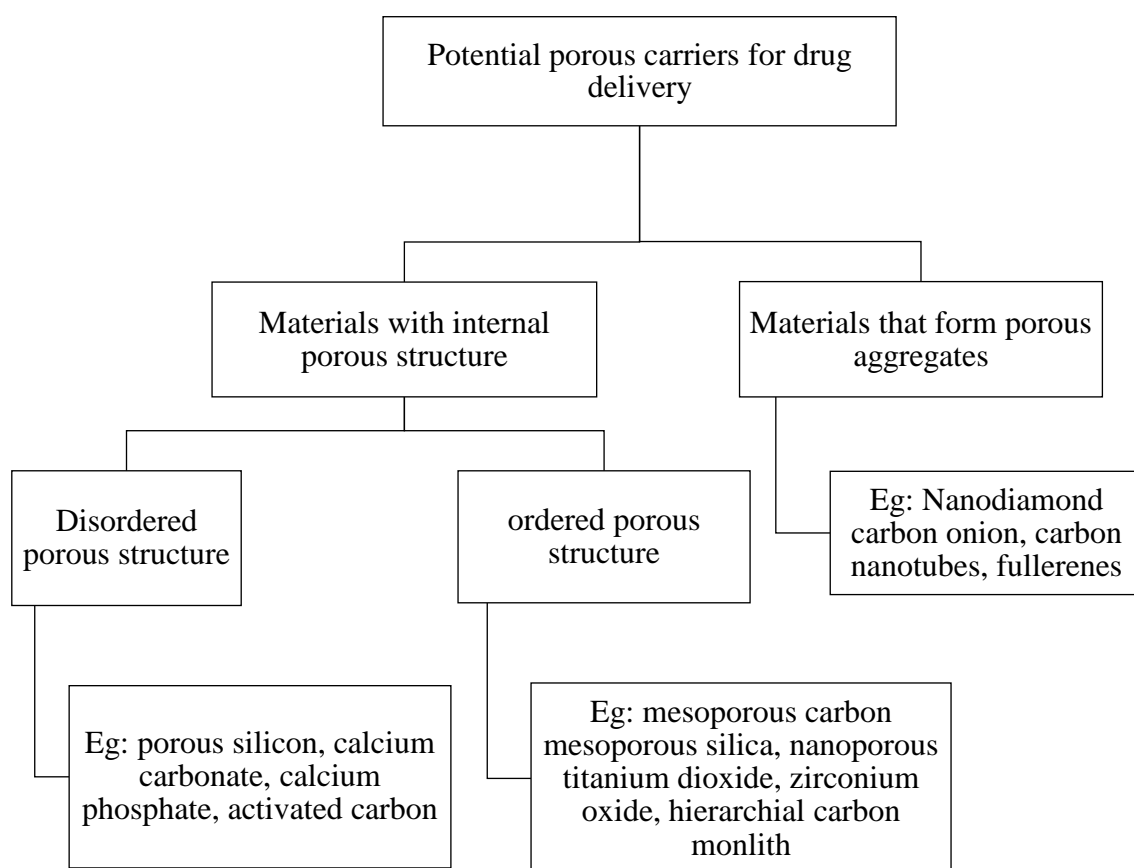
Figure 1-3: Potential porous carriers for amorphous drug delivery

Table 1-6: Advantages and limitations of materials that have been studied previously as drug carriers for amorphous drug delivery.

Porous material	Synthesis (Surface area)	Advantages	Limitations	Reference
Porous silicon	Electrochemical etching (Up to 1000 m^2/g)	Biodegradable; Ease of synthesis and fabrication.	Undergoes atmospheric oxidation; Requires surface modification for stability; Potential chemical interactions with drugs. Difficult up-scalability.	(Salonen, Laitinen, et al. 2005; Jarvis et al. 2012; Limnell 2011; Xu et al. 2013)
Porous silica	Sol-gel process (Up to 800 m^2/g)	Ease of synthesis.	Surface silanol groups can chemically interact with carboxyl groups of drugs via esterification resulting in irreversible drug adsorption or slower drug release; Siloxane bridges might also undergo hydrolysis.	(Kinnari et al. 2011; Wu et al. 2016; Zhang & Cresswell 2016; Kamarudin et al. 2015; Choudhari et al. 2014; Guo et al. 2013)
Ordered mesoporous silica (OMS)	Surfactant templating (Up to 1200 m^2/g)	Uniform porosity; Large surface area.	Expensive synthesis; Variable toxicity results; Chemical interactions between drugs and surface silanol groups; Siloxane bridges might undergo hydrolysis; Difficult up-scalability.	(Wang 2009; Manzano et al. 2008; Ng et al. 2013; Heikkilä et al. 2010)
Ordered mesoporous carbon	Hard templating method (Up to 1400 m^2/g)	Uniform porosity; Chemical inertness; Insolubility in biological fluids.	Synthesis involves the use of OMS as a template, thereby leading to high production costs; Poor wettability; Difficult up-scalability.	(X. Wang et al. 2011; Zhang, Zhi, et al. 2013; Zhang, Wang, et al. 2013; Zhao et al. 2012)

1.5.1. Silicon based materials

Porous silicon and silicon dioxide (silica) materials have been widely studied as drug carriers for amorphous drug delivery, due to their high surface area and tuneable porosity (Wang 2009).

1.5.1.1. Porous silicon

Porous silicon (pSi) is produced by electrochemical anodisation of silicon crystals in hydrofluoric acid solution. The pore diameter of porous silicon produced can vary from 1 nm to several µm and pore structure can be branched with interconnectivity or columnar without any interconnections, depending on the fabrication conditions. pSi produced from etching contains Si-Si bonds in the bulk structure and on the surface; the surface bonds are weak and react with hydrofluoric acid during synthesis, resulting in Si-H bonds. Unfavourably, this hydride (Si-H) surface of pSi is also unstable and undergoes slow oxidation on exposure to atmosphere and water vapour, resulting in siloxane (Si-O-Si) and silanol (Si-O-H) groups. Also, pSi with hydride surface undergoes degradation and converts into silicic acid in the biological media. Since the carrier needs to be inert in the process of drug loading and handling, pSi is often stabilised by oxidation, resulting in stable surface siloxane (Si-O-Si) and silanol (Si-O-H) groups, which also reduces the rate of dissolution in biological media. Stabilisation can also be achieved by carbonisation, which results in Si-C bonds, which are more stable than Si-O bonds (Lehto et al. 2013; Hecini et al. 2013).

Faster drug release was achieved when several poorly soluble drugs were loaded into pSi materials compared to the pure crystalline drug (Table 1-7); however, porous silicon is associated with limitations, such as potential drug-carrier interactions; silanol groups on the surface of pSi were found to react with carboxyl groups of drugs, which could be

disadvantageous when chemical interactions are not desired. Also, the challenging scale-up of the production and fabrication of pSi still needs to be addressed (Jarvis et al. 2012; Xu et al. 2013; Limnell 2011).

Table 1-7: Drug loading and release from porous silicon

Carrier	Surface area (m^2/g)	Drug (loading w/w, %)	Effect on drug release	Reference
Thermally carbonised porous silicon	248	Ibuprofen (30.4)	At pH 5.5, drug release from carrier was complete in 60 min whereas the unloaded drug required 240 min	(Salonen, Laitinen, et al. 2005)
	253	Itraconazole (11.3)	Drug release (pH 1.2) from the carrier was complete in 30 min whereas the release was only 30% for the unloaded drug.	(Kinnari et al. 2011)
Thermally oxidised porous silicon	222.4	Ibuprofen (36.5)	Drug release (pH 5.5) from the carrier at 160 min was 75% whereas the release was only 55% for the unloaded drug.	(Limnell et al. 2007)
	226	Itraconazole (11.2)	Drug release (pH 1.2) from the carrier was complete in 30 min whereas the release was only 30% for the unloaded drug.	(Kinnari et al. 2011)

1.5.1.2. Porous silica

Porous silica used in the drug delivery studies is an amorphous form of silicon dioxide, which contains siloxane groups (Si-O-Si) in the bulk structure and silanol groups (Si-OH) on the surface. Porous silica with a disordered porous structure (silica gel) is produced from alkoxysilanes via hydrolysis followed by condensation, and are commonly used as pharmaceutical excipients (Kinnari et al. 2011; Limnell 2011), whereas porous silica with an ordered mesoporous structure (Ordered mesoporous silica) is prepared via a template method, using different templates such as alkyl trimethyl ammonium ion surfactants or amphiphilic block copolymers; sodium silicate solution is added to the template containing solution and is thermally treated, followed by the removal of template by either calcination or solvent extraction (Mellaerts et al. 2008; Limnell 2011).

Ordered mesoporous silica (OMS) consists of a narrow pore size distribution in the nanometre range and can have a hexagonal unidirectional tube-like pore arrangement (Figure 1-4) or a three dimensional cubic pore arrangement, depending on the synthesis conditions (Heikkilä et al. 2010; Vallet-Regi- et al. 2007).

OMS materials prepared using different templates with different pore structures, namely MCM-41, SBA-15 and MCM-48, have been extensively studied as drug carriers, since they have an ordered pore network and homogenous size for better control on drug loading and release, compared to disordered porous silicon and porous silica.
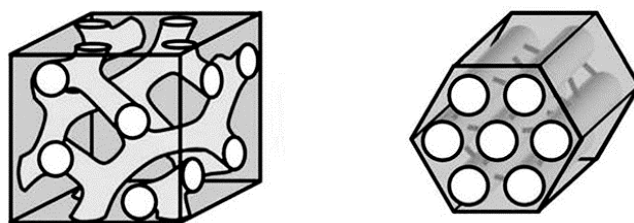
Figure 1-4: Cubic (Left) and Hexagonal (Right) type of pore symmetry of ordered mesoporous silica materials.

Table 1-8: Drug loading and release from porous silica

Carrier	Surface area in m^2/g	Drug loading (w/w, %)	Effect on drug release	Reference
MCM-41	1200	Ibuprofen (41)	Drug release (pH 7.4) from the carrier was complete after 10 hours, whereas the release was only 10% for the unloaded drug.	(Andersson et al. 2004)
	1036	Indomethacin (33)	Drug release in water from the carrier after 24 hours was 35%, whereas the release was only 28% for the unloaded drug.	(Ukmar et al. 2011)
SBA-15	550	Indomethacin (29.5)	Drug release (pH 1.2) from the carrier was 60% after 60min, whereas the release was less than 10% for the unloaded drug.	(Limnell 2011)
	776	Indomethacin (32)	Drug release in water from the carrier after 24 hours was 40%, whereas the release was only 28% for the unloaded drug.	(Ukmar et al. 2011)
	860	Ibuprofen (25.6)	Drug release in PBS was complete in 10 hours.	(Song et al. 2005)

Faster drug release was achieved when several poorly soluble drugs were loaded into OMS materials compared to the pure crystalline drug (Table 1-8); however, porous silica is also associated with limitations similar to that of pSi, namely potential drug-carrier interactions due to reactive surface silanol groups. Few studies have investigated functionalisation of surface silanol groups of OMS to achieve controlled release and targeted delivery (Table 1-9); surface functionalisation with long carbon chains are able to increase the hydrophobicity, thereby reducing the release rate. However, functionalisation can significantly decrease the pore diameter, resulting in reduced drug loading (Doadrio et al. 2006; Vallet-Regi- et al. 2007; Salonen et al. 2008).

Table 1-9: Functionalisation of porous silica and their potential applications in drug delivery

Chemical group	Applications in drug delivery	Reference
Aminopropyl folate	Cancer targeting; Overexpression of folate receptor on cancer cells may facilitate the uptake of the folate-modified silica particles.	(Slowing et al. 2006)
Alkyl chains	Controlled release; Hydrophobicity increases with increase in chain length, thereby resulting in slower drug release.	(Doadrio et al. 2006)
Thiol	Mucoadhesive drug delivery; The thiol groups covalently bind to glycoproteins in mucin.	(Q. Zhang et al. 2014)
Poly lysine (PLL) or polyethyleneimine (PEI)	RNA delivery; positively charged PLL or PEI groups can bind negatively charged nucleic acids.	(Hom, Lu et al. 2010)

Despite the extensive research on porous silica, there are still concerns about long-term effects of silica materials *in-vivo*, since exposure to crystalline silica has shown to cause adverse effects on the respiratory system and carcinogenic effects. Although porous silica investigated for drug delivery applications is amorphous in nature and considered to be less toxic unlike the crystalline form, long term effects of these particles still remain a debatable issue, due to variable results obtained from different cytotoxicity studies (Kwon et al. 2013). *In vitro* studies reported that cell membrane integrity weakened, resulting in reduced metabolism in Caco-2 cells when incubated with high concentrations of porous silica microparticles (0.2-14mg/mL) (Heikkilä et al. 2010). However, *in-vivo* studies in mice and rabbits showed no significant toxic effects when porous silica microparticles were administered orally (Jaganathan & Godin 2012), indicating that studies on bio-safety of porous silica are contradicting and needs further research.

1.5.2. Carbon based materials

Several porous carbon materials (Figure 1-5) have been studied as carriers for drug delivery applications (Table 1-10) due to their high surface area, chemical inertness, and high chemical and thermal stability (X. Wang et al. 2011; Chen et al. 2016). Carbon materials that have been studied as drug carriers are usually hydrophobic in nature and are insoluble in aqueous media (unless functionalised), which is advantageous for application in oral amorphous drug delivery, where dissolution of the carrier is not preferred due to potential cellular uptake leading to adverse effects.

Porosity in these carbon materials can be internal porosity (activated carbon and ordered mesoporous carbon) or can be aggregate created porosity (fullerenes, carbon onions, and

nanodiamonds). Both internal porosity and aggregate created porosity can be found in the case of carbon nanotubes (Presser et al. 2011).

Carbon
nanotube

Fullerene

Nanodiamond

Carbon onion

Amorphous carbon with small graphite like crystals
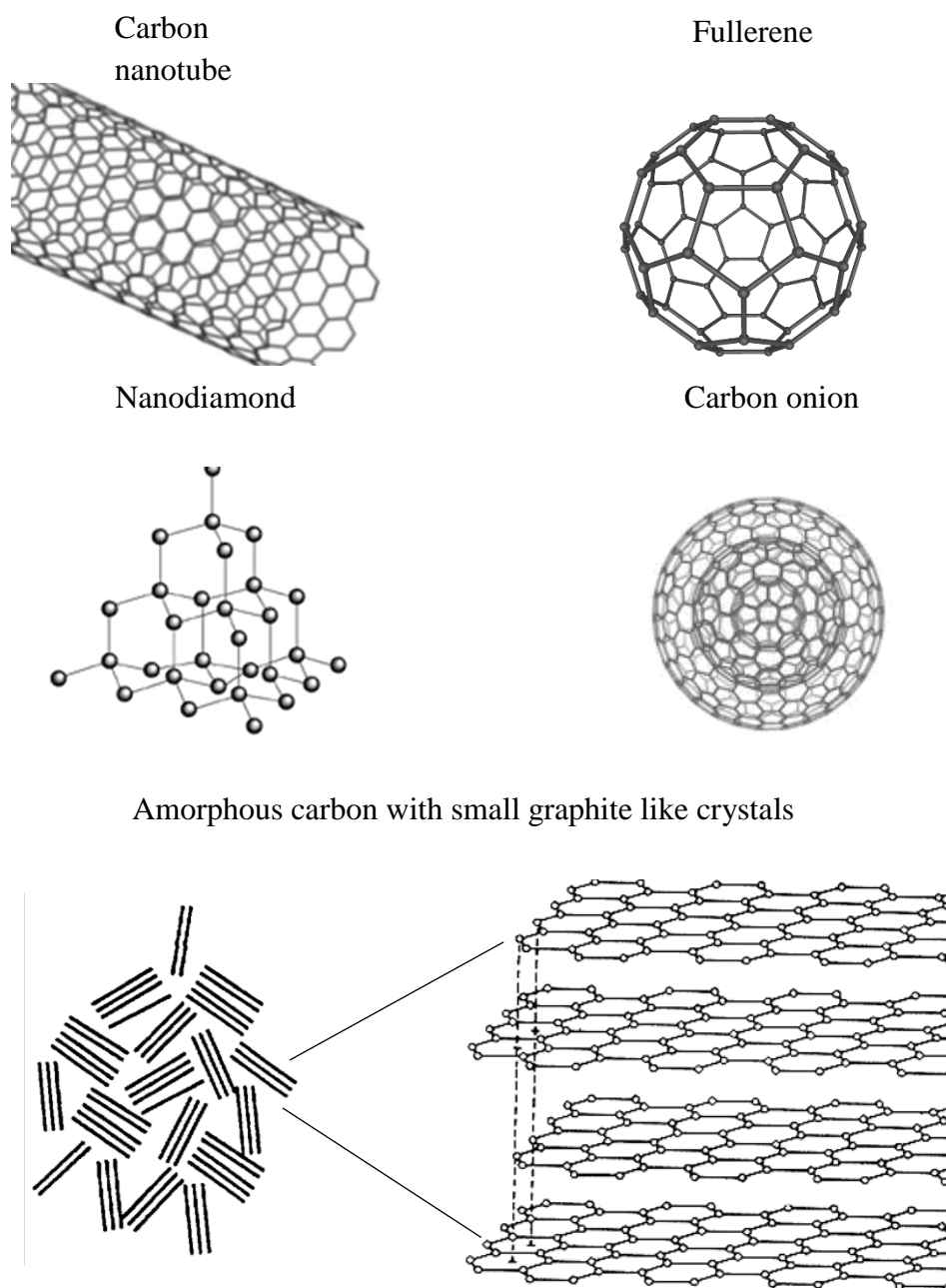
Figure 1-5: Molecular structure of different carbon allotropes that are potential drug carriers [Adapted from (Mochida et al. 2006)].

Table 1-10: Applications of porous carbon materials in drug delivery.

Carbon materials	Porosity	Possible adsorption mechanism[*]	Applications in drug delivery	Reference
Ordered mesoporous carbon (amorphous carbon with/without sp^2 graphite like crystallites)	Intra-particle	Pi-pi interactions when graphite like crystallites are present	Amorphous drug delivery	(Zhang, Zhi, et al. 2013)
Activated carbon (amorphous carbon with sp^2 graphitic crystallites)	Intra-particle	Pi-pi interactions	Anticancer drug delivery, lymphatic targeting	(Nakase et al. 2004; Mochida et al. 2006)
Fullerenes (single sp^2 graphene ring)	Aggregate created	Pi-pi interactions	Anticancer drug delivery	(Montellano et al. 2011; Blazkova et al. 2014)
Carbon onions (multiple sp^2 graphene rings)	Aggregate created	Pi-pi interactions	No specific research as drug carrier, however the ability to cross 'Blood brain barrier' was investigated.	(Pakhira et al. 2016)
Nanodiamond (sp^3 diamond core and sp^2 amorphous carbon)	Aggregate created	Interactions between functional groups and drugs	Gene delivery, Anticancer drug delivery	(Ho et al. 2010; El-Say 2011)
Carbon nanotubes (single or multiple sp^2 graphene structures)	Aggregate created and intra-particle	Pi-pi interactions	Anticancer drug delivery	(Bielicka et al. 2013; Terzyk et al. 2012; Wong et al. 2013)

[*] In addition to van der Waals forces

1.5.2.1. Activated carbon

Activated carbon (AC) is a porous material that consists of several small graphitic crystallites joined together, but without a long range order. Each graphitic crystallite consists of 1-5 layers of hexagonal and pentagonal rings of sp^2 carbon arranged in a near parallel fashion. AC is produced from carbonisation of a variety of carbon-rich materials (e.g. coal, wood, peat etc.), followed by either steam activation or chemical activation. Steam activation involves steam treatment of a carbon-rich source, such as wood, at 800-1100 ºC. Chemical activation involves carbonisation of carbon-rich material in the presence of an activating agent, such as phosphoric acid or zinc chloride, at 600-1000 ºC, followed by washing and drying (Olivier 2008; Mochida et al. 2006; Peter et al. 2008; Harris et al. 2008).

AC consists of a disordered three-dimensional interconnected pore structure, with a broad pore size distribution of micropores, mesopores, and macropores (Figure 1-6). Micropores, which contribute to the major part of the internal surface area, originate from the spaces between several randomly arranged small graphitic layers. Unlike graphite, where all the layers are arranged in a parallel manner, AC consists of randomly arranged layers. Macropores and mesopores of AC act as pathways that lead to micropores. Micropores of AC are slit-shaped and can exhibit higher packing density, which can result in higher loading compared to cylindrical shaped pores (Harris et al. 2008; Rodriguez-Reinso 2007).

Surface area and pore size distribution of AC depends on the synthesis conditions, and pore size distribution can be controlled by changing the type of raw material, activation temperature, proportion of activating agent, and duration of the treatment; AC prepared from coal was found to contain a wide range of mesopores, whereas coconut shell-based

49

AC showed more microporosity (Xia et al. 2010; Inagaki 2009; Marsh & Rodriguez-reinoso 2006).
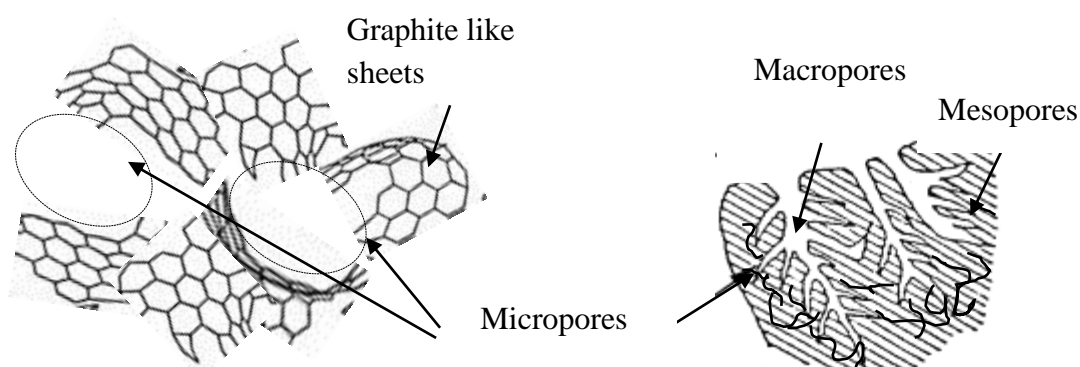
Figure 1-6: Schematic depiction of the porous structure of activated carbon and origin of micropores from the spaces between graphite-like sheets [Adapted from (Mochida et al. 2000; Enoki & Kobayashi 2005)]

1.5.2.1.1. Surface chemistry

The adsorption on AC is mostly physisorption and the interactions can be simply non-specific van der Waals forces or structure-specific Pi- Pi interactions that occur between the aromatic rings of the adsorbate and aromatic rings of graphene layers of AC (Figure 1-7). These possible interactions between aromatic drug molecules and AC can potentially result in stronger adsorption (Martinez & Iverson 2012; Haghseresht et al. 2002); however, the aromatic rings in AC are not arranged parallel to the pore wall and are present in a random fashion.

a)   b)   c)
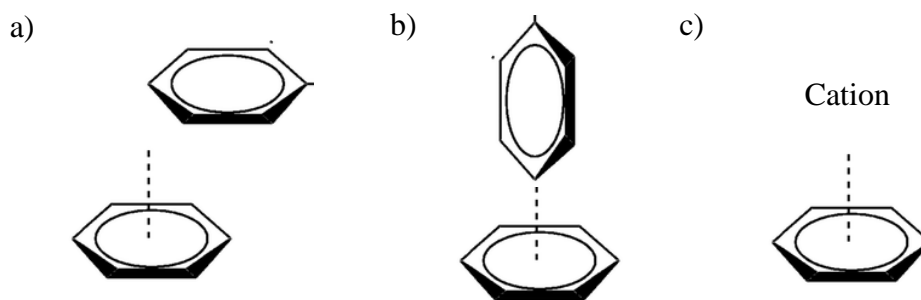
Cation

Figure 1-7: Illustration showing interactions between aromatic ring of adsorbate and the aromatic ring of AC: (a) Parallel displaced and (b) T-shaped; (c) interactions between positively charged adsorbate and the aromatic ring of AC [Adapted from (Martinez & Iverson 2012)(Matthews et al. 2014)].

However, adsorption on AC can also be affected by functional groups present on the edges (Figure 1-8) of graphene sheets, essentially oxygen-containing groups such as carboxyl, since these groups determine the hydrophilicity, which can affect the interaction with aqueous media. Acid treatment of AC was found to increase oxygen-containing functional groups (Table 1-11) and resulted in an increase in the adsorption of organic molecules from gaseous phase and a decrease in the adsorption of organic molecules from aqueous media (Li et al. 2002).

Treatment with HNO_3
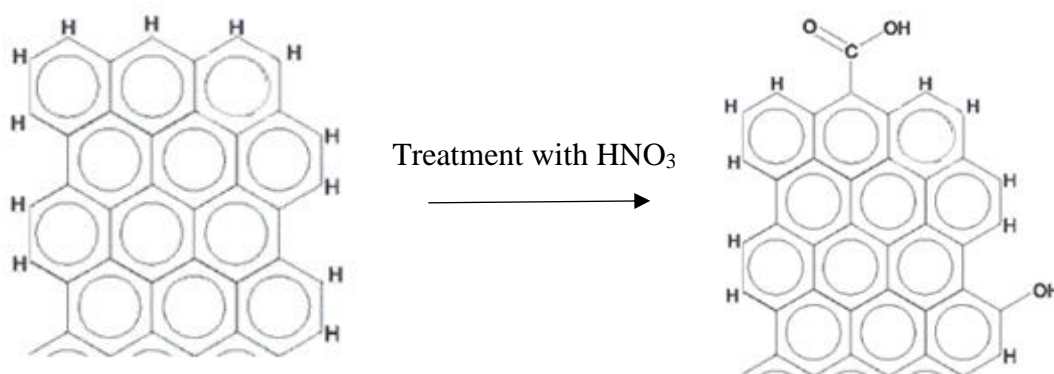
Figure 1-8: Effect of acid treatment on the surface chemistry of activated carbon. Several hydroxyl or carboxyl groups can be imparted resulting in increased hydrophilicity [Adapted from (Mochida et al. 2006)].

Table 1-11: Effects of surface functionalisation of activated carbon

Treatment	Effect on surface chemistry	Effect on adsorption	Reference
Exposure to oxygen at 200-700 ºC or treatment with H_2O_2 or HNO_3.	Increase in carboxylic, phenolic and hydroxyl groups	Hydrophilicity increases with increased number of oxygen groups. Adsorption of organic compounds in aqueous media decreases	(Li et al. 2002)
Heat treatment at 700 ºC in inert atmosphere	Removes oxygen group but might produce free radical edge sites	Hydrophobicity increases. Adsorption of organic compounds in aqueous media increases.	(Knappe et al. 2004; Boehm 2008)
Exposure to ammonia and chlorine at 400-900 ºC	Increase in pyridine type structures and amine groups	Hydrophobicity increases. Adsorption of organic compounds in aqueous media increases.	(Knappe et al. 2004)

1.5.2.1.2. Biological safety and potential applications in drug delivery

AC is extensively used in water purification and is also clinically used as an antidote to remove poisonings (Liang et al. 2013; Olson 2010; Juurlink 2016) AC administered orally was not absorbed from the gut and the clinical studies on safety of orally administered AC showed no serious adverse effects (Wang, Cui et al. 2012) and minor side effects (e.g. constipation, abdominal distention etc.,) were observed on use of AC as an antidote (Chang, Kelly et al. 2006).

AC has also been investigated as a drug carrier for cancer targeting and sustained delivery of anticancer drugs; when injected into the tumours in mice, AC loaded with methotrexate was found to increase the duration of active exposure period of the drug to the tumour by releasing the drug slowly for a prolonged period of time, thereby suppressing the tumour growth at a higher rate compared to the unloaded drug (Nakase et al. 2004). Also, AC

was found to have an affinity towards the lymph nodes when injected near the tumour site (Guo et al. 2011; Yokota et al. 2000).

Table 1-12: Potential clinical applications of activated carbon

Potential applications	Result	Reference
Chemotherapy	Drugs adsorbed on to AC nano particles were selectively delivered to regional lymph nodes and retained at the site of injection for a longer duration in rats and cancer patients.	(Guo et al. 2011; Hagiwara & Takahashi 1987; Shah et al. 1998)
Antacid	Calcium carbonate or sodium carbonate adsorbed on the activated carbon was able to maintain ideal pH and neutralise gastric acidity without any rebound effect *in vitro*.	(Linares et al. 2006; Linares et al. 2007)
Photo thermal cancer therapy	When exposed to laser radiation, PVP dispersed AC nano particles were able to convert light into heat energy and resulted in tumour growth suppression at the site of injection in mice.	(Chu et al. 2013)
Lymph node staining	AC of particle size < 200 nm was readily absorbed into regional lymphatics and blackened lymph nodes when injected.	(Yokota et al. 2000)
Controlled release	AC containing temperature responsive hydrogel was used to increase the drug loading capacity and mechanical strength of the hydrogel for controlled release.	(Yun et al. 2008)
Amorphous drug delivery	AC and crystalline drugs were mixed using a mortar and pestle resulted in the loss of crystallinity over a period of time.	(Konno et al. 1986)

Whilst few studies have explored the use of AC for anticancer drug delivery, as noted in Table 1-12, there is not much information on the drug loading efficiency, drug release kinetics and application as an amorphous drug carrier.

AC is inexpensive, commercially available, non-toxic and has a high surface area to volume ratio, which can favour the development of an efficient, cost-effective and safe carrier for oral drug delivery.

1.5.2.2. Ordered mesoporous carbon

Ordered mesoporous carbon (OMC) is an sp^2 form of carbon, similar to AC, and can contain small graphitised crystallites; however, unlike activated carbon, OMC contains a narrow pore size distribution with a uniform pore symmetry and is prepared by a soft template or hard template method. The soft template method involves use of surfactants as templates to allow self-assembly of carbon molecules to form nanostructures, similar to the preparation of OMS, whereas the hard template method involves a physical template, such as OMS, on which the carbon source precipitates or polymerises before undergoing calcination at high temperatures (Pan et al. 2010; Darmstadt et al. 2008; Niu et al. 2013).

Several studies have been performed using OMC as an amorphous drug carrier due to its chemical inertness, low toxicity and stronger adsorption compared to OMS materials. OMC was found to be stable in the gastric environment without getting absorbed by intestinal cells, which can be advantageous for application in oral drug delivery (Zhang, Zhi, et al. 2013). Cytotoxicity studies on Caco-2 cells and gastric irritation tests in mice also showed that OMC is non-toxic and did not induce any irritation (Niu et al. 2013; Zhao et al. 2012).

OMC (839 m^2/g) prepared using SBA-15 as a template was studied for ibuprofen loading and a loading of 24% could be achieved (X. Wang et al. 2011), which is almost similar to the ibuprofen loading (25.6%), achieved when SBA-15 (860 m^2/g) was used as a carrier

(Song et al. 2005), indicating that there is no significant difference in the drug loading capacity between OMC and OMS materials. However, there is no information on the fraction of crystallinity in the loaded drug, which could give a better understanding of the difference in the ability to produce and stabilise the amorphous drug, between OMS and OMC materials.

OMC was found to be poorly wettable in biological media due to its hydrophobic surface; therefore, carboxylation of these materials was performed by treating with a mixture of sulphuric and nitric acids, which resulted in an increased wettability (Zhang, Zhi, et al. 2013). Site-selective release of drug from OMC was also achieved by incorporating Fe nanoparticles in the carbon walls (Yuan et al. 2009). OMC functionalised with thermo-responsive polymer was found to achieve a controlled release of the drug between 20-25 ℃ (Zhu et al. 2011), indicating the modifiable surface chemistry of amorphous carbon for application in controlled drug delivery. However, synthesis of OMC involves the application of surfactant template method similar to OMS, which is an expensive and complicated process to scale up.

1.5.2.3. Nanodiamond

Nanodiamonds (ND) are synthesised through detonation of carbon containing explosive mixtures, such as trinitrotoluene and hexogen. ND produced from this method are spherical in nature in the size range of 2-10 nm and consist of a crystalline diamond core surrounded by an amorphous shell of sp^3 and sp^2 carbons containing several functional groups and, therefore, exhibit properties different from that of micro diamonds (El-Say 2011; Ho et al. 2010).

ND particles often aggregate into porous clusters due to strong interactions between the surface functional groups, reaching several hundred of nanometres in size. Also, the presence of these functional groups was found to be advantageous for drug delivery application due to the hydrophilicity imparted and high cellular internalisation since pi-pi interactions are not present due to the absence of aromatic graphene rings in the structure (Chen et al. 2016).

ND was investigated for application in sustained anticancer drug delivery by functionalising with sodium alginate and was found to exhibit less toxic effects *in vitro* compared to the drug alone (Cui et al. 2016). Furthermore, the surface interaction between the drug and ND facilitated slow release of the drug and inhibited the precipitation of the poorly water soluble drug. Also, drug adsorbed on to porous ND clusters was found to increase the dispersibility of the drug in aqueous media, indicating the potential of ND clusters in improving the solubility of poorly soluble drugs (Chen et al. 2016). However, there is no adequate information on the drug loading capacity or drug release kinetics.

The toxicity of NDs on the respiratory system was studied by the intratracheal administration in mice and no toxic effects were found when a concentration of up to 1mg/kg was used. However, a dose dependent toxicity was observed in several internal organs when high concentrations were used (1-20mg/kg) (Zhu et al. 2012). There is no clarity about the biocompatibility of ND due to contradicting toxicity studies and needs further research on the long-term effects before they can be considered safe for clinical use. Also, the application of ND in drug delivery systems is often associated with limitations, such as the requirement of incorporating functional groups to improve the interaction between the drug and ND (El-Say 2011).

1.5.2.4. Carbon nanotubes

Carbon nanotubes (CNT) are cylindrical graphene tubes of few nanometres in diameter and up to several micro metres in length. CNT can be single walled (SWCNT) or multiwalled (MWCNT), with an inner tube diameter ranging from 1-3 nm and outer tube diameter ranging from 2-100 nm. CNT are synthesised through arc discharge method, chemical vapour deposition, and laser ablation method (He et al. 2013).

Carbon nanotubes have accessible internal porosity and also have high external surface area due to their shape; however, internal drug loading is limited due to the restricted space in the tube and most of the drug loading studies have been performed by adsorbing the drugs on the external surface. Several drugs have been loaded into CNT by chemisorption (paclitaxel and cisplatin) and by π-π stacking (doxorubicin) to investigate the applications in intracellular delivery, since CNT was found to have an ability to cross cell membranes by hydrophobic interactions, π-π stacking interactions, electrostatic adsorption and covalent bonding. Despite their higher cellular uptake, application of CNT for intracellular delivery is still controversial due to the toxicity concerns associated with these nano materials (He et al. 2013; Wong et al. 2013).

Carbon nanotubes are hydrophobic in nature and insoluble in aqueous solutions and are usually functionalised with polyethylene glycol (PEG) to improve their solubility, biocompatibility and to reduce their toxicity. PEG-CNT were found to be less toxic compared to aggregated unfunctionalised CNT when given intratracheally and intraperitoneally, indicated by *in-vivo* studies in animal models (Liu, Robinson et al. 2011). No toxicity, mortality or tissue damage was shown when water soluble hydroxylated SWCNT were studied for bio distribution in mice through oral,

intraperitoneal subcutaneous and intravenous routes (Liu, Robinson et al. 2011); however, accumulation was observed in stomach, kidneys, and bone after 30 minutes of administration, which were eventually cleared in unchanged form (Yang, Luo et al. 2012). However, some studies have shown that CNT was broken down by myeloperoxidase in the neutrophils of mice (Kagan, Konduru et al. 2010). Also, inhalation studies indicated that CNT could lead to inflammation and pulmonary toxicity (Bergin & Witzmann 2013). The toxicity and metabolism of CNT were found to depend on the surface functionalisation, solubility, shape, aggregation and chemical composition, due to which the cytotoxicity results from several studies are contradicting, which makes it difficult to generalise the toxicity of the CNT for drug delivery applications. Despite the animal studies indicating the safety of oral administration of CNT even at high concentrations (Liu et al. 2011), application of these materials for amorphous oral drug delivery can be challenging due to their potential pulmonary toxicity and complexity of production.

1.5.2.5. Fullerenes

Fullerenes are hollow molecules with spherically arranged graphene sheets and can be produced via arc discharge method which involves an arc discharge between two graphite electrodes in water, during which graphite undergoes vapourisation resulting in the deposition of carbon soot on the surface of the container. The carbon soot is then scrapped and collected followed by boiling with toluene. The toluene carbon mixture is then evaporated to produce fullerene crystals (Kyesmen et al. 2016). These fullerene aggregates/crystals referred to as fullerites can reach up to 300 µm in size which have micropores from molecular defects of fullerenes and may also contain mesopores from

point defects and stacking defects in the aggregation (Suárez-García et al. 2008; Nikonova et al. 2016). These aggregates can have three preferential adsorption sites: 1) between the four fullerene molecules 2) channels formed between two adjacent molecules and 3) on the surface of each molecule. Although no drug delivery studies have been performed using the fullerites, water-soluble fullerene derivatives were studied as drug carriers for intracellular delivery where drugs such as paclitaxel, doxorubicin were covalently attached to fullerene molecules (Montellano, Da Ros et al. 2011).

Fullerenes, when administered orally to rats were excreted in faeces unchanged, while trace amounts passed through the gut wall and were observed in urine, indicating the uptake by intestinal cells; however, no toxic effects were reported. When given intravenously, water-soluble fullerenes were found to be less toxic compared to the insoluble fullerenes (Kolosnjaj-Tabi et al. 2012). Few studies have reported that cell viability reduced in bovine macrophages and enhanced the production of tumour necrosis factor (Mao et al. 2013). Despite few reports on the toxic effects of fullerenes, these are considered to be less toxic compared to carbon nanotubes.

1.5.2.6. Carbon onion

Carbon onion, which is also called onion-like carbon (OLC), consists of spherical closed graphene shells that were first observed when carbon soot was exposed to a radiating beam of a transmission electron microscope. The layered structure of these shells resembles the structure of an onion and can be considered as concentrically arranged fullerenes separated by 3-4 Angstroms (Terrones & Terrones 2003; McDonough & Gogotsi 2013; Choucair & Stride 2012).

OLC has been prepared using several techniques, such as arc discharge, which involves discharge between two carbon electrodes in the water; plasma spraying, which involves accelerating of ND particles using fast travelling arc plasma; and electron beam irradiation, which involves irradiating carbon soot. However, only minute quantities can be prepared from the aforementioned methods and larger quantities of OLC can be prepared via thermal annealing of detonation nanodiamonds (ND) and the size of each onion depends on the size of the nanodiamonds used for the synthesis (Costa et al. 2014; Sano et al. 2002; Gubarevich et al. 2003).

The transformation of ND to OLC (Figure 1-9) involves graphitisation from the surface to the core; as the temperature increases, ND undergoes a phase transformation from sp^3 to sp^2 carbon, in order to reduce the surface energy, and finally forms completely merged graphitised carbon shells. The merging of graphite shells causes a significant decrease in the surface energy for the graphitised particles, which could be the driving force for the formation of spherical OLC (Bielicka et al. 2013).

OLC produced from ND undergo aggregation that can reach up to several µm in size due to the van der Waals forces that hold the molecules/onions together, resulting in the formation of aggregate created porosity formed by the space between multiple onions, which may be used as strong adsorption sites for drug molecules (Zeiger, Jäckel, et al. 2015; Reinert et al. 2015).

ND

OLC with few graphene shells on the surface and a ND core

OLC with several graphene shells and without a ND core

900-1300 °C

>1300 °C
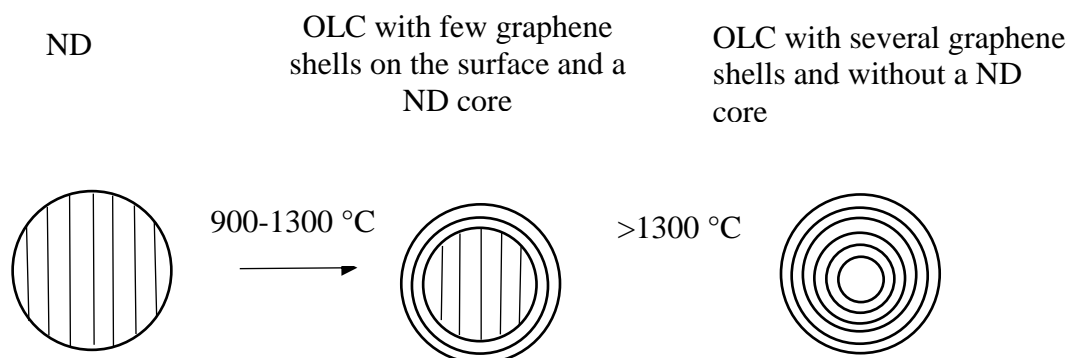
Figure 1-9: Illustration of the transformation of sp3 carbon in nanodiamond (ND) from the surface to the core with an increase in temperature resulting in the formation of carbon onion (OLC) [Adapted from (Cebik et al. 2013)].

OLC contains concentrically arranged graphene layers that are strong potential sites of adsorption for drugs (Figure 1-10) due to the possibility of pi-pi interactions between aromatic rings of graphene layers of OLC and the aromatic rings of the drug. OLC can exhibit much stronger drug adsorption inhibiting crystallisation of the loaded drug compared to AC, since the graphitic layers in AC are not arranged parallel to the pore wall and are present in a random fashion. (Bielicka et al. 2013; Popov et al. 2012; Enoki & Kobayashi 2005; White 2015)

However, the porous structure of OLC contains aggregate created mesoporosity with some microporosity, with a relatively low surface area in the range of 200-600 m^2/g compared to that of AC, which can exhibit a surface area of up to 2000 m^2/g depending on the synthesis conditions (Zeiger, Jäckel, et al. 2015).
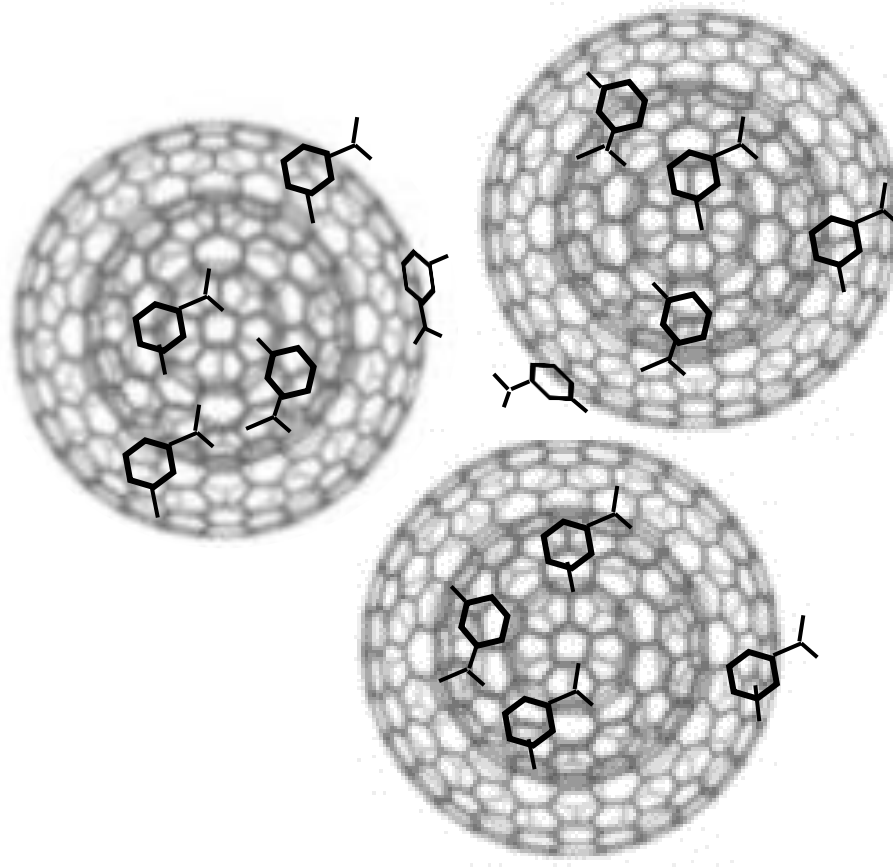
Figure 1-10: Illustration showing the potential adsorption of aromatic molecules on OLC aggregates via parallel displaced pi- pi interactions [Adapted from (McDonough et al. 2012)].

Biocompatibility of OLC has been investigated by few researchers and no significant toxicity was observed. Human skin fibroblasts exposed to OLC with a diameter of 30 nm produced from arc discharge method showed less toxic effects compared to carbon nanotubes. Rat derma fibroblasts were exposed to OLC functionalised with poly ethylene glycol and the cell viability was over 80%, even at high concentrations tested (3000 µg/mL). However, there is limited research on the cytotoxicity studies of OLC, making any conclusions on the safety of OLC difficult (Bartelmess & Giordani 2014).

No specific research has been performed on the application of OLC as a drug carrier; however, the ability of acid treated OLC to cross the blood-brain barrier has been studied recently in mice. OLC, when injected into mice were found to enter the brain without causing any perfusion and cleared out from the body without depositing for long period, indicating the potential of OLC to carry the drug to the brain (Pakhira et al. 2016). OLC was also studied for application in cellular imaging, due to their ability to undergo cellular internalisation (Bartelmess & Giordani 2014).

1.6. Thesis aim and objectives

Although numerous studies about porous carrier based drug delivery have been published, there are still many limitations, such as low drug loading efficiency, the crystallinity of the loaded drug, poor chemical stability, potential toxicity and high costs of production. With the above limitations in mind, the aim of this work is to investigate the application of activated carbon and carbon onion as porous drug carriers in order to develop safe, efficient, and less expensive porous carriers.

The main objectives of current work include:

1. Evaluate cell cytotoxicity of activated carbon and carbon onion micro-particles on Caco-2 cells.

2. Investigate drug loading into activated carbon and carbon onion using paracetamol and ibuprofen as model drugs.

3. Determine drug loading capacities of carbon onion and activated carbon under different loading conditions.

4. Investigate factors affecting drug loading and solid state characteristics of the drug loaded.

5. Investigate drug release behaviour from activated carbon and carbon onion.

Chapter 2 **- Materials and Methods**
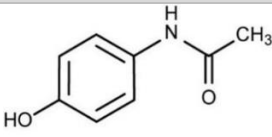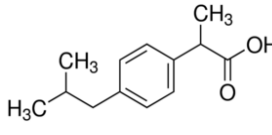
2.1. Materials

AC used for drug loading studies in Chapter 3 and 4 was Norit® Darco® G60 type. Three other types of activated carbon were used to study the effect of porosity in Chapter 5. All four types of AC were purchased from Sigma Aldrich, UK and the information about the manufacturing conditions is shown in Table 2-1. Nanodiamond (ND) (particle size<10nm, purity ≥97%) used in the preparation of carbon onion was purchased from Sigma-Aldrich, UK. Paracetamol powder (purity 98-102%) was purchased from Sigma, UK and Ibuprofen powder (purity 99%) was purchased from discovery Fine chemicals, UK. Properties of paracetamol and ibuprofen are presented in Table 2-2. Ethanol, sodium lauryl sulphate, sodium dihydrogen phosphate, disodium hydrogen phosphate, sulphuric acid, nitric acid, dimethyl sulfoxide and sodium hydroxide were purchased from Fisher, UK. Caco-2 cells were purchased from ATCC. Dulbecco's Modified Eagles Medium (DMEM, with 4500 mg/L glucose, L-glutamine, sodium pyruvate, sodium bicarbonate, amino acids and vitamins), foetal Bovine Serum, trypsin-EDTA solution, anti-mycotic solution (with 10,000 units penicillin, 10 mg streptomycin and 25 μg amphotericin B per mL), Hank's balanced salt solution, MTT dye, phosphate buffered saline, trypan blue were purchased from Sigma-Aldrich, UK.

Table 2-1: Activated carbon specifications, Sigma Aldrich, UK.

Product name	AC Norit® Darco® G60	AC Darco® KB-G	AC For Cell culture	AC Meets USP testing requirements
Product code	05100	675326	C9157	C7606
Source	Lignin	Wood	N/A	100% natural origin
Manufacturing conditions	Steam activation	Chemical activation	Steam activation and washed with hydrochloric acid	Steam activation processed to meet standards required for medicinal use

Table 2-2: Properties of model drugs

Model drug	Structure	Molecular weight	Melting point (Glass transition)	pKa	BCS class	Reference
Paracetamol		151.16	169 °C (22.85)	9.4	III	(Kalantzi et al. 2006; Sibik et al. 2014)
Ibuprofen		206.3	74.8 °C (-45.15)	4.9	II	(Limnell 2011; Dudognon et al. 2008)

2.2. Particle size analysis

Particle size analysis of carrier was performed using HELOS/BR Laser diffractometer (Sympatec GmbH, Germany). 0.5 % (*w/v*) carrier suspension was prepared in ethanol and was analysed for particle size in the measuring range of 0.1 to 500 µm.

2.3. Cytotoxicity studies

In vitro cytotoxicity studies of activated carbon and carbon onion were performed with human colon carcinoma cells. Caco-2 Cells were cultured in 75 cm^2 culture flasks using Dulbecco's modified Eagle's medium with 10% FBS, 1% L-glutamine and 1% antimycotic solution. Cells were incubated at 37^{0}C in an atmosphere of 5% CO$_2$ and 95% relative humidity, and the growth medium was changed every 2 days.

Cells between passages 100 and 120 were used in the toxicity studies. Cells were washed with HBSS and were harvested using trypsin-EDTA solution. The cell suspension was diluted to achieve a density of 10^4 cells/ml using DMEM and was added to 96 well plates at 100 µL per well such that each well has a density of 1000 cells. The cells were incubated for 24 hours. The medium was removed after 24 hours and the carrier-DMEM suspensions with different concentrations of the carrier (10-800µg/mL) were added to 96-well plates at 100 µL per well and incubated for 24 h. Caco-2 cells without carrier suspension added was used as a control. The medium was removed after 24 hours of incubation and the cells were washed with PBS to remove any carrier particles. 100 µL of fresh medium and 20 µL of 5mg/mL MTT in PBS solution was added to each well and incubated for 4 hours. After 4 hours the medium containing MTT was removed and replaced with 100 µL DMSO. The absorbance of the resulting formazan solution was determined at 492 nm on a SynergyTM HT microplate reader. Percentage of cell viability was calculated using equation -4:

$$\text{Percentage cell viability} = \frac{\text{Absorbance of sample}}{\text{Absorbance of control}} \times 100 \qquad \text{(Equation -4)}$$

2.4. Drug loading into activated carbon

2.4.1. Solution adsorption

1000 mg of AC was added to 10 mL of saturated solution of drug in ethanol (saturation solubility of paracetamol and ibuprofen at 20 °C is 150 and 698 mg/mL of ethanol respectively) and the suspension was stirred (stirring speed-100 rpm) at 20 °C for 24 hours. Post loading, the suspension was centrifuged at 1500 rpm, the supernatant was removed and the sediment was dried at 40 °C for 24 hours. The concentration of drug in the supernatant was determined to estimate the amount of drug adsorbed. The unloaded/free drug was found to crystallise as a top layer due to the evaporation of the solvent, as shown in Figure 2-1. This top crystalline layer of the sediment was removed and analysed for drug content. The bottom layer was collected, sieved (mesh 150-opening size 104 µm) to remove any agglomerates and was labelled as drug/AC complex.

Aston University

Illustration removed for copyright restrictions

Figure 2-1: Schematic representation of solution adsorption method used in the preparation of drug/carrier complex and photographic image showing crystallisation of drug after drying the sediment obtained by centrifugation. Top white crystalline layer was separated and the bottom layer was labelled as drug/carrier complex.

2.4.2. Effect of drug loading method

To understand the effect of loading method on loading efficiency and solid state characteristics, three different solvent based loading methods were compared.

1)   Rotary evaporation (RE): 1000 mg of AC was added to a 500 mL round-bottomed flask containing 10 mL of the saturated drug-ethanol solution at 25°C (Saturation solubility of paracetamol and ibuprofen at 25 °C is 165 and 970 mg/mL of ethanol, respectively (Gracin & Rasmuson 2002; Wang et al. 2010)). Ethanol was extracted under a vacuum pressure of 5 torr using a rotary-evaporator with a water bath set to 25 °C, and a runtime of 1 hour. Residual solid was allowed to dry for 24 hours in an oven at 40 °C.

2)   Solution adsorption -filtration (SA-F): 1000 mg of AC was added to 10 mL of the saturated drug-ethanol solution and the suspension was stirred (100 rpm) at 25 °C for 1 hour, followed by filtration under vacuum. The residue obtained was allowed to dry for 24 hours in an oven at 40 °C.

3)   Solution adsorption -centrifugation (SA-C): drug-carrier suspension was prepared similar to the SA-F method; however, post stirring, the suspension was centrifuged for 10 minutes at 1500 rpm. The supernatant was removed and the residue/sediment obtained was allowed to dry for 24 hours in an oven at 40 °C. After 24 hours of drying, white crystalline drug layer was found on the surface of the sediment, which was removed, while the bottom layer was considered as drug/carrier complex, as described in the previous chapter.

2.4.3. Effect of contact time

1000 mg of activated carbon was added to 10 mL of saturated drug solution (saturation solubility of paracetamol and ibuprofen at 20 °C is 150 and 698 mg/mL of ethanol, respectively) and was allowed to undergo stirring (100 rpm) at 20 °C for 1 hour, 4 hours, 6 hours, 15 hours and 24 hours.

2.4.4. Effect of temperature

To understand the effect of temperature on drug loading, drug loading was performed at four different temperatures. 1000 mg of AC was added to 10 mL of saturated drug solution (concentration of PA: 150 mg/mL of ethanol and concentration of IBU: 690 mg/mL) and was allowed to undergo stirring for 4 hours at 20, 25, 30, and 35 °C.

2.4.5. Effect of initial drug concentration

To determine the effect of concentration of drug in the loading solution on the loading efficiency, drug loadings were performed by SA-C method using four different drug concentrations (concentrations of 25, 50, 100, 150 mg of PA per mL of ethanol and concentrations of 350, 450, 550, 690 mg of IBU per mL of ethanol). 1000 mg of activated carbon was added to 10 mL of drug solution and was allowed to undergo stirring (100-rpm) at 20 °C for 4 hours.

2.4.6. Drug loading using saturated drug solution at different temperatures

Saturated PA solutions at four different temperatures were used for loading (saturated solubility of PA is 150, 165, 183, 199 mg/mL of ethanol at 20, 25, 30, 35 °C respectively (Granberg & Rasmuson 1999)) to determine the maximum PA loading that could be achieved without any crystallisation.

2.4.7. Effect of carrier dose

To investigate the effect of quantity of carrier on drug loading efficiency, varying amounts of carrier was added to 10 mL of saturated drug solution (concentration of PA: 150 mg/mL of ethanol and concentration of IBU: 690 mg/mL) and was allowed to undergo stirring (100 rpm) at 20 ºC for 4 hours.

2.5. Modification of surface chemistry of activated carbon

To consider the effects of the surface chemistry of the carrier on drug loading and release, AC was treated to modify its surface chemistry with HNO_3, NaOH and a mixture of H_2SO_4/HNO_3 separately, as reported previously in the literature (Li et al. 2005; Chiang et al. 2002; Li et al. 2003). In a typical procedure, 1 g of AC (G60- type) was added to 100 mL of 3:1- $H_2SO_4(65\%)/HNO_3(96\%)$ solution and was stirred for 3 hours at room temperature. The solution was then decanted and AC was washed with ultrapure water until a neutral pH was achieved. The AC was then dried at 70 ºC in an oven for 24 hours and was referred to as AC-H_2SO_4/HNO_3.

Also, 1 g of AC was treated separately with 100 mL of 6N HNO_3 solution and 100 mL of 2M NaOH solution while stirring at room temperature for 5 hours and 24 hours, respectively. Post-treatment with HNO_3 and NaOH solution, AC samples were washed and dried as described previously and the treated ACs were referred to as AC- HNO_3 and AC-NaOH, respectively.

2.6. Preparation of carbon onions from thermal annealing of detonation nanodiamond

Nanodiamond (ND) powder (primary particle size < 10 nm, ≥ 97% trace metal basis) used in the preparation of carbon onions was purchased from Sigma-Aldrich, UK. Samples of ND were placed in quartz crucibles and thermally annealed in a carbolite TZF furnace under flowing nitrogen atmosphere. The samples were annealed at a heating rate of 5°C/min to three different annealing temperatures: 900; 1000; and 1100°C, with holding time of 2 hours. During the process of annealing, all three samples were held for 0.5 hours when they reached temperatures of 350 and 700°C, to remove adsorbed water molecules and acidic groups, respectively (Zeiger, Jäckel, et al. 2015). Approximately 100 mg of ND sample was annealed at each temperature. After the thermal treatment, the annealed samples were allowed to cool down to room temperature under nitrogen atmosphere. The annealed samples are referred to as ND-900, ND-1000 and ND-1100, which stand for precursor (nanodiamond) and annealed temperature.

2.7. Drug loading into carbon onion

2.7.1. Effect of contact time

Drug loading was performed using solution adsorption-centrifugation method at different stirring times. 500 mg of OLC was added to 5 mL of saturated solution of drug in ethanol (saturation solubility of paracetamol and ibuprofen at 20 °C is 150 and 698 mg/mL of ethanol, respectively) and the suspension was stirred (stirring speed-100 rpm) at 20 °C for four different durations (0.25, 0.5, 1, 2, 4 hours). Post loading, the suspension was centrifuged at 1500 rpm, the supernatant was removed and the precipitate was dried at 40 °C for 24 hours. After 24 hours of drying, white crystalline drug layer was found on the

surface of the sediment, which was removed, while the bottom layer was considered as drug/OLC complex.

2.7.2. Effect of initial concentration on drug loading

Drug loadings were performed by SA-C method using three different drug concentrations (concentrations of 50, 100, 150 mg of PA per mL of ethanol and concentrations of 300, 500 and 698 mg of IBU per mL of ethanol). 100 mg of OLC was added to 10 mL of drug solution and was allowed to undergo stirring (100-rpm) at 20 °C for 1 hour.

2.8. Determination of drug loading using UV spectroscopy

50 mg of drug/carrier complex was added to 100 ml of ethanol and was stirred for 24 hours at 25°C. The solution was filtered using 0.45 µm syringe filters (0.2 µm syringe filters were used for samples containing carbon onion) and the concentration of the drug in the filtrate was determined by UV spectroscopy (Jenway, UK) at wavelengths of 257nm and 264nm for paracetamol and ibuprofen respectively. Loading efficiency was calculated using equation -5:

$$Loading\ efficiency\ (\%) = \frac{weight\ of\ the\ drug\ in\ complex}{weight\ of\ complex} \times 100 \qquad \text{(Equation-5)}$$

Calibration curves were constructed for paracetamol and ibuprofen. Stock solutions of paracetamol were prepared by dissolving 20 mg in 100 mL ethanol and standards were prepared by diluting the stock solution with ethanol to achieve concentrations of 2, 4, 6, 8 and 10 µg/mL. Calibration curve constructed to relate the absorbance and drug concentration is shown in Figure 2-2.
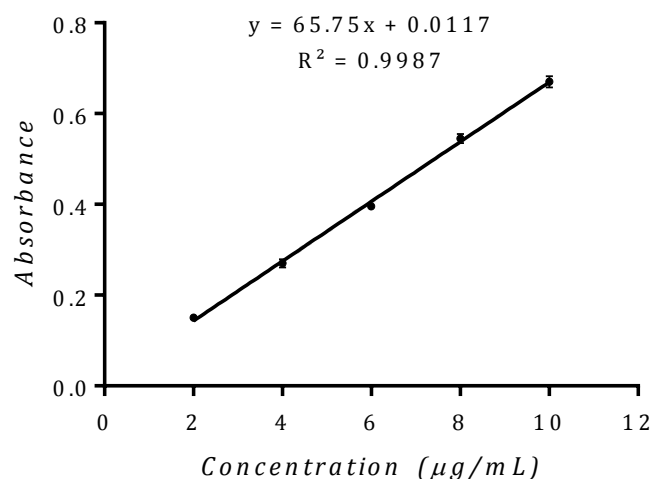
Figure 2-2: Calibration curve for paracetamol in ethanol at 257nm. Concentration of the drug in the solution was determined by UV spectroscopy. Each experiment was carried out in triplicate with the average mean result recorded ± the standard deviation (represented as error bars)

Stock solutions of ibuprofen were prepared by dissolving 100 mg in 100 mL ethanol and Standards were prepared by diluting the stock solution with ethanol to achieve concentrations of 0.2, 0.3, 0.4, 0.5 and 0.6 mg/mL. Calibration curve constructed to relate the absorbance and drug concentration is shown in Figure 2-3.
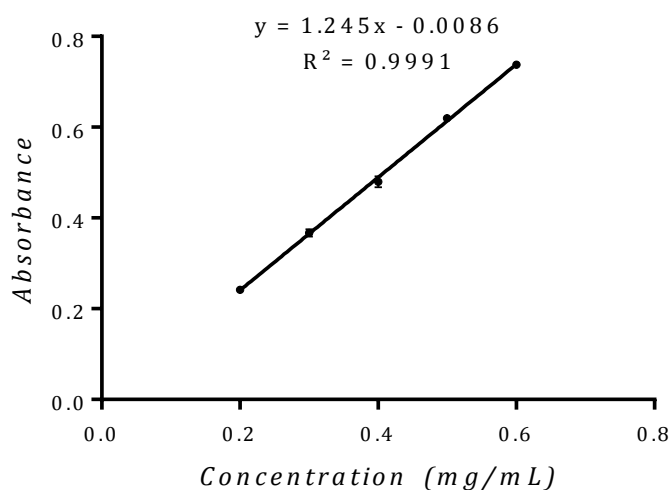
Figure 2-3: Calibration curve for ibuprofen in ethanol at 264nm. Concentration of the drug in the solution was determined by UV spectroscopy. Each experiment was carried out in triplicate with the average mean result recorded ± the standard deviation (represented as error bars)

2.9. Differential Scanning calorimetry (DSC)

DSC measures the changes in the heat flow as a function of temperature, as the sample is being heated. The presence of crystalline drug can be detected from the melting peak of DSC curves. The analysis was performed using a Q100 DSC (TA Instruments, UK). Sample (2-3 mg) was transferred to Tzero aluminium pan and temperature scan was performed at a heating rate of 10°C/min under nitrogen gas. Percentage crystallinity was calculated from the melting enthalpy using equation-6 (Kong & Hay 2002):

$$\frac{Xc(\%)}{Xc^{\circ}(\%)} = \frac{\Delta Hm}{\Delta Hm^{\circ}} \qquad \text{(Equation-6)}$$

Where $Xc(\%)$= percentage of crystallinity in the drug/carrier complex and $Xc^{\circ}(\%)$ = percentage of crystallinity in physical mixture containing equivalent amount of drug and carrier as that of complex and is considered to be 100%. ΔHm = melting enthalpy of the drug/carrier complex and ΔHm° = melting enthalpy of physical mixture containing equivalent amount of drug and carrier as that of complex.

2.10. Powdered X-ray diffraction analysis (XRD)

X-ray diffraction is a non-destructive technique used to study the structure of crystalline materials. Sample is bombarded with X-rays through a range of angles and the intensity of the X-rays diffracted is recorded. To determine the solid state of the drug in the drug/carrier complex, XRD diffraction was performed using a Bruker D8 ADVANCE diffractometer (Bruker, USA) with a Cu–Kα source operated at 30 kV and 30 mA. The angular range (2θ) was 10 to $50°$ with a step size of $0.02°$. Diffraction spectra of carbon containing samples were baseline corrected using EVA software.

2.11. Attenuated total reflectance-Fourier transform infra-red (ATR-FTIR) spectroscopy

FTIR involves exposing the sample to Infrared radiation during which the sample absorbs radiation at certain wavelengths. The degree of absorption at different wavelengths is characteristic of the molecular structure of the sample. FTIR was used to investigate possible interactions between the drug and the carrier and was performed using a Nicolet iS5 spectrometer (Thermo Fisher Scientific, UK) equipped with an iD5 ATR accessory with a laminated diamond crystal at an angle of incidence of 42°. The spectra were obtained in the range of 500-4000 cm^{-1} (wavenumber) at a spatial resolution of 4 cm^{-1} and were an average of 16 scans.

2.12. Nitrogen sorption analysis

In this technique, the sample is exposed to nitrogen at cryogenic temperature and the amount of nitrogen adsorbed at each pressure is calculated from which the surface area of the sample can be calculated. The porosity of the carrier before and after drug loading was investigated by nitrogen adsorption technique using a Micrometrics ASAP 2420 (Accelerated surface area and porosimetry system, Micrometrics, USA). Adsorption-desorption isotherms were obtained at 77 K in the relative pressure range between 0.01 and 0.9. Prior to analysis, all samples were degassed at 40°C for 24 hours. The specific surface area of the sample was determined from adsorption isotherm according to Brunauer–Emmett–Teller (BET) model assuming multilayer adsorption. The quantity of gas adsorbed as monolayer was determined using equation-7 (Thommes 2010):

$$\frac{1}{Q(\frac{P^O}{P}-1)} = \frac{1}{Q_m C} + \frac{C-1}{Q_m C} \times \frac{P}{P^o}$$ (Equation-7)

Where P is the partial vapour pressure of adsorbate gas, P_o is the saturated pressure of adsorbate gas (760 Torr for N_2), Q is the total quantity of gas adsorbed at relative pressure (P/P^o), Q_m is the monolayer quantity of gas adsorbed and C is a BET constant. Q_m was obtained from linear plots of $\frac{1}{Q(\frac{P^0}{P}-1)}$ vs the relative pressure ($\frac{P}{P^o}$) in the linear relative pressure range of 0.1-0.3 (Plonska-Brzezinska et al. 2011). From the value of Q_m so determined, the BET Specific surface area (BET$_{SSA}$) was calculated using Equation-8:

$$SSA = \frac{Q_m NA}{22400}$$ (Equation-8)

Where N is the Avogadro constant($6.022 \times 10^{23}\ mol^{-1}$), A is the cross-sectional area of one adsorbate molecule (0.162 nm^2 for N_2), 22400 is the volume occupied by one mole of adsorbate at STP in millilitres.

Pore size distribution of the sample was computed with the ASAP 2420 software using non-local density functional theory (NLDFT) model assuming slit-shaped pores since BET model does not take pore morphology into account.

2.13. Scanning electron microscopy (SEM)

SEM focuses beams of electrons on the surface of a sample and the interactions between the sample surface and beam of electrons are used to obtain images of the surface of the sample. SEM Images presented in chapter 3 were recorded with a VEGA3 SEM (TESCAN, Czech Republic) at an acceleration voltage of 15kV. Prior to imaging, samples were coated with 10nm gold using a Q150 ES sputter coater (Quorum

technologies, UK). SEM images presented in chapter 6 were recorded with an XL30 ESEM-FEG (Philips, Netherlands) at an acceleration voltage of 10kV.

2.14. High-resolution transmission electron microscopy (HRTEM)

In this technique, a thin sample is exposed to high energy beam of electrons which travel through the sample and the interactions between the sample and the electrons give information about the crystal structure on a molecular level. Transmission electron microscope images were recorded using 2010F (JEOL) microscope operating at 200 kV and using a Gatan Ultrascan 4K camera. Prior to analysis, the sample powders were suspended in ethanol and sonicated for 1 hour to separate agglomerates. 5 µl of the suspension was allowed to dry onto lacey carbon grid.

2.15. Raman spectroscopy

Raman spectroscopy was used to investigate the transformation of nanodiamond to carbon onion (graphitization). This technique involves exposing the sample to laser light and detecting the scattered light. Some amount of scattered light is shifted to a different energy to that of incident laser rays. Plotting the intensity of shifted light for each energy of light results in Raman spectra which can give information on the crystalline structure of the sample. Spectra were measured on a Renishaw InVia Raman microscope with a 532 nm excitation source. The acquisition time was 10 seconds and 3 accumulations were recorded.

2.16. X-ray Photo electron spectroscopy (XPS) and X-ray excited Auger electron spectroscopy (XAES)

XPS provides information about the chemical composition of the surface of materials (usually 3-10nm depth). Materials are exposed to X-rays and electrons from the inner

shells are emitted. The kinetic energy of the emitted electrons is determined which gives the binding energy of the electrons which is characteristic of elements. The chemical composition and sp^3/sp^2 bonding ratio of the samples were determined using a Thermo Scientific ESCALAB 250 electron spectrometer. Analysis conditions include X-ray source with excitation energy of 15KeV, pass energy of 20 eV with a step size of 0.1 eV, dwell time of 50 ms and X-ray spot size of 500 µm. The samples were placed on an adhesive copper plate at a chamber pressure of 5×10^{-10} mbar during the analysis. X-ray excited Auger peaks (C KLL) at higher binding energy were analysed to obtain carbon phase information.

2.17. *In vitro* drug release studies

Drug release was studied with a USP Type II dissolution apparatus at 37 °C with paddle stirring speed of 100 rpm. Powders were filled in hard gelatin capsules size 000 and 0.1 M sodium phosphate buffer at different pH, with or without 1% Sodium dodecyl sulphate was used as dissolution medium. Samples were withdrawn at specific time intervals and replaced with fresh dissolution medium. The samples were filtered using 0.45 µm syringe filters (0.2 µm syringe filters were used for samples containing carbon onion) and concentration of drug was determined using UV spectrophotometer (Jenway, UK).

2.18. Statistical analysis

Each experiment was carried out in triplicate with the average mean result recorded ± the standard deviation (represented as error bars). Statistical analysis was carried out on the data by one way ANOVA (analysis of variance) followed by the post-hoc Tukey's or Dunnett's multiple comparison test using Graph pad prism software (Version 6.0 for Windows) unless stated. Statistically significant differences are noted for $p < 0.05$ ($p < 0.05$; [**] $p < 0.01$; [***] $p < 0.001$; [****] $p < 0.0001$).

Chapter 3 **- Application of activated carbon as a porous carrier for amorphous drug delivery**

Some of the results presented in this chapter have been published in the paper:

3.1. Introduction

Application of porous materials, such as porous silica, as carriers to improve the solubility or dissolution rate of drugs has been largely demonstrated in various research papers (Vallet-Regi et al. 2001; Salonen et al. 2008; Zhang et al. 2010). Drug adsorbed in the pores of the carrier is present in an amorphous state and the restricted space in the pores inhibits the crystallisation of the drug. The amorphous form of drugs have disordered molecular packing and higher internal energy compared to the crystalline form, leading to improved solubility and dissolution, especially in drugs with high crystal energy (Salonen, Laitinen, et al. 2005; Yu 2001; Preisig et al. 2014). In addition, adsorption of the drug to the carrier can also improve the dissolution due to the higher surface area exposed to the dissolution medium. However, most of the carriers investigated so far are often associated with limitations, such as expensive synthesis, low loading efficiency, poor stability, reactivity with drugs and safety concerns (Salonen, Laitinen, et al. 2005; Jarvis et al. 2012; Xu et al. 2013; Kinnari et al. 2011). Hence, it is crucial to develop more efficient carriers that can overcome these limitations.

Of interest during this study is the application of activated carbon as a porous carrier to study mechanisms of drug loading and release, since this material has several properties such as high porosity, commercial availability, low cost and chemical inertness, qualifying it for oral drug delivery. AC consists of a three-dimensional interconnected pore structure, with micropores (pore width <2 nm), mesopores (pore width 2-50 nm) and macropores (pore width >50 nm). AC is extensively used in drinking water treatment and is also clinically used as an antidote to remove poisonings. Despite, the favourable properties, the literature on the application of activated carbon for drug delivery is sparse.

Various drug loading methods such as solvent evaporation, supercritical CO_2, melting and solution adsorption have been studied previously for drug loading into porous carriers, however, solution adsorption also called as immersion is the most widely used method. Solution adsorption involves drug loading by immersing the carrier in a saturated or high concentrated drug solution and stirring for a specific duration followed by separating the drug-loaded carrier complex by filtration or centrifugation (Salonen, Paski, et al. 2005; Li-hong et al. 2013; Piotto & Bettotti 2017).

3.2. Aims and Objectives

The aim of this chapter is to investigate the application of activated carbon (AC) as a porous carrier for amorphous drug delivery using paracetamol and ibuprofen as model drugs. To achieve this, the main objectives were to:

1. Investigate the particle size of AC (Norit® Darco® G60 type) and study the cytotoxicity of AC using Caco-2 cells.

2. Perform drug loading using solution adsorption method and determine the drug loading efficiency

3. Study the solid state characteristics of the drug loaded in to AC and investigate the interactions between drugs and AC in order to understand if the drug loading was due to physical adsorption or chemical interaction.

4. Investigate if the drug loading is reversible and to understand the kinetics of drug desorption.

5. Identify the sites of adsorption of the drug and analyse the porosity of AC before and after drug loading.

3.2.1. Characterisation of activated carbon

Cellular uptake of microparticles is much lower compared to nanoparticles, therefore the risk of toxicity associated with microparticles can be much lower. However, studies (Desai et al. 1996; Heikkilä et al. 2010; Desai et al. 1997; He & Park 2016) have shown uptake of microparticles of size up to 10 µm by intestinal epithelium, with particles of size < 5 µm transported through lymphatics and particles of size > 5 µm retained in the Peyer's patches, suggesting the importance of considering the toxicity of microparticles of size < 10 µm. Also, the particle size of the carrier may affect the drug release rate; smaller particles can exhibit faster drug release due to higher surface to volume ratio and shorter pore length (Y. Zhang, Wang, et al. 2014; Burguete et al. 2012). Therefore, the particle size of activated carbon used in this study was determined by laser diffraction.

AC used in this study has a particle size in the range of 0.55- 87.5 µm, with nearly 40% of the particles ≤ 10 µm in size (Figure 3-1 and Table 3-1), indicating the possibility of internalisation by cells. Hence, toxicity studies were performed on Caco-2 cells to determine the feasibility of application of AC in oral drug formulations.

Caco-2 cells were incubated with media containing AC in concentrations of 10-800µg/mL, with cell survival rate subsequently evaluated by MTT assay (Figure 3-2). There was a statistically significant difference in the survival rate between cells exposed to different concentrations of AC ($p < 0.0001$, one-way ANOVA). A post hoc test showed that there was no statistically significant difference ($p > 0.05$, Dunnett's multiple comparison test), for AC in concentrations of 10-200 µg/mL; however, for the concentrations ≥ 400 µg/mL, significant toxicity was observed ($p < 0.01$, Dunnett's multiple comparison test), which could be attributed to adsorption of nutrients in the culture medium by activated carbon (Fröhlich 2012; Baeza-Squiban et al. 2011).

Nevertheless, even at the highest concentration (800 µg/mL) tested, the cell viability was still over 80%, suggesting that application of AC with a particle size above 0.45 µm could be safe for oral drug delivery.
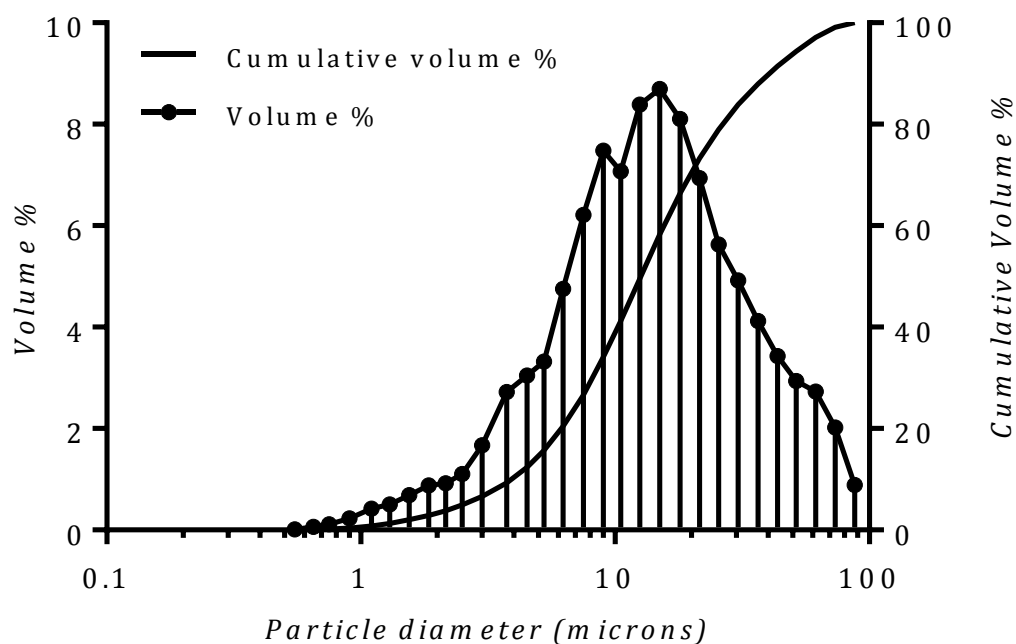
Figure 3-1: Particle size distribution of activated carbon. 25 mg of carrier was dispersed in 200 mL of ethanol and then analysed for particle size using laser diffraction (HELOS, Sympatec GmbH, Germany) in the measuring range of 0.1 to 500 µm.

Table 3-1: Particle size characteristics of activated carbon from laser diffraction analysis.

Material	X90[a] (µm)	X50[b] (µm)	X10[c] (µm)	Volume mean diameter (µm)	Span
Activated carbon	40.59 ± 0.53	12.62 ± 0.09	3.92 ± 0.02	17.85 ± 0.15	2.91 ± 0.02

[a] Particle dimension corresponding to 90% of the cumulative undersize distribution
[b] Median particle dimension
[c] Particle dimension corresponding to 10% of the cumulative undersize distribution
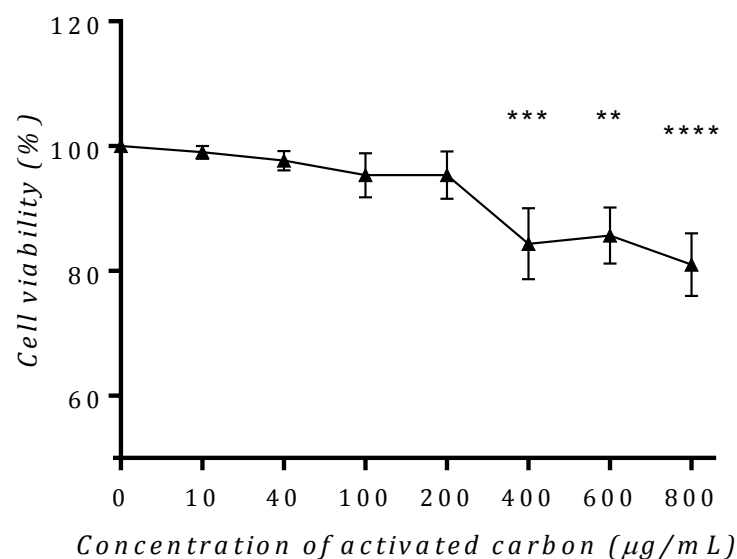
Figure 3-2. Cytotoxicity of activated carbon against Caco-2 cells. MTT assay was used to analyse the survival rate of Caco-2 cells incubated with different concentrations of activated carbon. Statistically significant differences compared to control (0 µg/mL) are noted for $p < 0.05$ ($^{**}p < 0.01$; $^{***}p < 0.001$; $^{****}p < 0.0001$, one-way ANOVA and Dunnett's multiple comparison test).

3.2.2. Determination of drug loading efficiency

Drug loading was performed as described in section-2.4.1. The sediment obtained after centrifugation was allowed to dry for 24 hours, during which residual ethanol was evaporated, leaving a crystalline layer of the drug on the top of the sediment. Also, due to the tight packing of particles in the sediment, the evaporation process was slowed down, which can give enough time for the drug to be diffused into the deeper pores (Preisig et al. 2014). The quantity of drug present in the supernatant, crystalline layer of the sediment and complex are presented in Table 3-2. The loading efficiency was found to be 20.7 % and 44.4 % for paracetamol (PA) and ibuprofen (IBU), respectively. The higher drug loading of IBU is attributed to the higher initial concentration of IBU in the loading solution, due to its higher maximum solubility in ethanol compared to PA. Although the loading efficiency was higher, the fraction of adsorbed to the unadsorbed drug was lower for IBU compared to that of PA, which could be due to better interstitial

86

accommodation with the ethanol leading to stronger interactions between IBU and ethanol (Domańska et al. 2009) since among many aspects, adsorption depends on the solubility of the adsorptive (drug) and solution chemistry (Radke & Prausnitz 1972). It was also found that analysis of free drug in the supernatant solution can give a false estimation of drug loading capacity, since it does not consider the top crystalline layer of the sediment.

Table 3-2: Comparison of ibuprofen and paracetamol loading in activated carbon

Drug	Initial quantity of drug [a] (mg)	Quantity of drug in the complex (mg)	% Loading efficiency (drug/complex)	Quantity of drug (mg)	
				Supernatant [b]	Crystalline layer [c]
PA	1500	208 ± 12.5	20.7 ± 1	985.5 ± 12	320.5 ± 6
IBU	6900	643 ± 77.7	44.4 ± 4	5592.4 ± 159	662.3 ± 174

[a] per 10mL of Ethanol
[b] supernatant obtained from centrifugation
[c] top crystalline layer of the sediment.

3.2.3. Solid-state analysis of drug

DSC and XRD techniques were used to detect any crystalline drug in the complex. Pure paracetamol exhibited a melting peak at 169 °C, characteristic of monoclinic Form I crystalline paracetamol (Qi et al. 2008). In the case of PA/AC phy mix containing an equivalent amount of PA and AC as that of complex, a melting peak at 169 °C similar to that of pure PA was observed. However PA/AC complex did not show any crystallinity, suggesting that the paracetamol is completely amorphous in the complex (Figure 3-3). Pure ibuprofen and a physical mixture containing an equivalent amount of IBU and AC as that of complex exhibited a melting peak at 74.8 °C indicative of crystalline drug (Cano et al. 2001; Xu et al. 2004). However, unlike PA/AC complex, IBU/AC complex exhibited a melting peak at 74.8 °C, suggesting the presence of crystallinity (Figure 3-4).

To determine the amount of crystallinity, melting enthalpies of IBU/AC phy mix and IBU/AC complex were compared (Table 3-3) and the percentage crystallinity in the IBU/AC complex, was found to be about 19% of the total drug present in the IBU/AC complex (which is equivalent to 122 mg of IBU, since the total IBU present in IBU/AC complex is 643 mg). This suggests that the true loading efficiency for IBU is 39% and loading higher than this could lead to crystallisation of ibuprofen. To obtain IBU/AC complex with no crystallinity, the concentration of IBU in the loading solution needs to be adjusted, suggesting that saturated drug solution for loading is not suitable in all cases, especially for drugs with high solubility in the loading solvent, which could result in higher loading leading to crystallisation. Hence, it is important to optimise drug loading conditions to obtain drug/carrier complexes with 100% amorphous drug and will be investigated in the next chapter. Also, melting enthalpies of both PA/AC phy mix and IBU/AC phy mix were not equivalent to that of pure PA and IBU respectively. Possible reasons for such differences could be: (1) drug-AC interactions leading to reduced intermolecular forces in the drug and; (2) adsorption of drug into the pores of AC during the process of melting (Wang et al. 2012; Chen et al. 2012). The exact mechanism on how these can lead to changes in melting enthalpy requires further investigation.

Table 3-3: Melting enthalpies and melting temperatures obtained from DSC thermograms of pure drugs, drug/carrier complexes, and drug/carrier physical mixtures.

Sample	Drug carrier ratio (*w/w*)	Melting Enthalpy (J/g)	Melting temperature (°C)	% Crystallinity
IBU	1:0	130.3	74.8	100
IBU/AC phy mix	0.8:1	83.4	74.8	100*
IBU/AC complex	0.8:1	15.78	72	19
PA	1:0	181	169.2	100
PA/AC phy mix	0.25:1	27.1	169.2	100*
PA/AC complex	0.25:1	-	-	0

* Crystallinity in the physical mixture is considered as 100% to calculate the crystallinity in the complex relative to that of physical mixture.

Aston University

Illustration removed for copyright restrictions

Figure 3-3: DSC curves of paracetamol (PA), activated carbon (AC), paracetamol loaded activated carbon (PA/AC complex) and physical mixture of paracetamol and activated carbon (PA/AC phy mix). No melting peak was found in PA/AC complex indicating that the drug loaded was completely amorphous. Note that the heat flow scale is arbitrary.

Figure 3-4: DSC thermograms of ibuprofen (IBU), activated carbon (AC), ibuprofen-loaded activated carbon (IBU/AC complex) and physical mixture of ibuprofen and activated carbon (IBU/AC phy mix). IBU/AC complex exhibited a melting peak and from the melting enthalpy, percentage crystallinity was found to be 19% of the total drug loaded. Note that the heat flow scale is arbitrary.

The results from DSC were confirmed by X-ray diffraction studies (Figure 3-6 and Figure 3-5). PA and PA/AC Phy mix showed characteristic diffraction peaks at 15.4°, 18.1°, 20.3°, 23.3°, 24.2° and 26.4°, corresponding to crystalline PA (I.-C. Wang et al. 2011). XRD patterns of pure IBU and IBU/AC phy mix showed characteristic peaks at 11.8°, 16.4°, 17.4°, 20° and 22° (2θ), corresponding to crystalline IBU (Liu et al. 2014; Martín et al. 2009).

In the case of drug/carrier complexes, XRD patterns of PA/AC complex did not show any peaks corresponding to crystalline PA, suggesting that the drug was completely present in an amorphous form. However, IBU/AC complex exhibited diffraction patterns corresponding to crystalline IBU; however, the peaks at 20° and 22° were less intense, suggesting reduced crystallinity of IBU.

Figure 3-5: XRD patterns of paracetamol (PA), activated carbon (AC), paracetamol loaded activated carbon (PA/AC complex) and physical mixture of paracetamol and activated carbon (PA/AC phy mix). No diffraction pattern was found in PA/AC complex corresponding to crystalline PA indicating that the drug loaded was completely amorphous. Note that the intensity scale is arbitrary.

Figure 3-6: XRD patterns of ibuprofen (IBU), activated carbon (AC), ibuprofen-loaded activated carbon (IBU/AC complex) and physical mixture of ibuprofen and activated carbon (IBU/AC phy mix). IBU/AC complex exhibited a diffraction pattern corresponding to crystalline IBU however, the peaks at 20° and 22° were less intense. Note that the intensity scale is arbitrary.

Results from DSC and XRD studies suggest, in the case of PA/AC complex, PA was effectively loaded into the pores of AC in an amorphous state. However, with IBU/AC complex, the loaded drug was not completely amorphous, which could be attributed to the higher loading, which in turn is a result of higher concentration of drug in the loading solution compared to PA. This indicates the effect of initial drug concentration on the loading efficiency and solid state characteristics and will be investigated in the next chapter. Nevertheless, both PA and IBU loaded into AC were successfully converted into the amorphous form.

3.2.4. Drug carrier interactions

It is important to consider possible chemical interactions between the drugs and AC, since these interactions can affect the chemical nature and stability of the drugs loaded. FTIR spectra of AC did not show any significant peaks (Figure 3-7 and Figure 3-8), whilst the sloping of the spectra towards the right in samples containing AC is due to an increase in the absorption by carbon with an increase in wavelength (decrease in wavenumber), since the depth of penetration of radiation increases at higher wavelengths (Wilhelm 1996).

FTIR spectra of PA and PA/AC phy mix (Figure 3-7) showed a strong peak at 3310cm^{-1} and a broad peak at 3200 cm^{-1}, corresponding to secondary amide N-H stretching and phenol O-H stretching, respectively. Also, a sharp peak corresponding to carbonyl C=O stretching at 1645 cm^{-1} was found. Spectra of IBU and IBU/AC phy mix (Figure 3-8) showed a sharp peak corresponding to carboxylic acid (C=O) stretching at 1710 cm^{-1} and characteristic three peaks between 2960-2860 cm^{-1}, corresponding to C-H stretching.(Lai et al. 2017)

No significant peaks corresponding to PA were found in the case of PA/AC complex (Figure 3-7) and could be due to the absence of PA on the surface or in the superficial

pores. Since the depth of penetration of IR into the samples is only about 0.2 - 5 µm, drug deposited in the deeper pores may not be detected (Kazarian & Chan 2013). PA/AC complex with higher drug loading could help study about possible chemical interactions between PA and AC and will be discussed in the next chapter.

Spectra of IBU/AC complex was found to be similar to that of IBU, with no significant shift in the existing peaks and no new peaks found, indicating the absence of any chemical interactions (Figure 3-8). The presence of peaks in the spectrum of IBU/AC complex unlike that of PA/AC complex, could also indicate the presence of IBU as separate drug crystals or as a layer adsorbed on the external surface of AC, further supporting results from DSC and XRD.

Aston University

Illustration removed for copyright restrictions

Figure 3-7: FTIR spectra of paracetamol (PA), activated carbon (AC), paracetamol-loaded activated carbon (PA/AC complex) and physical mixture of paracetamol and activated carbon (PA/AC phy mix). No chemical interactions could be detected between PA and AC. Note that the transmittance scale is arbitrary.

Figure 3-8: FTIR spectra of ibuprofen (IBU), activated carbon (AC), ibuprofen-loaded activated carbon (IBU/AC complex) and physical mixture of ibuprofen and activated carbon (IBU/AC phy mix). No chemical interactions could be detected between IBU and AC. Note that the transmittance scale is arbitrary.

3.2.5. Surface morphology

The above studies demonstrate that, in the case of PA/AC complex, PA is completely amorphous, loaded into the pores and is absent on the surface of AC, while IBU/AC complex contained crystalline and possibly surface adsorbed IBU. To examine the surface morphology and to identify sites of adsorption of the drug in the complex, SEM images were obtained (Figure 3-9). However, in IBU/AC complex, small particles of approximately 2 µm in size adsorbed on the surface could be seen, indicated by an arrow in Figure 3-10 (c). When this particular area in IBU/AC complex with adsorbed particles was magnified, the surface morphology looked completely different to that of pure AC (Figure 3-10 (d)), and the presence of these particles could be due to the surface crystallisation of IBU as previously indicated by DSC, XRD and FTIR studies.
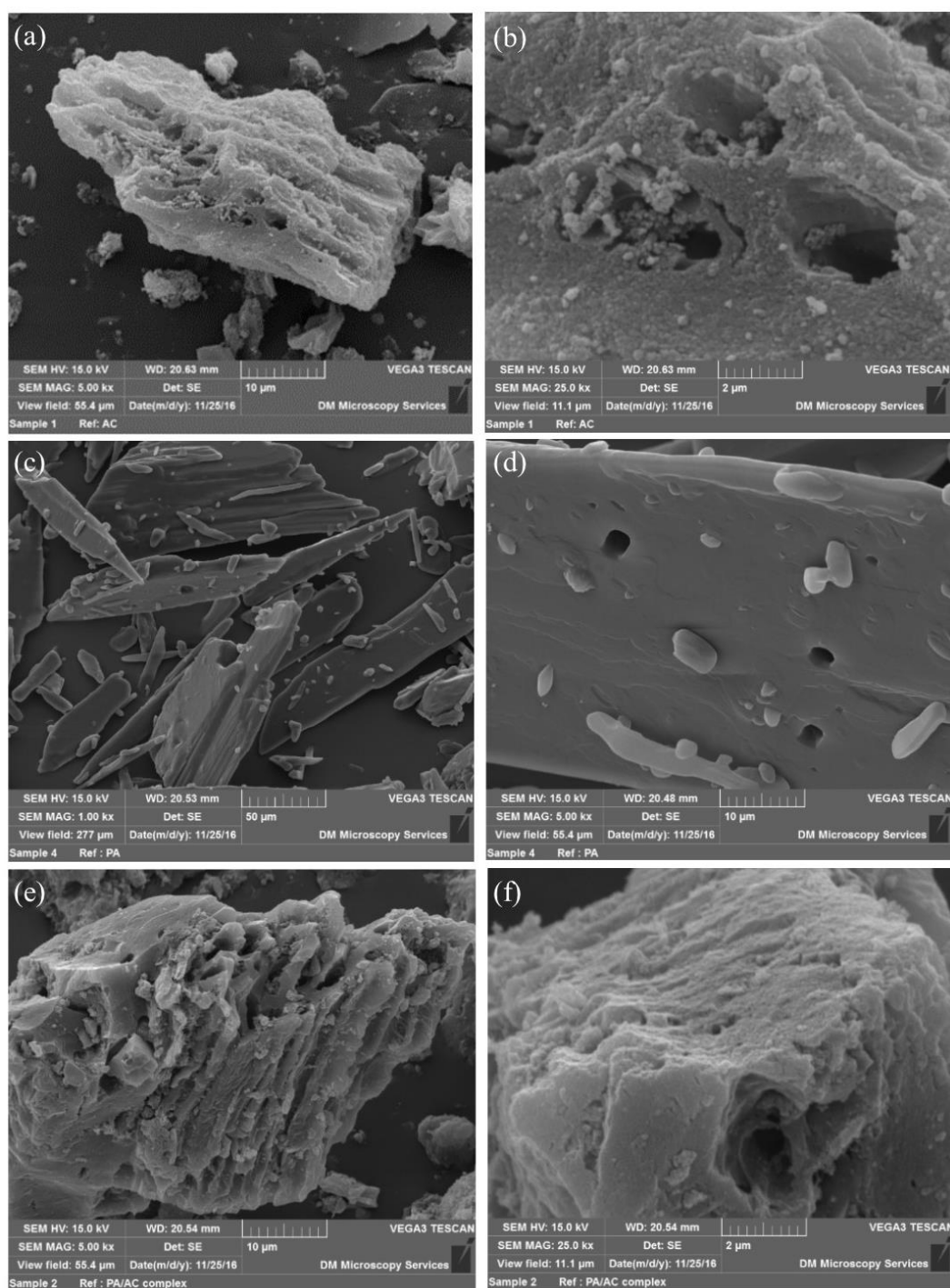
Figure 3-9: SEM images of (a) and (b) activated carbon, (c) and (d) paracetamol, (e) and (f) paracetamol loaded activated carbon with 25% loading.
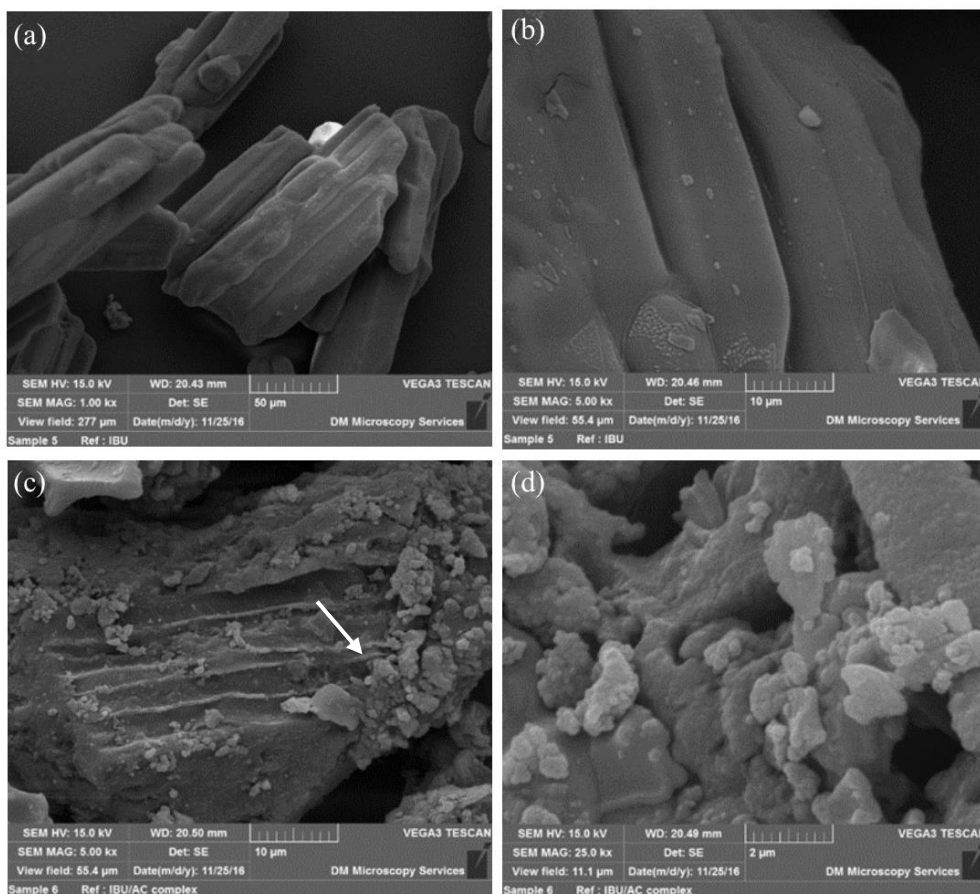
Figure 3-10: SEM images of (a) and (b) ibuprofen, (c) and (d) ibuprofen loaded activated carbon with 44% loading showing surface crystallised ibuprofen.

3.2.6. *In vitro* drug release studies

The dissolution profiles of pure drug and drug/carrier complex are presented in Figure 3-11 and Figure 3-12. Phosphate buffer at pH 5.8 and pH 7.2 was used as dissolution medium for paracetamol and ibuprofen, respectively, according to BP specifications (Pharmacopoeia 2016). Prior to the study, all the samples were put in hard gelatin capsules, which took approximately 3 minutes to disintegrate; hence, drug release has commenced at 3 min in all the samples.

Compared to crystalline PA, the dissolution rate of PA/AC complex was slightly higher until 10 min, after which drug release from the complex slowed down and reached an end point at 20 min with an incomplete release (54 %). No further drug release was observed

even after 72 hours and this incomplete PA release from the complex could be attributed to poor wettability of AC (powder samples floating on the surface of the dissolution medium could be observed), leading to inaccessibility of dissolution medium to deeper pores. Therefore, sodium phosphate buffer with 1% SDS was used as dissolution medium to improve the wettability of carbon. Indeed, the complete release was achieved for PA/AC complex in the presence of SDS. There was a statistically significant difference in the drug release between pure crystalline PA and PA/AC complex ($p < 0.0001$, two-way ANOVA), which could be due to the amorphous nature of PA loaded into porous AC. Compared to pure crystalline drug, amorphous drug present in the pores of AC has a higher surface area in contact with the dissolution media, which can result in faster release; thus, the drug loaded into AC, compared to the pure crystalline drug, favoured faster release.

Aston University

Illustration removed for copyright restrictions

Figure 3-11: Dissolution profiles of paracetamol (PA) and paracetamol loaded activated carbon (PA/AC complex) determined at pH 5.8. Curves PA-SDS and PA/AC complex-SDS represent dissolution profiles determined in media containing 1% SDS. Statistically significant differences are noted for $p < 0.05$, (**** $p \leq 0.0001$, two-way ANOVA and Bonferroni's multiple comparison test).

In the absence of SDS, similar to PA/AC complex, drug release from IBU/AC complex was incomplete (no further release was observed even after 72 hours) with 61% release (Figure 3-12 (a)); however, was higher than PA/AC complex (total release was 56%), and could be due to the presence of higher amount of IBU in the superficial pores of AC or due to the presence of crystalline ibuprofen outside the pores of AC.

In the presence of SDS, drug release from IBU/AC complex was complete, reaching an endpoint within 15 minutes; however, there was no statistically significant difference in the drug release between crystalline IBU and IBU/AC complex ($p > 0.5$, two-way ANOVA), which could be due to the higher solubility of IBU at pH 7.2. IBU is a weak acid with pKa 4.9 and its solubility is lower at acidic pH (Rivera-Leyva et al. 2012). Therefore, sodium phosphate buffer at pH 5.5 with and without SDS (Figure 3-12 (b)), was used as dissolution medium to reduce the solubility of IBU. In the absence of SDS, drug release from IBU/AC complex was incomplete similar to that at pH 7.2, indicating that pH did not have any effect on the wettability of carbon. It was observed that disintegration of gelatin capsules at pH 5.5 was faster compared to pH 7.2, due to which a higher initial release (within 5 min) was observed at pH 5.5 compared to pH 7.2 (Zhao et al. 2004).

In the presence of SDS, there was a statistically significant difference in the drug release between pure crystalline IBU and IBU/AC complex ($p < 0.0001$, two-way ANOVA); however, when drug release data from IBU/AC complex at pH 7.2 was compared with IBU/AC complex at pH 5.5 (Figure 3-13), no statistically significant difference was found ($p > 0.5$, two-way ANOVA), indicating that: (1) the difference observed in the drug release between IBU and IBU/AC complex at pH 5.5 is due to reduction in the drug release rate of pure crystalline IBU and not due to increase in the drug release from IBU/AC complex; (2) that drug release from IBU/AC complex was less pH dependent.

Nevertheless, compared to the pure crystalline IBU, IBU/AC complex favoured faster release (at pH 5.5), further supporting results from PA/AC complex release studies.

Figure 3-12: Dissolution profiles in sodium phosphate buffer determined at (a) pH 7.2 and (b) pH 5.5. Curves IBU and IBU/AC complex represent pure ibuprofen and ibuprofen-loaded activated carbon. Curves IBU-SDS and IBU/AC complex-SDS represent dissolution profiles determined in media containing 1% SDS. Statistically significant differences are noted for $p < 0.05$ (****$p < 0.0001$, two-way ANOVA and Bonferroni's multiple comparison test).
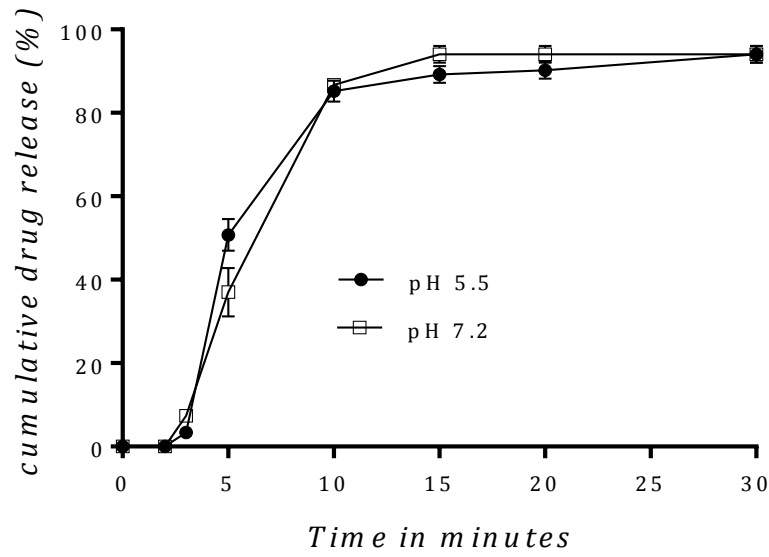
Figure 3-13: Comparison of dissolution profiles of ibuprofen-loaded activated carbon complex determined at pH 7.2 and pH 5.5 in sodium phosphate buffer with 1% SDS. Statistically significant differences are noted for $p < 0.05$ (two-way ANOVA).

Drug release profiles obtained in the presence of SDS for PA and IBU were fitted with simplified Higuchi model which describes drug release based on Fick's law of diffusion (equation-9) which can be used to describe diffusion controlled system where drug release is from an insoluble matrix (Costa et al. 2001; Izquierdo-Barba et al. 2005):

$$f_t = K_H t^{1/2} \qquad \text{(Equation-9)}$$

Where K_H is the Higuchi constant and f_t is the fraction of drug released at time t

Higuchi square root of time plots for both drug loaded complexes (Figure 3-14), display a two-step release with an initial burst effect, which could be attributed to the drug release from superficial macropores and mesopores followed by slow release which could be attributed to drug release from deeper micropores. Results also show that kinetic

constants for PA and IBU are different indicating the influence of the chemical nature of drug (Table 3-4).
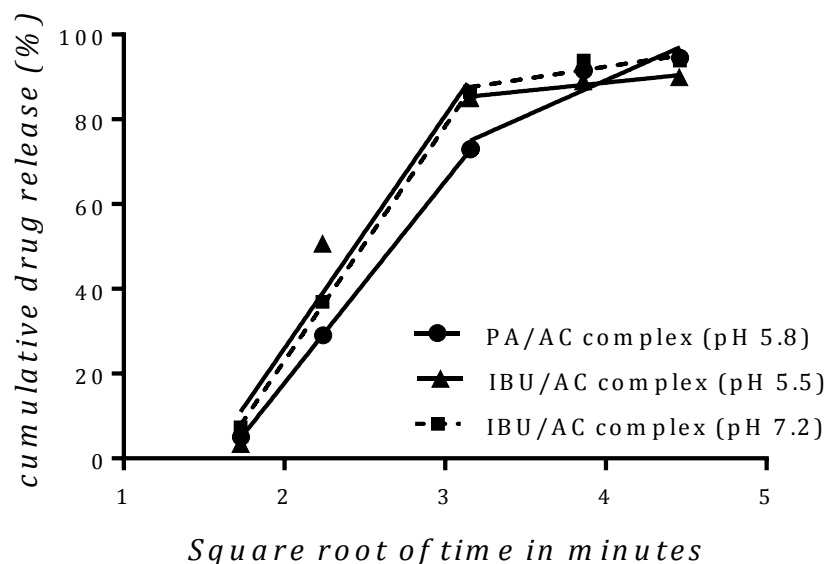
Figure 3-14: Two step regression linear utilising Higuchi's square root of time plot for drug release from complex in the presence of SDS. In brackets pH of the dissolution medium. Each point represents the mean of n=3 determinations.

Table 3-4: Kinetic parameters of drug release from paracetamol and ibuprofen loaded activated carbon

Sample	Higuchi diffusion two step		
	Duration	Rate constant	Linear regression coefficient
PA/AC complex at pH 5.8	3-10 min	47.54	1
	10-20 min	16.88	0.8854
IBU/AC complex at pH 5.5	3-10 min	54.75	0.9342
	10-20 min	3.87	0.9202
IBU/AC complex at pH 7.2	3-10 min	55.22	0.9994
	10-20 min	5.72	0.7913

3.2.7. Porosity analysis to determine the sites of adsorption

Adsorption isotherms and pore size distribution curves of AC before and after drug loading are shown in Figure 3-15 and Figure 3-16, with the data from N_2 sorption studies summarised in Table 3-5. The adsorption/desorption isotherm of AC exhibited a typical type IV isotherm and a hysteresis loop, characteristic of microporous materials with significant mesoporosity (Chen et al. 2010). The pore size distribution of pure AC shows the presence of pores in the range of 2-14 nm. For PA/AC physical mixture, reduction in surface area and pore volume was observed, but the pore size distribution was similar to that of AC indicating that the drug was not present inside the pores of AC. However, for IBU/AC physical mixture, pore size distribution became broader and the exact reason for this is not clear, however could be due to adsorption of IBU on AC due to hydrophobic interactions.

Table 3-5: Surface areas and pore volumes obtained from Nitrogen sorption of pure activated carbon (AC), ibuprofen loaded activated carbon (IBU/AC complex) and paracetamol loaded activated carbon (PA/AC complex)

Sample	Specific surface area[a] (m²/g)	Total pore volume [b] (cm³/g)	Micropore volume [b] (cm³/g)
AC-untreated	1027.4	0.81	0.33
AC-Post treatment	994.6	0.77	0.32
PA/AC complex	127	0.31	0.016
IBU/AC complex	101.8	0.23	0.014
PA/AC phy mix	673.5	0.57	0.21
IBU/AC phy mix	30.9	0.17	0

[a] Calculated by BET method
[b] Calculated by NLDFT method
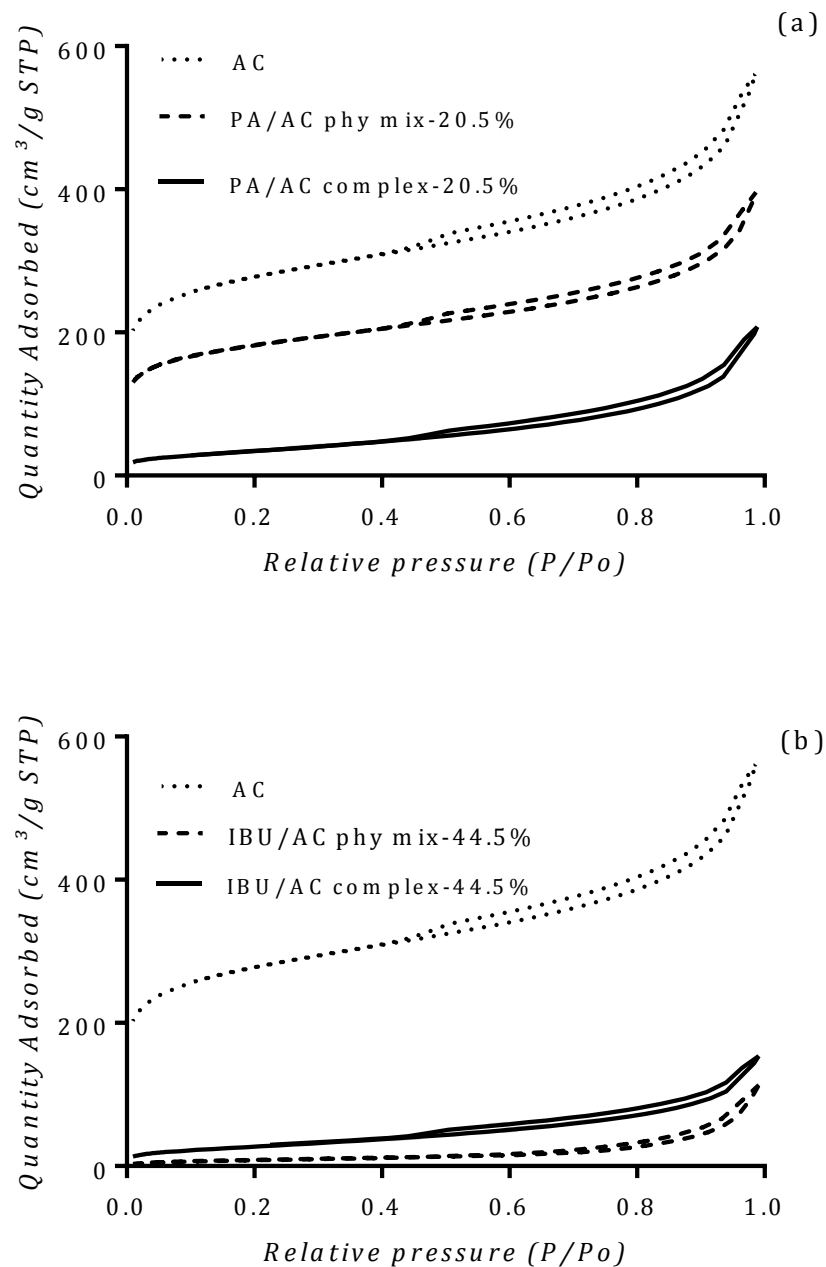
Figure 3-15: Nitrogen adsorption/desorption isotherms at 77 K of activated carbon (AC) before and after drug loading showing, (a) paracetamol loaded activated carbon (PA/AC complex) and physical mixture of paracetamol and activated carbon (PA/AC phy mix); (b) ibuprofen-loaded activated carbon (IBU/AC complex) and physical mixture of ibuprofen and activated carbon (IBU/AC phy mix).

Figure 3-16: (a) Nitrogen adsorption/desorption isotherms at 77 K (b) Pore size distribution (2-14nm) calculated using NLDFT slit-shaped pore model, of pure activated carbon (AC), ibuprofen-loaded activated carbon (IBU/AC complex) and paracetamol loaded activated carbon (PA/AC complex).

3.3. Conclusion

The potential for activated carbon as an amorphous drug carrier was investigated, using paracetamol and ibuprofen as model drugs. Solution adsorption is the most commonly used method for drug loading into a porous carrier. Hence, drug loaded AC (drug/AC) complex was prepared by solution adsorption where AC was immersed in saturated drug solution at 20C and stirred for 24 hours. UV analysis revealed that drug loading of 20.7 ± 1 and 44.4 ± 4 % (*w/w)* was achieved for PA and IBU, respectively. Higher loading of IBU is attributed to the higher concentration of IBU in the loading solution, indicating the effect of concentration in the loading solution on the loading efficiency. Solid-state analysis showed that PA present in the PA/AC complex was completely amorphous, whereas 19% of the IBU in IBU/AC complex was found to be crystalline. FTIR studies could not detect any drug in PA/AC complex, which could be due to the absence of surface adsorbed drug in PA/AC complex, since the depth of penetration is < 5 µm and drug deposited in the deeper pores could not be detected. Whereas, FTIR was able to detect IBU in IBU/AC complex, which could be attributed to the higher loading and presence of surface adsorbed drug or crystalline drug particles. However, no chemical interactions could be detected between IBU and AC, confirming physical adsorption. The higher loading of IBU and presence of crystallinity in the IBU/AC complex indicated that using saturated drug solution for drug loading is not applicable to all drugs, and optimum concentration of drug in the loading solution needs to be determined for every drug due to the difference in the solubility and chemical characteristics of the drug. Therefore, optimisation of drug loading method is necessary and will be discussed in chapter 4.

In vitro release studies were performed in phosphate buffer with and without the addition of 1% sodium lauryl sulphate. All the powder samples were loaded into gelatin capsules to eliminate powders floating on the surface of the dissolution media. Drug release was

complete within 20 min (in the presence of 1% SDS) for both PA/AC complex and IBU/AC complex and exhibited faster initial release compared to the pure drug, which could be attributed to the presence of amorphous drug and a higher surface that is in contact with the dissolution media. The release rate of both PA/AC and IBU/AC complexes was found to be diffusion controlled with an initial burst followed by slow release and the rate constant was dependant on the characteristics of the drug. Also, IBU release from the complex was found to be independent of pH of the dissolution medium which could be due to the higher influence of properties of the carrier; however, further studies are needed to confirm this effect and will be discussed in chapter-5. Cytotoxicity studies revealed that Caco-2 cells incubated with media containing 800 µg/mL of activated carbon (particle size of 0.45- 87.5µm) showed cell survival rate above 80%, suggesting the low toxicity of these particles. The low toxicity, high drug loading capacity and ability to stabilise amorphous drug supports the potential of activated carbon as an amorphous drug carrier.

Chapter 4 -**Towards development of activated carbon as a drug carrier: optimisation of drug loading method**

4.1. Introduction

Drug loading into porous carriers has shown to improve the dissolution rate of the drug, since the loaded drug is shown to exhibit an amorphous nature. However, the loading method and loading parameters can affect the diffusion of the drug into the pores of the carrier, thereby affecting the loading efficiency, solid state characteristics and drug release kinetics (Ahern et al. 2013); therefore, it is important to investigate the influence of loading factors on the performance of activated carbon (AC) as a drug carrier.

Solution impregnation (solution adsorption) and solvent evaporation are the most commonly used drug loading methods, due to their simplicity and relatively low cost (Lai et al. 2017; Preisig et al. 2014). Solution impregnation involves immersion of the carrier in a saturated drug solution to allow the drug molecules to diffuse into the pores of the carrier, whereby the drug-loaded carrier particles are then collected by filtration or centrifugation. Solvent evaporation involves the addition of a carrier to a drug solution and evaporation of the solvent by rotary evaporation to obtain drug-loaded carrier particles. In this study, loading methods will be compared to understand the subsequent impact on the properties of drug/AC complex.

In addition to the loading method, initial drug concentration can also affect the drug loading efficiency and solid state characteristics of the loaded drug (Kinnari et al. 2011). High concentrations of drug in the loading solution acts as the driving force for the diffusion of the drug into the pores of the carrier, therefore a high concentration of the drug is required to achieve maximum drug loading (Lai et al. 2017). However, a high concentration of drug in the loading solution can also lead to crystallisation on the surface of the carrier particles or as separate crystals. Indeed, as seen in the previous chapter, it was shown that paracetamol (PA) loaded into AC was completely amorphous, with a

loading efficiency of 20.7%, whereas ibuprofen (IBU) loaded AC was found to contain 19% crystallinity, with a loading efficiency of 44.4%. Therefore, in order to obtain PA/AC complex with higher loading and IBU/AC complex without crystallinity, the optimum concentration of drug in the loading solution needs to be determined. In addition, these results can also demonstrate how the nature of the drug itself may further impact on loading efficiency and solid state characteristics since chemical nature of the drug affects the drug-carrier interactions thereby affecting the drug loading process.

Also, loading parameters such as contact time, temperature, and carrier dose can also have an effect on the loading efficiency and investigating the effects of these factors is essential for design and operation of experiments for drug loading into activated carbon (Lai et al. 2017; Yi et al. 2016).

4.2. Aims and objectives

The aim of this current chapter is to investigate the effects of loading parameters, namely loading method, contact time, loading temperature, and carrier dose on drug loading and release. To achieve this, the main objectives of this study were to:

1) Compare the characteristics of the loaded drug in the drug/carrier complexes obtained using three different solvent based loading methods.

2) Investigate the effects of contact time, temperature and carrier dose on loading efficiency.

3) Determine the optimum initial drug concentration in the loading solution to achieve drug loading without any crystallinity.

4) Identify the interactions between drug and carrier in complexes with different loadings.

4.3. Results and Discussion

4.3.1. Effect of drug loading method on loading efficiency and solid state characteristics

In the previous chapter, solution adsorption followed by centrifugation (SA-C) was used to prepare drug/carrier complex to investigate the potential of AC as a porous carrier. In this study, to understand the effect of loading method on loading efficiency and solid state characteristics, drug/carrier complex was prepared using three different solvent based loading methods namely rotary evaporation (RE), solution adsorption -filtration (SA-F) and solution adsorption -centrifugation (SA-C) as described in section-2.4.2. The quantity of drug in the complex was determined by UV spectroscopy and drug loading efficiency was calculated, as described in section-2.8. Percentage drug crystallinity in the complex was determined by comparing the melting enthalpy with that of a physical mixture containing an equivalent quantity of drug, as described in section-2.9.

Table 4-1: Comparison of loading efficiencies and solid state characteristics of drug/carrier complexes prepared by three different methods (stirring speed: 100 rpm, temperature: 25 ºC; initial PA and IBU concentration: 165 and 970 mg/mL of ethanol respectively; solution volume: 10 mL; AC dose: 1000 mg; contact time: 1 hour).

Method	% Drug loading		Melting enthalpy, J/g (Melting point , °C)		% Crystallinity	
	PA	IBU	PA	IBU	PA	IBU
RE	60.3 ± 1.7	88.5 ± 1.2	45 ± 4 (168)	77 ± 4.2 (74.2)	46.3 ± 4.1	62.1 ± 3.4
SA-F	23.4 ± 5.2	54.5 ± 7.1	9 ± 2 (168)	30.45 ± 3 (69.8)	30 ± 6.7	37.7 ± 3.8
SA-C	18 ± 3.4	48.4 ± 4.7	-	15.23 ± 3.8 (72.3)	-	22.1 ± 5.4

Statistically significant difference was found in the loadings ($p<0.0001$, one-way ANOVA) obtained from three different methods (Table 4-1). Also a post hoc test showed that there was no significant difference ($p>0.5$, one-way ANOVA followed by Tukey's test) in the loading between SA-F and SA-C methods and could be due to the fact that the loading methods are very similar except with the post loading collection process, however, the complex prepared by SA-C method showed lower crystallinity (Figure 4-1 and Figure 4-2) and could be due to slower evaporation of solvent from the sediment obtained after centrifugation, allowing enough time for the surface adsorbed drug to diffuse into the pores of AC. Whereas, in the case of the SA-F method, vacuum filtration could have led to the crystallisation of the drug due to the rapid removal of the solvent.

The drug/AC complex prepared by RE method showed the highest loading (Table 4-1), since this method involves removal of loading solvent by evaporation leaving behind all the drug added. However, the complex obtained from this method also showed the highest amount of crystallinity and is attributed to the rapid evaporation of solvent leading to less contact time for the drug to diffuse into the pores, thereby resulting in the crystallisation of the drug (Runt & Rim 1982).

Also, SA-F exhibited lower crystallinity due to the efficiency of separation of unbound drug by filtration compared to RE which removed the solvent alone by evaporation. With increase in drug loading, % crystallinity was found to increase and could be due to the saturation of the carrier at some point, indicating that increasing the loading above its capacity will lead to crystallisation of the drug.
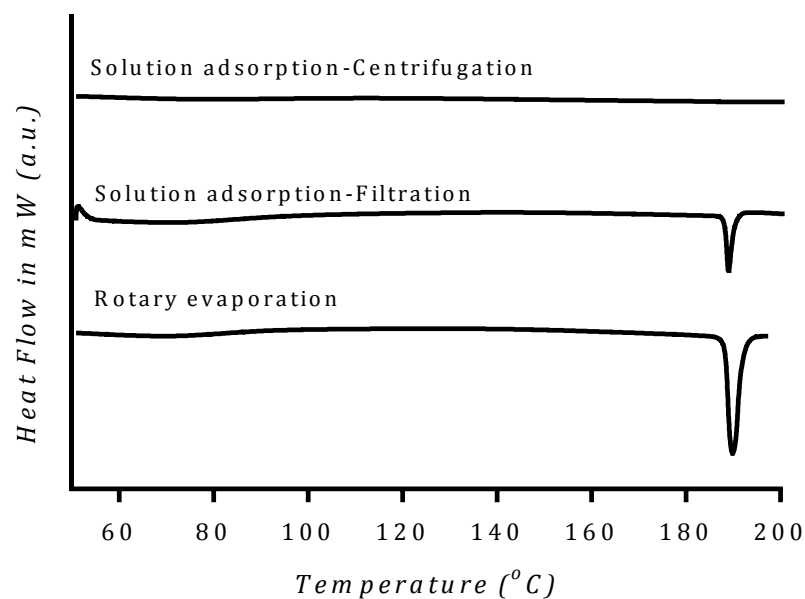
Figure 4-1: DSC curves of paracetamol loaded activated carbon samples (PA/AC complex) prepared by three different methods. No melting peak was found in PA/AC complex prepared by Solution adsorption-Centrifugation method indicating that the drug loaded is completely amorphous. Note that the heat flow scale is arbitrary.
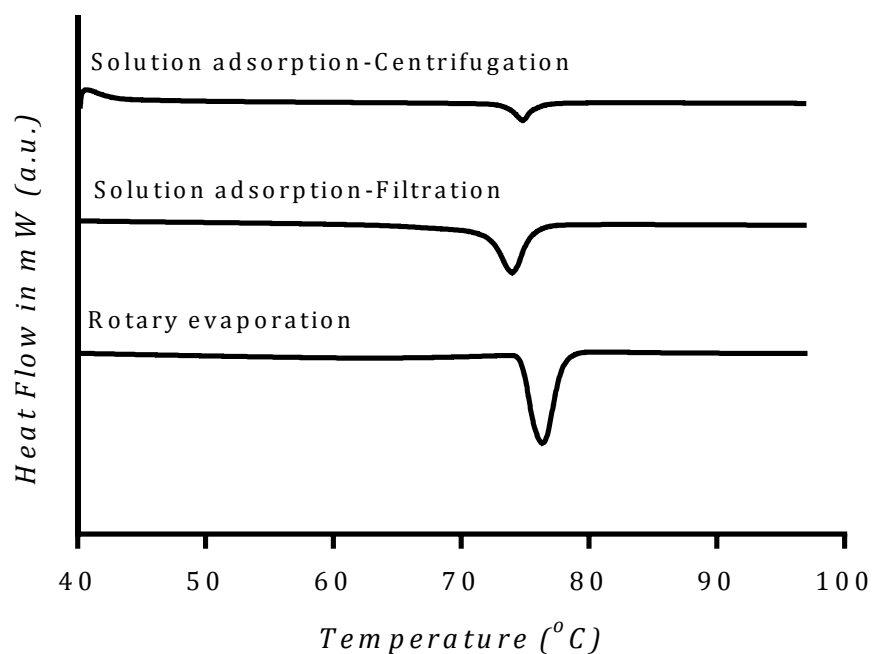
Figure 4-2: DSC curves of ibuprofen-loaded activated carbon samples (IBU/AC complex) prepared by three different methods. Melting peaks were found in the complex obtained from all three methods indicating the presence of crystallinity. Note that the heat flow scale is arbitrary.

112

Also, melting temperatures were found to be different (Figure 4-2) for IBU/AC complexes obtained from different methods, which could be attributed to the difference in the rate of evaporation of ethanol leading to changes in the crystal habit. For e.g. rapid evaporation of solvent leads to formation of cavities during the crystal growth process (Viseras et al. 1995; Zhang et al. 2015; Lee et al. 2007). Also, higher loading in IBU/AC complex compared to PA/AC complex prepared from all three methods could be attributed to the higher concentration of IBU in the loading solution due to its higher maximum solubility in ethanol compared to PA. Although all three methods resulted in crystallisation of drug, the complex prepared by the SA-C method exhibited the least crystallinity, therefore all subsequent loadings were performed using this method.

4.3.2. Investigating the effect of contact time between drug and carrier on the loading efficiency

Diffusion of drug molecules into the pores of the carrier depends on the contact time between the drug and the carrier, therefore allowing enough time for maximum drug loading is crucial (Thomas 1983). To determine the contact time required for maximum loading, drug loading was performed at different stirring times as described in section-2.4.3.

Results from both PA and IBU loading (Figure 4-3) showed a statistically significant difference in the drug loading between complexes obtained at different contact times ($p < 0.05$, one-way ANOVA). A post hoc test showed that loading increased significantly with an increase in contact time up to 4 hours ($p < 0.05$, one way ANOVA followed by Tukey's test) and there was no statistically significant difference ($p > 0.05$, Tukey's multiple comparison test) in the drug loading of complexes obtained at contact time of 4-

24 hours, suggesting that equilibrium was reached at 4 hours. Therefore, all subsequent loadings were performed for 4 hours. Also, a high drug loading (16.4% and 35% for PA and IBU, respectively) was achieved within 1 hour of stirring and could be attributed to the rapid adsorption of the drug due to large concentration gradient and ease of accessibility of adsorption sites in the superficial pores. The contact time required to reach an equilibrium depends on various factors such as porosity of the carrier, solute/adsorbate and solvent and therefore needs to be determined based on the loading conditions (Yi et al. 2016).
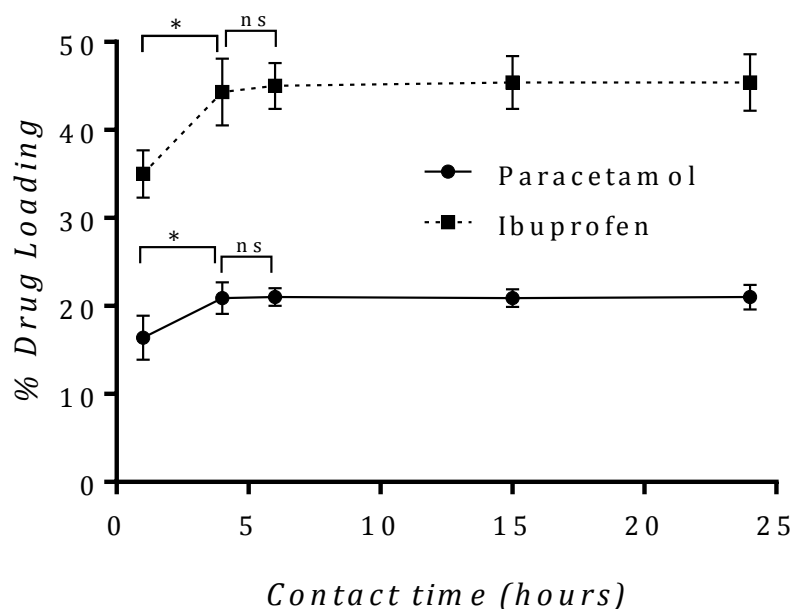
Figure 4-3: Effect of contact time on loading efficiency (stirring speed: 100 rpm; temperature: 20 ℃; initial PA and IBU concentration: 150 and 698 mg/mL of ethanol respectively; solution volume: 10 mL; AC dose: 1000 mg). Results are the mean of triplicate experiments ± SD. Statistically significant differences are noted for $p < 0.05$ (*$p < 0.05$; ns-no significance; one-way ANOVA and Tukey's multiple comparison test).

4.3.3. Effect of Temperature on loading efficiency

Temperature affects the interactions between the drug (solute) and the solvent, thereby affecting the adsorption of the drug by the porous carrier (Garzón et al. 2004). Therefore,

to understand the effect of temperature on drug loading, drug loading was performed at four different temperatures as described in section-2.4.4.

With the increase in temperature, a statistically significant difference was found in the drug loading ($p < 0.05$, one-way ANOVA), suggesting that drug loading was temperature dependent. Loading efficiency decreased with increase in the temperature (Figure 4-4) and is similar to the results obtained from previous research. Reduction of drug loading at higher temperatures is due to reduced adsorption of molecules that tend to stay in the solution due to higher energy. Also, the decrease in the loading was found to be higher in the case of IBU than PA, suggesting that the influence of chemical characteristics of the drug due to drug-solvent interactions (Chen et al. 2011; Yi et al. 2016).
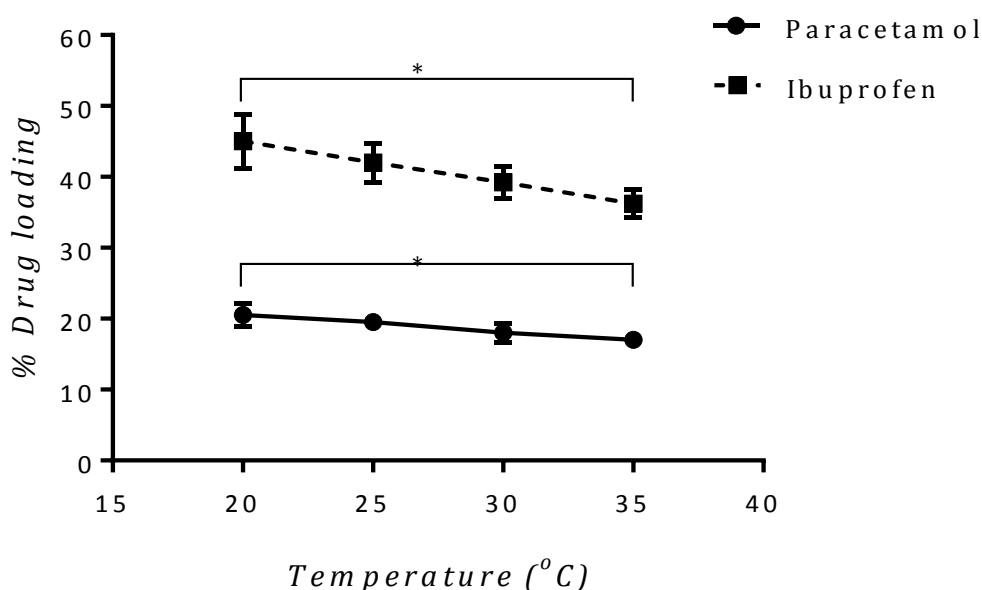
Figure 4-4: Effect of temperature on loading efficiency (stirring speed: 100 rpm; initial PA and IBU concentration: 150 and 698 mg/mL of ethanol respectively; contact time: 4 hours; solution volume: 10 mL; AC dose: 1000 mg). Results are the mean of triplicate experiments ± SD. Statistically significant differences are noted for $p < 0.05$ (*$p < 0.05$, one-way ANOVA and Tukey's multiple comparison test).

4.3.4. Investigating the effect of initial drug concentration in the loading solution on loading efficiency and solid state characteristics

To determine the effect of concentration of drug in the loading solution on the loading efficiency, drug loadings were performed by SA-C method using four different drug concentrations as described in section-2.4.5. UV results indicated that, with the increase in the drug concentration, a statistically significant difference was found in the drug loading ($p < 0.01$, one-way ANOVA). Drug loading reached a maximum when the drug concentration in the loading solution reached the saturation point (Figure 4-5), indicating that drug loading increases with increase in the initial concentration of drug in the loading solution. However previous research found that high drug loading achieved was associated with high amounts of crystallinity indicating the disadvantages of using high initial drug concentration for loading (Lai et al. 2017).

Solid state analysis was performed on drug/carrier complex with different loadings and lower drug loading was found to be advantageous in the case of IBU/AC complex, since thermal studies revealed that crystallinity decreased with a decrease in the drug loading (Table 4-2), whereby IBU/AC complex with a loading of 30.2% was completely amorphous. These results indicate that IBU/AC complex with complete amorphous drug loading could be achieved when the initial drug concentration in the loading solution was 350 mg/mL. These results might also suggest that the maximum IBU loading that could be achieved without any crystallinity is less than 34.6%, since crystallinity was found in the IBU/AC complex with a loading $\geq$ 34.6 %, which is slightly less than the maximum IBU loading (39%) estimated from the previous chapter.
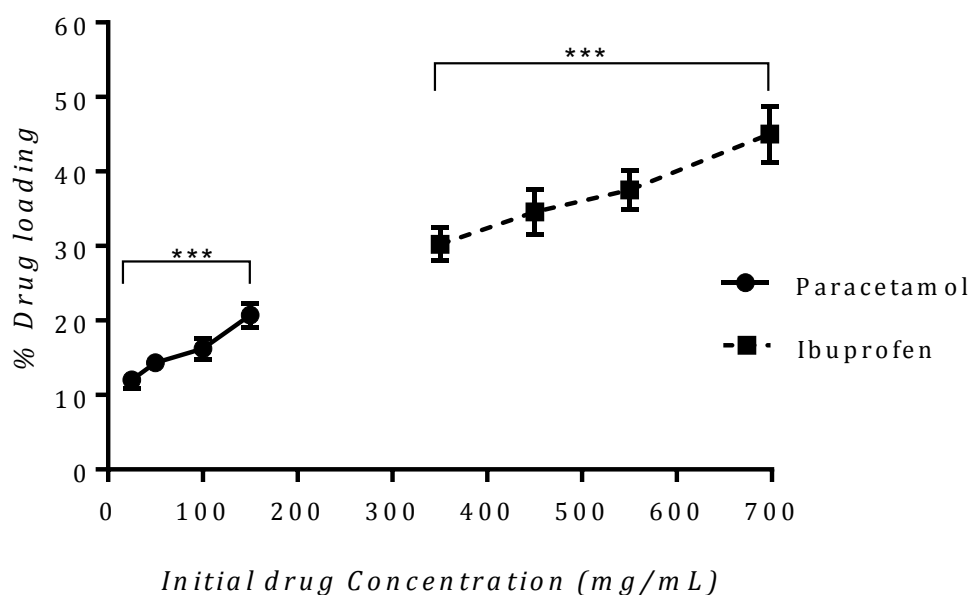
Figure 4-5: Effect of initial drug concentration on loading efficiency (stirring speed: 100 rpm; temperature: 20 °C; solution volume: 10 mL; AC dose: 1000 mg; contact time: 4 hours). Results are the mean of triplicate experiments ± SD. Statistically significant differences are noted for $p < 0.05$ (*** $p < 0.001$, one-way ANOVA and Tukey's multiple comparison test).

Table 4-2: Effect of initial drug concentration on loading efficiency and solid state characteristics of IBU/AC complexes (stirring speed: 100 rpm; temperature: 20 °C; solution volume: 10 mL; AC dose: 1000 mg; contact time: 4 hours).

Initial drug concentration (mg/mL of ethanol)	% Drug loading	% Crystallinity
350	30.2 ± 2.2	-
450	34.6 ± 3	6 ± 1.5
550	37.5 ± 2.6	10 ± 3.4
698 (saturation point)	45 ± 3.7	19 ± 2.8

No crystallinity was found in the case of PA/AC complex obtained at all four drug concentrations, with the highest drug loading achieved being 20.7%, when the initial drug concentration used was 150 mg/mL, indicating that higher loading could be achieved if the initial PA concertation in the loading solution is further increased; however, this is the maximum concentration (150 mg/mL) that could be achieved at 20 °C. Therefore,

saturated PA solutions at four different temperatures were used for loading as described in section-2.4.6, to determine the maximum PA loading that could be achieved without any crystallisation.

Results indicated that PA loading increased with an increase in the initial drug concentration (Table 4-3), reaching a maximum of 26.8% when the initial PA concentration in the loading solution was 199 mg/mL at 35 ºC. Also, it has to be noted that this higher temperature could have reduced the drug loading since drug loading decreased with increase in the temperature in the previous study and the true loading at a concentration of 199mg/mL could have been higher than 26.8% if a lower temperature (25 ºC) was used; however, it is not possible to reduce the temperature since this will result in reduced solubility of the drug.

Further, PA was found to be loaded in a completely amorphous state in all the samples, indicating that drug loading higher than 26.8% could be achieved without leading to crystallisation of drug. Therefore, loading of at least 26.8% for PA and 30.2% for IBU could be achieved without any crystallisation, when an initial drug concentration of 199 mg/mL and 350 mg/mL was used for loading PA and IBU, respectively. The difference in the optimum required concentration between PA and IBU could be attributed to the higher melting point of PA compared to IBU since drugs with higher melting point readily undergo crystallisation (Brent 2015).

Table 4-3: Effect of initial drug concentration on loading efficiency (stirring speed: 100 rpm; solution volume: 10 mL; AC dose: 1000 mg; contact time: 4 hours).

Temperature (ºC)	Drug concentration (mg/mL of ethanol)	% Drug loading
20	150	20.7 ± 1
25	165	22 ± 1.8
30	183	24.6 ± 2
35	199	26.8 ± 2

4.3.4.1. Effect of loading efficiency on the interactions between drug and carrier

To understand the effect of loading efficiency on drug-carrier interactions, FTIR spectroscopy was used to study drug/carrier complexes. FTIR spectrum of drug/AC complex with different loadings were compared with that of pure drug (Figure 4-6 and Figure 4-7).

FTIR spectra of PA/AC complex with 26.8% drug loading showed a peak at 3310 cm^{-1}, a broad peak at 3200 cm^{-1}, and a sharp peak at 1645 cm^{-1}, corresponding to secondary amide N-H stretching, phenol O-H stretching, and carbonyl C=O stretching, respectively, similar to that of pure PA. In the case of PA/AC complex with 24.6% loading, peaks corresponding to N-H and O-H stretching could not be identified, although the peak corresponding C=O stretching could be observed. There could be three reasons for this: (1) Lower intensity of N-H and O-H peaks compared to C=O peak; (2) the presence of the drug in the deeper pores in the complex. The depth of penetration of IR increases with a decrease in the wavenumber, therefore, drug located in the deeper pores could be identified better at lower wavenumbers (Oelichmann 1989; Kazarian & Chan 2013); (3) Lower drug loading leading to reduced intensity of the peaks, since no FTIR peaks could be identified in the PA/AC complex with a drug loading of 20.7% (section 3.4.4).

Both IBU/AC complexes with loading 30.2% and 44.4% showed a sharp peak, corresponding to carboxylic acid (C=O) stretching at 1710 cm^{-1}, and characteristic three peaks between 2960-2860cm^{-1}, corresponding to C-H stretching, similar to that of pure IBU (Lai et al. 2017). However, the intensity of the peaks was found to decrease with a decrease in the drug loading.

Nevertheless, spectra of drug/AC complex was found to be similar to that of pure drug in both PA and IBU. No significant shift in the position of existing peaks was found and no new peaks were found, indicating the absence of any chemical bonding between functional groups and AC since chemisorption can result in drug potency in some cases and can also lead to irreversible drug adsorption or slower drug release which can be disadvantageous when immediate release is preferred (Guo et al. 2013; Choudhari et al. 2014). Also, the presence or absence of peaks in the FTIR spectra doesn't seem to indicate the presence of crystalline drug on the surface of AC, since peaks could be seen in the FTIR spectra of PA/AC complexes with no crystallinity.
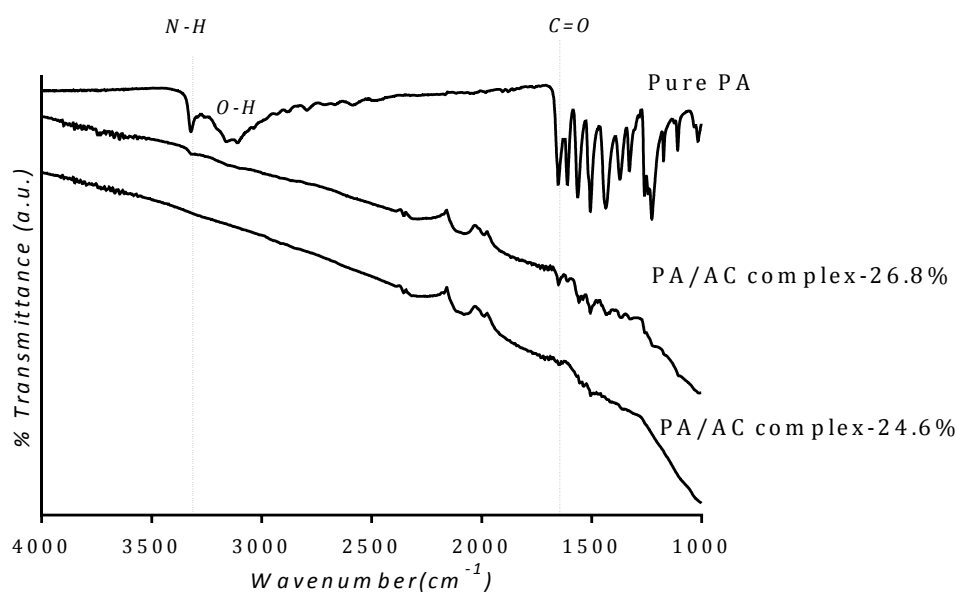
Figure 4-6: FTIR spectra of paracetamol (PA), paracetamol-loaded activated carbon (PA/AC complex) with different loadings, showing peaks corresponding to amide, phenol and carbonyl groups of PA. No chemical interactions could be detected between PA and AC. Note that the transmittance scale is arbitrary.
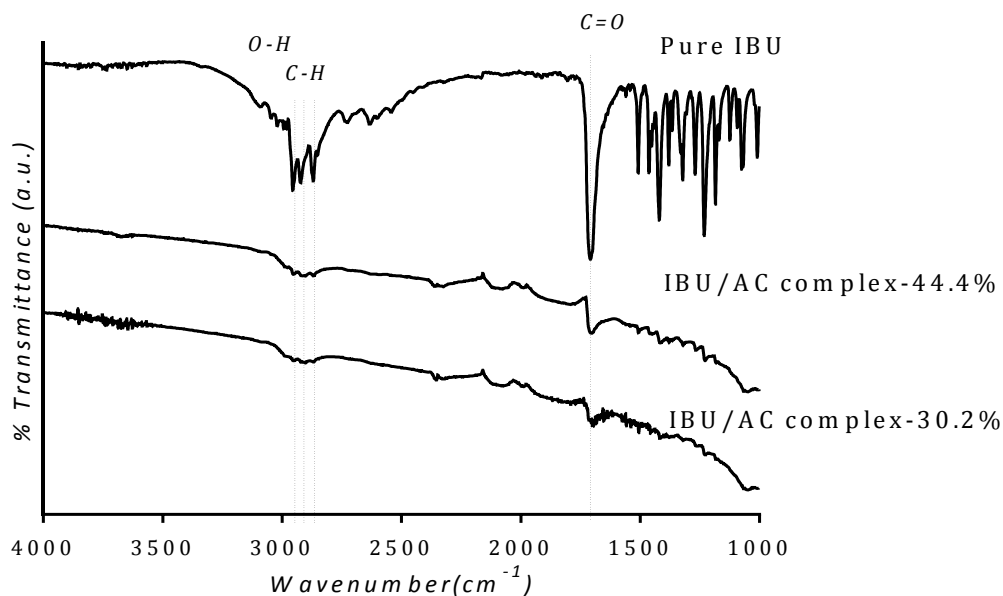
Figure 4-7: FTIR spectra of ibuprofen (IBU), ibuprofen-loaded activated carbon (IBU/AC complex) with different loadings, showing peaks corresponding to methyl and carboxylic acid groups of IBU. No chemical interactions could be detected between IBU and AC. Note that the transmittance scale is arbitrary.

4.3.5. Effect of carrier dose on loading efficiency

Previous studies suggest that the quantity of carrier can affect the drug loading, thereby affecting the release rate (Lai et al. 2017). Therefore, to investigate the effect of quantity of carrier on drug loading efficiency, drug loading was performed using varying amounts of carrier as described in section-2.4.7.

Drug loading results (Figure 4-8 and Figure 4-9) showed a statistically significant difference in the total quantity of drug loaded ($p < 0.001$, one-way ANOVA) and loading efficiency ($p < 0.05$, one-way ANOVA) between complexes prepared using different carrier doses. A post hoc test showed that total quantity of drug loaded increased significantly for PA ($p < 0.01$, Tukey's multiple comparison test) and IBU ($p < 0.05$, Tukey's multiple comparison test) with an increase in the carrier dose from 500 to 1000 mg (per 10 mL drug solution); however, no significant difference ($p > 0.05$, Tukey's

121

multiple comparison test) was found when the carrier dose was increased from 1000 to 1500 mg (per 10 mL drug solution) for both PA and IBU.

Although the total amount of drug loaded increased, loading efficiency decreased significantly ($p<0.001$, one way ANOVA) due to an increase in the quantity of the carrier in complex and was in agreement with previous reports (Lai et al. 2017). Also it can be suggested that the drug loading results were influenced by the quantity of the carrier alone, since the initial drug concentration was kept constant (no changes in the drug-solvent interactions).
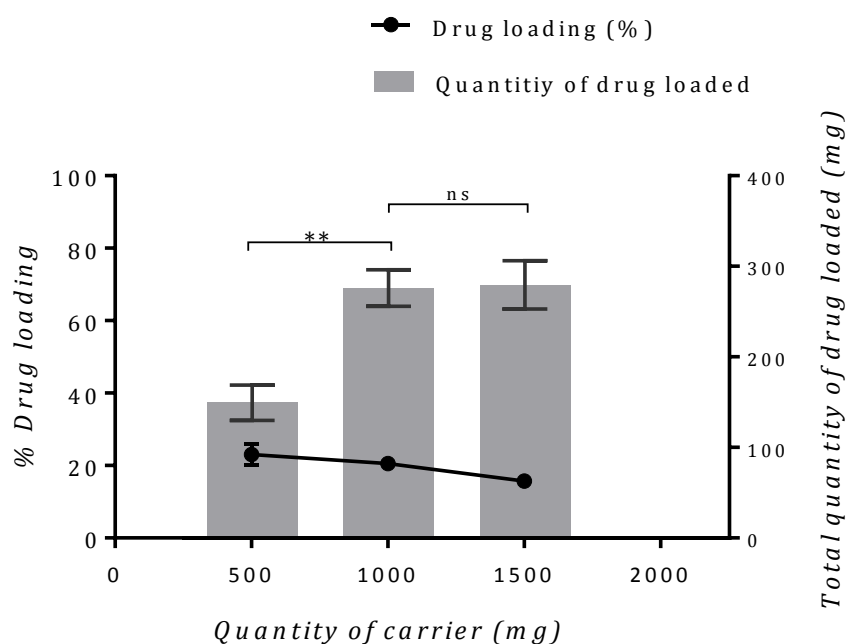
Figure 4-8: Effect of carrier quantity on PA loading efficiency (stirring speed: 100 rpm; initial PA concentration: 150 mg/mL of ethanol respectively; contact time: 4 hours; solution volume: 10 mL; temperature: 20 °C). Results are the mean of triplicate experiments ± SD. Statistically significant differences are noted for $p < 0.05$ (** $p < 0.01$; one-way ANOVA and Tukey's multiple comparison test).
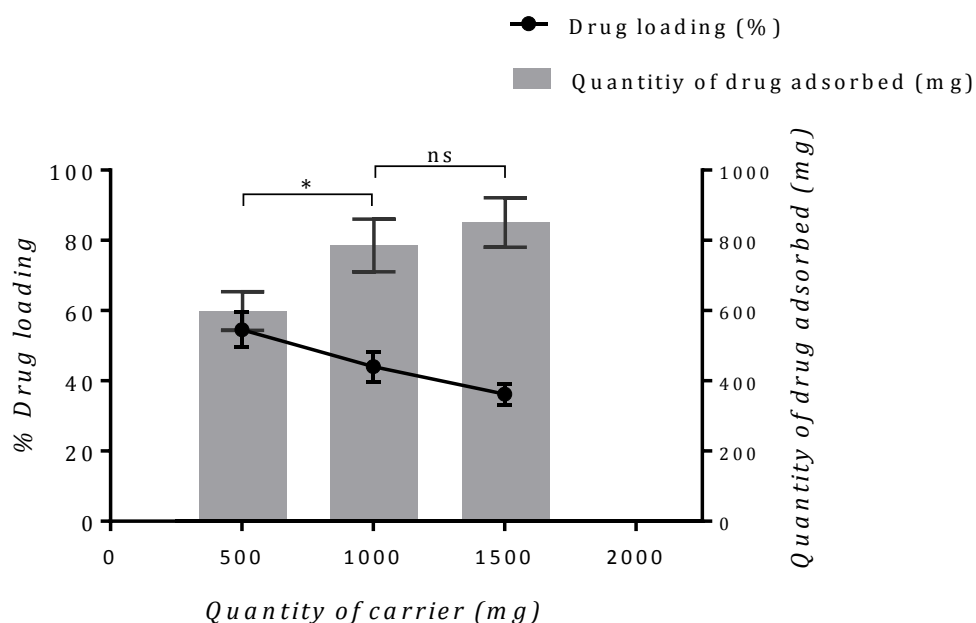
Figure 4-9: Effect of carrier quantity on IBU loading efficiency (stirring speed: 100 rpm; initial IBU concentration: 698 mg/mL of ethanol respectively; contact time: 4 hours; solution volume: 10 mL; temperature: 20 ℃). Results are the mean of triplicate experiments ± SD. Statistically significant differences are noted for $p < 0.05$ (*$p < 0.05$; one-way ANOVA and Tukey's multiple comparison test).

4.4. Conclusions

The work in this chapter showed that the loading efficiency and solid state characteristics of the drug loaded into activated carbon are influenced by a range of factors, such as the loading method, the concentration of drug in the loading solution, temperature, contact time and carrier dose. Three different loading methods were compared and it was found that high drug loading could be achieved with solvent evaporation, although this method also showed a very high drug crystallinity (46.3% for PA and 62.1% for IBU). Complexes prepared by solution adsorption-centrifugation method showed the lowest crystallinity and was used for all subsequent drug loadings. Initial drug concentration was also found to affect solid state characteristics, with results indicating that drug/carrier complex without any crystallinity could be achieved by adjusting the drug concentration in the

loading solution; the optimum concentration to achieve a complex without crystalline drug was found to be 199 mg/mL and 350 mg/mL for PA and IBU, respectively, and the loading achieved was 26.8% for PA and 30.2 % for IBU. Also, no chemical interactions could be detected between the drug and the carrier even at higher drug loading, supporting the physical adsorption of the drug.

Drug loading into activated carbon was found to reach an equilibrium in 4 hours, indicating that stirring time of 4 hours would be sufficient to achieve maximum loading. Also, drug loading decreased with increase in the temperature and could be due to increase in drug-solvent interactions at a higher temperature. Drug loading was found to increase with an increase in the quantity of AC up to 1000 mg per 10 mL of drug solution, after which no significant increase in drug loading could be seen. Overall, these studies have demonstrated that successful optimisation of drug loading into activated carbon must consider several factors to achieve maximum loading without any crystallisation.

Chapter 5 -**Effect of surface chemistry and porosity of activated carbon on drug loading and release**

5.1. Introduction

When employing a porous carrier, such as activated carbon, in the realm of drug delivery, the key properties of surface chemistry and porosity are important characteristics, since, amongst other aspects, they may affect the drug loading and release profiles (Lai et al. 2017; Limnell et al. 2007). Results from previous chapters have shown the potential of activated carbon as a drug carrier with a high drug loading capacity and with an ability to inhibit crystallisation of loaded drug; however, complete drug release could not be achieved in the absence of SDS and was attributed to the poor wettability of AC, leading to inaccessibility of the dissolution medium to the deeper micropores. Activated carbon is generally hydrophobic and has poor wettability, due to its preparation method involving high-temperature treatment, resulting in the loss of functional groups (Liu et al. 2008). However, several oxygen-containing groups, such as phenol, carboxyl, and lactone, might still be present in low quantities at the edges of the micropores, due to the presence of free valence carbon atoms at these sites. The quantity of such oxygen-containing groups on the surface can affect the polarity of AC, thereby affecting interaction with water (Ahnert H. A.; Pinto, N. G. 2009). Oxygen groups on the surface of AC can interact with water molecules through hydrogen bonding, thereby increasing the hydrophilicity of AC, which, in turn, may affect the drug loading and release (Hayati & Mahmoodi 2012; Yin et al. 2007). Several modification techniques, such as acidic treatment, basic treatment, heat treatment and impregnation with surfactants have been studied previously to increase oxygen-containing groups on AC surface (Table 5-1). However, such modifications also resulted in some disadvantages, such as reduction in surface area, reduction in adsorption capacity and release of SO_2 or NO_2 gases (Yin et al. 2007; Ahnert H. A.; Pinto, N. G. 2009; Li et al. 2002).

Table 5-1: Types of treatments used for modification of surface chemistry of carbon based materials

Treatment	Effect on surface chemistry and porosity of carbon based materials	Reference
Boiled in HNO_3 (5N) solution for 10 hours under a reflux.	Total acidic groups of AC increased by 6 times and BET surface area decreased from 604 m^2/g to 399 m^2/g.	(Jaramillo et al. 2010)
Treated with H_2SO_4/HNO_3 (3:1) at room temperature for 3 hours.	The increase in the carboxylic and hydroxyl groups in carbon nanotubes.	(Li et al. 2005)
Immersed in HNO_3/H_2SO_4 mixture at 100 ºC under N_2 atmosphere for 24 hours.	Hydroxyl and epoxy groups increased from 1.58 to 10.08% in graphite.	(Shin et al. 2013)
Boiled in HNO_3 (4M) solution for 1 hour.	Total acidic groups of AC (mmol/g) increased by 22.8 times and total basic groups (mmol/g) decreased by 4.6 times.	(Ahnert H. A.; Pinto, N. G. 2009)
Heated with conc H_2SO_4 for 3 hours at 80 ºC.	Total acidic groups of AC (mmol/g) increased by 2.2 times and BET surface area increased from 991 to 1113 m^2/g.	(Terzyk & Rychlicki 2000)
Treated with HNO_3 (6N) solution for 5 hours at room temperature	BET surface of AC decreased from 1136 to 1088 m^2/g and carboxyl groups increased from 2 to 29 mmol/100g.	(Li et al. 2003)
Treated with 1-5 N NaOH for 24 hours at room temperature	The total surface oxygen-containing groups of AC (meq/g) increased by 1.86 times when treated with 2N and 4N NaOH.	(Chiang et al. 2002)
Treated with 35% NaOH solution for 24 hours	BET surface area in AC decreased from 1013 to 807 m_2/g and base value increased from 173 to 420 meq/g.	(Park & Jang 2002)

In addition to surface chemistry, the porosity of the carrier might also affect drug loading and release. Carriers with smaller pore size and longer pore channel were found to exhibit slower drug release (Zhang et al. 2010; Horcajada et al. 2004), indicating that carriers with a high fraction of micro porosity and large particle size could be disadvantageous in achieving faster release.

5.2. Aim and objectives

The aim of this current chapter, therefore, is to investigate the effects of carrier characteristics, namely surface chemistry and porosity, on drug loading and release. To achieve this, the main objectives of this study were to:

1. Modify the surface chemistry of AC (G60 type) by three different surface treatment methods.
2. Investigate the surface chemistry and porosity of surface treated AC, using XPS, FTIR, and nitrogen sorption techniques.
3. Evaluate the effect of surface treatment of AC on drug loading and release.
4. Evaluate the effect of porosity on drug loading and release using four different types of AC.

5.3. Results and Discussion

5.3.1 Effect of surface chemistry of activated carbon on drug loading and release

To consider the effects of the surface chemistry of the carrier on drug loading and release, AC was treated to modify its surface chemistry with HNO_3, NaOH and a mixture of H_2SO_4/HNO_3 separately, as described in section 2.7. The treated ACs were referred to as AC- HNO_3 and AC-NaOH, respectively. Treatment with strong acids, such as nitric acid, is the most commonly used method to incorporate oxygen groups, where the extent of oxidation was found to depend on the concentration and temperature of the oxidant (Jaramillo et al. 2010). Furthermore, nitric acid in the presence of sulphuric acid is a stronger oxidant and can penetrate the deeper layers of carbon structure, potentially enabling more extensive oxidation of the carrier surfaces (Shin et al. 2013). Basic treatment has also been employed to modify the surface chemistry of AC and was found to improve the adsorption of organic compounds; during treatment with NaOH, hydroxyl ions might react with the surface functional groups of AC, resulting in an increase in the number of lactone, carboxylic and phenolic functional groups (Chiang et al. 2002).

5.3.1.1. Characterisation of surface chemistry of modified activated carbon

The surface chemistry of AC before and after surface treatment was examined using XPS analysis. XPS spectra of all samples (Figure 5-1) showed two peaks corresponding to carbon (C 1s) and oxygen (O 1s), marked at 284 eV and 532 eV, respectively, while spectra of $AC-H_2SO_4/HNO_3$ and $AC-HNO_3$ showed an additional peak corresponding to nitrogen (N 1s), marked at 400 eV. Peaks corresponding to tin (Sn 2p) and silver (Ag 3d), marked at 495 eV and 377 eV, respectively (Daniel et al. 2013), were also found in AC-H_2SO_4/HNO_3 could have originated from the internal structure of AC as a result of

opening of some pores during treatment with the mixture of H_2SO_4 and HNO_3 or could be from contamination during analysis (Terzyk 2001).

Relative atomic contents (Table 5-2) were calculated from the peak areas and results indicated that, post treatment, the atomic percentage of carbon decreased while the atomic percentage of nitrogen and oxygen increased, indicating the increase in the number of oxygen containing groups. AC treated with a mixture of H_2SO_4 and HNO_3 exhibited the highest percentage of surface oxygen content compared to HNO_3 and NaOH treatments and could be due to the stronger oxidising nature of nitric acid in the presence of sulphuric acid (Shin et al. 2013).

Table 5-2: The relative atomic contents of carbon, oxygen, and nitrogen of activated carbon before and after surface treatment determined from XPS analysis.

Sample	Relative atomic contents		
	C (%)	O (%)	N (%)
AC	95.69	4.31	--
AC-NaOH	93.96	6.04	--
AC- HNO_3	91.09	8.16	0.75
AC-H_2SO_4/HNO_3	70.17	27.78	2.06
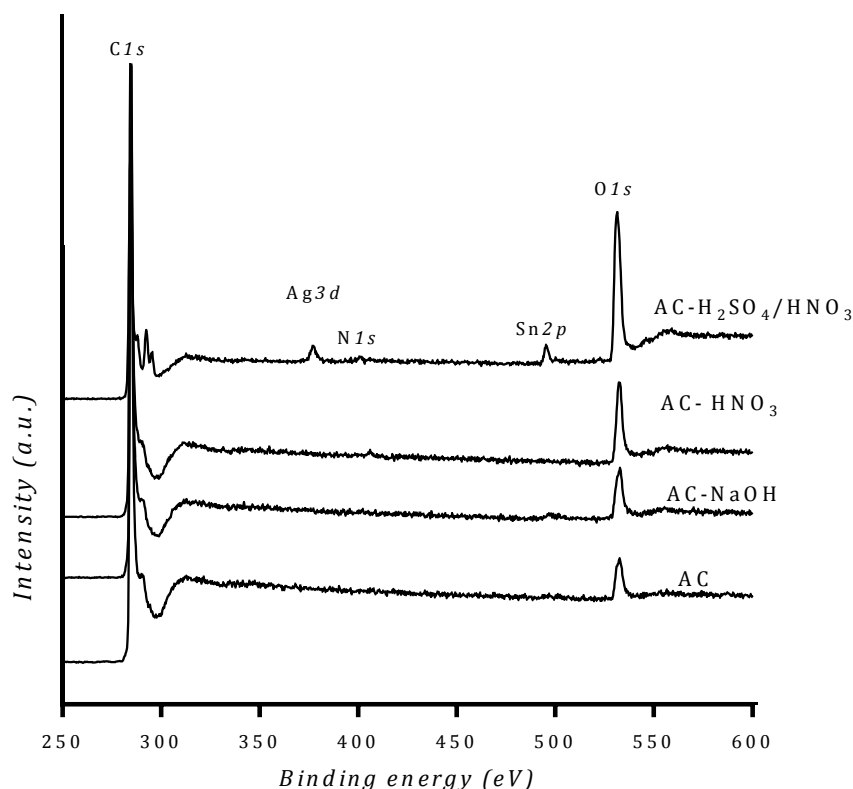
Figure 5-1: XPS spectra of pristine activated carbon (AC) and surface treated activated carbon (AC- HNO₃, AC- NaOH, and AC- H₂SO₄/HNO₃). The major peaks are marked for Carbon (C 1s), Nitrogen (N 1s) and Oxygen (O 1s) present on the surface. Note that the intensity scale is arbitrary.

FTIR was employed to further confirm the presence of surface oxygen groups and to identify the types of functional groups present on the surface of treated AC. No significant difference was found in the FTIR spectra of AC, AC-NaOH, and AC-HNO₃, since there was only a slight increase in the oxygen content post treatment (Table 5-2). However, AC-H₂SO₄/HNO₃ exhibited a broad band between 2600 and 3500 cm^{-1}, which can be attributed to O-H stretch, and a strong absorption band at 1717 cm^{-1}, which can be assigned to C=O groups, indicating the presence of carboxylic acid groups. The peak at 1560 cm^{-1} is attributed to carboxylate anion stretch mode (Atieh et al. 2010; Rios et al. 2003). FTIR studies suggested that AC treated with a mixture of H₂SO₄ and HNO₃ is an

131

effective method to incorporate oxygen groups compared to treating with NaOH or HNO$_3$ supporting the results from XPS.
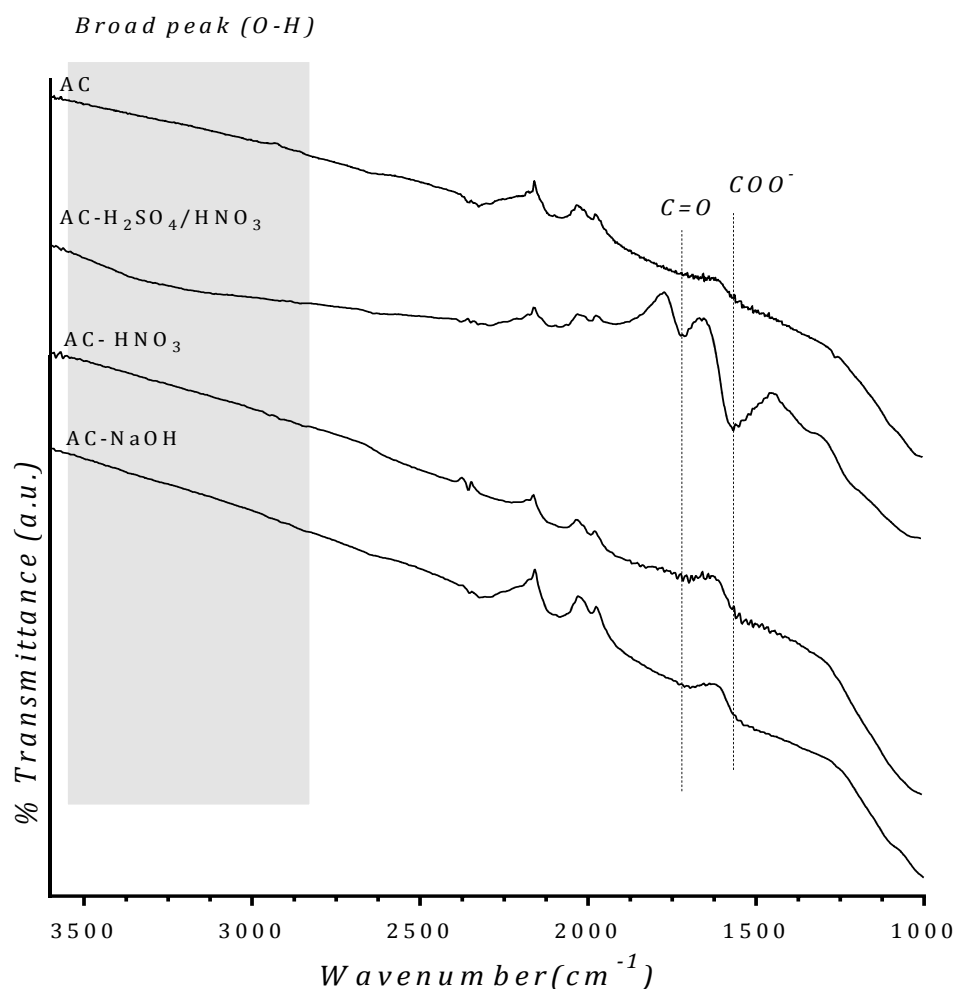
Figure 5-2: FTIR analysis of pristine activated carbon (AC) and surface treated activated carbon. AC treated with a mixture of H$_2$SO$_4$ and HNO$_3$ (AC-H$_2$SO$_4$/HNO$_3$) exhibited peaks corresponding to carboxylic acid groups. Note that the transmittance scale is arbitrary.

5.3.1.2. Characterisation of porosity of modified activated carbon

The porosity of AC before and after surface treatment was studied using nitrogen sorption analysis. The adsorption/desorption isotherms (Figure 5-3) of AC- HNO$_3$ and AC- NaOH was found to be very similar to that of pristine AC, indicating that there was no significant change in the porosity due to surface treatment with HNO$_3$ and NaOH; however, a significant reduction in the absorption was found in the adsorption/desorption isotherm

132

of AC-H_2SO_4/HNO_3, indicating a reduction in the porosity due to treatment with mixture of H_2SO_4 and HNO_3 solution. Similar results were found in previous reports where the porosity reduced by 34% (Bhatnagar et al. 2013) and could be due to the penetration of acid through breaking of the graphitic layers (Shin et al. 2013).

Specific surface area and pore volume were determined using BET and NLDFT theory and revealed that surface area and pore volume were reduced by 5.3 and 6.2 times, respectively, in AC-treated with AC-H_2SO_4/HNO_3 (Table 5-3). Nevertheless, although pore volume reduced significantly for AC-H_2SO_4/HNO_3, the pore size distribution was found to be similar to that of pristine AC indicating that reduction in the surface area and pore volume is due to the destruction of significant amount of pores and not due to the narrowing of pores by surface oxygen groups. Conversely, for AC-HNO_3, although there was no significant difference in the surface area and pore volume compared to pristine AC, pore size distribution curves (Figure 5-4) revealed that pore size distribution became broader in the range of 5-14 nm and shifted towards lower pore size, which could be due to the increase in surface oxygen groups resulting in narrowed pores (Strelko & Malik 2002).

No difference in the pore size distribution could be seen in the case of AC-NaOH and could be due to the lower amount of surface oxygen content compared to other samples Porosity analysis suggested that treatment with a mixture of H_2SO_4 and HNO_3 solution is disadvantageous despite the increase in surface oxygen content, due to the reduction in the porosity.
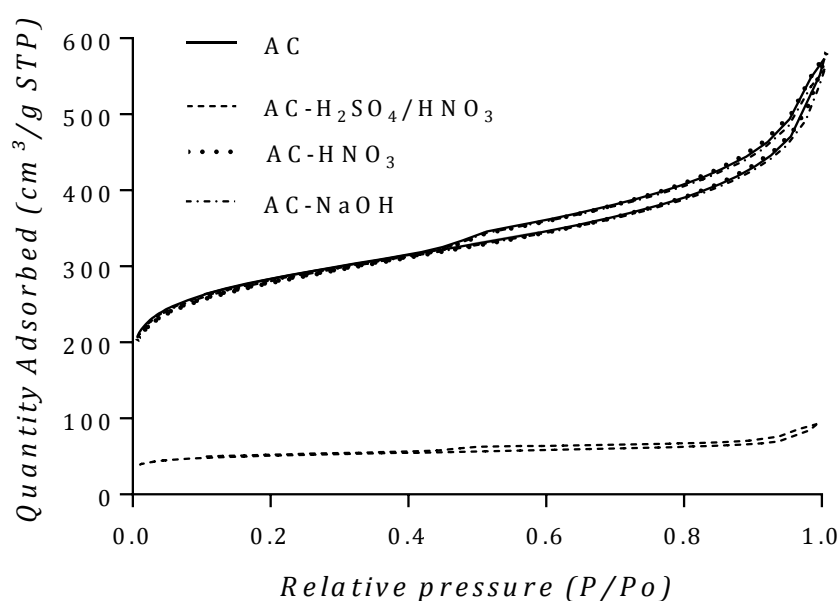
Figure 5-3: Nitrogen adsorption/desorption isotherms at 77 K of pristine activated carbon and surface treated activated carbon. Significant reduction in the adsorption was observed in the activated carbon treated with a mixture of H_2SO_4 and HNO_3 (AC-H_2SO_4/HNO_3).

Table 5-3: Surface area and pore characteristics determined from nitrogen sorption analysis of pristine activated carbon and surface treated activated carbon. Significant reduction in the surface area and pore volume was observed in the activated carbon (AC-H_2SO_4/HNO_3) when treated with a mixture of H_2SO_4 and HNO_3 solution.

Sample	Specific surface area[a] (m^2/g)	Total pore volume[b] (cm^3/g)	Micropore volume[b] (cm^3/g)
AC	1027.4	0.81	0.33
AC- HNO_3	1008.8	0.83	0.33
AC-NaOH	1021.7	0.79	0.32
AC-H_2SO_4/HNO_3	193.7	0.13	0.066

[a]Calculated using Brunauer-Emmett-Teller (BET) theory
[b]Determined by NLDFT theory assuming slit-shaped pores.

134
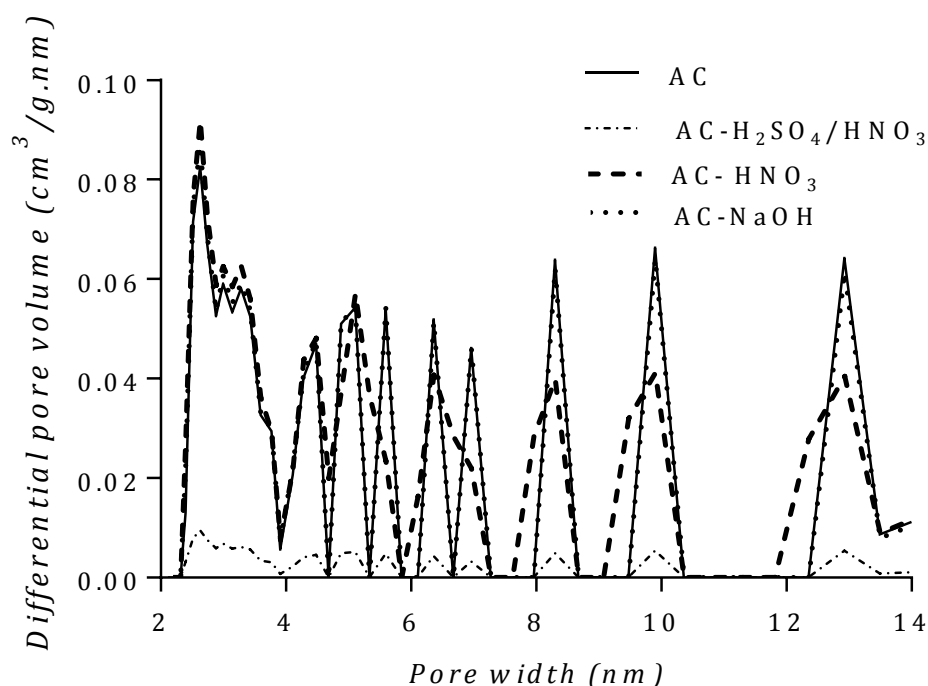
Figure 5-4: Pore size distribution (2-14nm) calculated using NLDFT slit-shaped pore model of pristine activated carbon (AC) and surface treated activated carbon. Despite significant reduction in the pore volume, pore size distribution of AC-H₂SO₄/HNO₃ was found to be similar to that of pristine AC.

5.3.1.3. Drug loading and release from modified activated carbon

To determine the effect of surface chemistry on drug loading and release, PA was loaded into AC, AC-HNO$_3$, AC-NaOH, and AC-H$_2$SO$_4$/HNO$_3$ using the previously optimised solution adsorption-centrifugation method. 1000 mg of AC was added to 10 mL of saturated PA solution (150 mg/mL of ethanol) and was allowed to undergo stirring (100 rpm) at 20 °C for 4 hours.

Statistically significant differences ($p < 0.001$, one-way ANOVA) in the drug loading was observed for AC before and after surface treatment (Figure 5-5). Also, a post hoc test showed that there was no statistically significant difference ($p > 0.05$, Dunnett's multiple comparison test) in the drug loading for AC- HNO$_3$ and AC-NaOH compared to that of pristine AC, and the difference in the drug loading was only in the case of AC-

H_2SO_4/HNO_3. To determine whether the difference in the drug loading was due to the porosity or surface oxygen content of AC, a Pearson's r test was used. A stronger and a more significant positive correlation ($r = 0.999$, $p < 0.001$) was found between the surface area of AC and % drug loading compared to the surface oxygen content of AC, indicating that the lower drug loading in the case of $AC-H_2SO_4/HNO_3$ was due to the reduction in the porosity, since drug loading decreases with decrease in the porosity; effect of porosity on drug loading will be discussed in the later parts of this chapter.
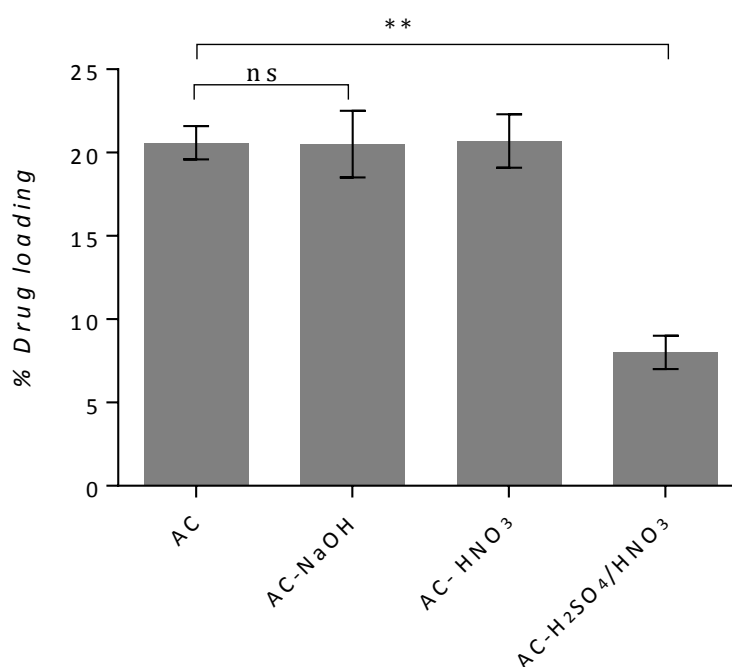
Figure 5-5: Drug (paracetamol) loading efficiency of pristine activated carbon (AC) and surface treated activated carbon (AC-NaOH, AC-HNO$_3$, and AC-H$_2$SO$_4$/HNO$_3$). Statistically significant differences compared to control (AC) are noted for $p < 0.05$ (** $p < 0.01$, one-way ANOVA and Dunnett's multiple comparison test). Results are the mean of triplicate experiments ± SD.

To study the effect of surface treatment on drug release, 50 mg of drug/carrier complex was added to 100 mL of phosphate buffer (pH 5.8) and was allowed to undergo stirring for 24 hours. Statistically significant differences ($p < 0.0001$, one-way ANOVA) in the drug release were observed for AC before and after surface treatment (Figure 5-6). Also, a post hoc test showed that there was no statistically significant difference ($p > 0.05$,

Dunnett's multiple comparison test) in the drug release between AC-NaOH compared to that of pristine AC, indicating that treatment with NaOH was ineffective in improving the drug release.

To determine whether the difference in the drug release was due to the porosity or the surface oxygen content of AC, a Pearson's r test was used. In contrast to drug loading, a stronger and a more significant positive correlation (r =0.991, p <0.01) was found between the surface oxygen content of AC and % drug release compared to the surface area of AC. Also, a complete drug release was achieved in the case of AC-H_2SO_4/HNO_3 and could be attributed to increased wettability due to surface oxygen groups, thereby leading to increased accessibility of dissolution medium to the pores. However, complete drug release could be due to the adsorption of drug in the superficial mesopores and macropores since most of the microporosity is lost during the treatment.
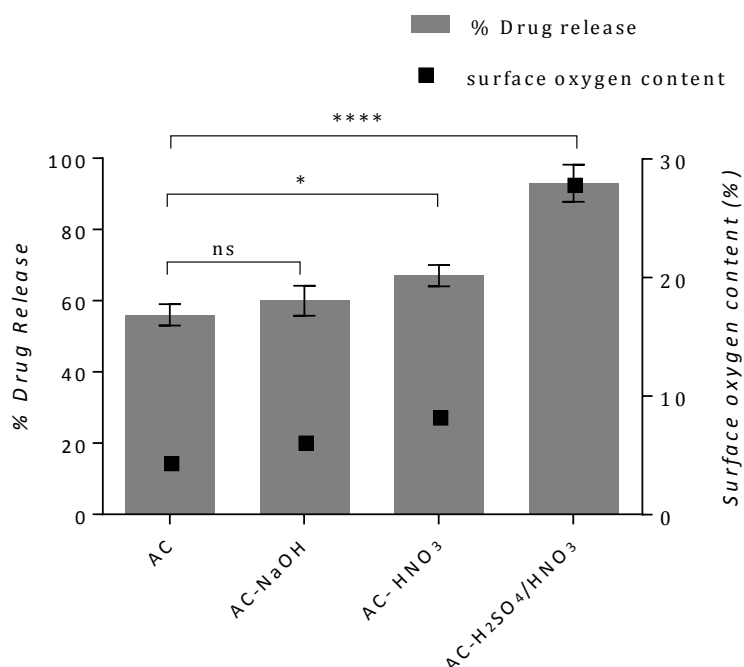
Figure 5-6: Effect of the surface oxygen content of pristine and surface treated activated carbon on drug (paracetamol) release. Drug release was determined in phosphate buffer post stirring for 24 hours. Statistically significant differences compared to control (AC) are noted for $p < 0.05$ (* $p < 0.05$; **** $p < 0.0001$, one-way ANOVA and Dunnett's multiple comparison test). Results are the mean of triplicate experiments ± SD.

5.3.2. Effect of porosity of activated carbon on drug loading and release

5.3.2.1. Particle size and porosity analysis of activated carbon

To determine the effect of porosity on loading and release, different types of AC were purchased and drug loading was performed using PA as a model drug. Prior to drug loading, AC samples were characterised for particle size and porosity. AC used in the previous chapters is also used in this particular study and will be referred to as AC-G60 In addition, three other types of AC obtained under different manufacturing conditions were also used and will be referred to as AC-KB, AC-USP, and AC-C9157.

Laser diffraction studies revealed that all the samples have a broad particle size (Figure 5-7 and Table 5-4). The average particle size of AC-G60, AC-USP, and AC- C9157 is very similar and is in the range of 29-35 µm, whereas the particle size of AC-KB is much lower, with an average size of 19.82 µm.
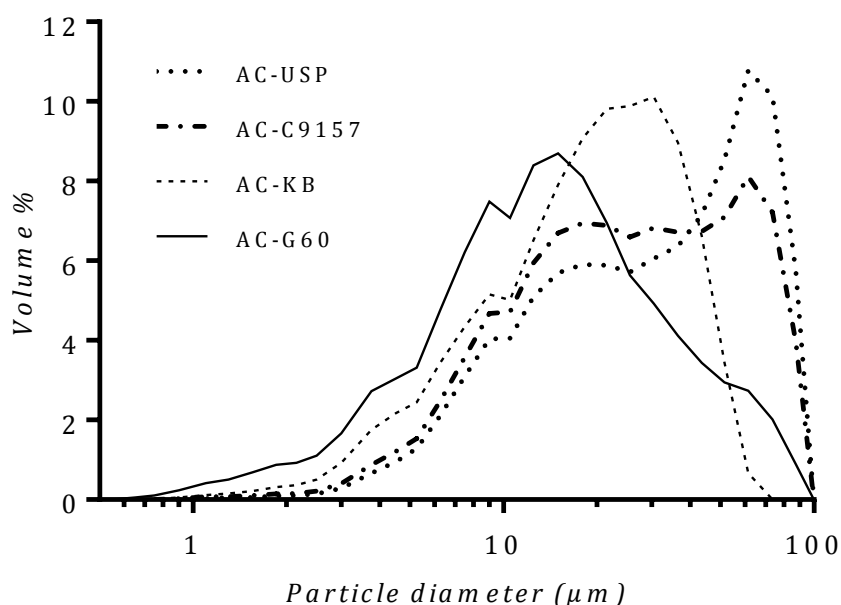
Figure 5-7: Particle volume size distribution of four different types of activated carbon obtained from laser diffraction analysis. All samples have a broad particle size distribution in the range of 0.5 to 100 µm.

Table 5-4: Particle size characteristics of four different types of activated carbon obtained from laser diffraction analysis.

Material	X90[a] (µm)	X50[b] (µm)	X10[c] (µm)	Volume mean diameter (µm)	Span
AC-G60	40.59 ± 0.53	12.62 ± 0.09	3.92 ± 0.02	17.85 ± 0.15	2.91 ± 0.02
AC-KB	37.25 ± 0.31	17.83 ± 0.22	5.53 ± 0.14	19.82 ± 0.21	1.78 ± 0.02
AC-C9157	63.34 ± 1.55	23.46 ± 0.76	7.19 ± 0.23	29.92 ± 0.86	2.39 ± 0.03
AC-USP	68.43 ± 0.12	29.41 ± 0.16	7.91 ± 0.1	34.33 ± 0.09	2.06 ± 0.01

[a]Particle dimension corresponding to 90% of the cumulative undersize distribution
[b]Median particle dimension
[c]Particle dimension corresponding to 10% of the cumulative undersize distribution

Porous characteristics of the four types of AC were studied using nitrogen sorption analysis. The adsorption/desorption isotherm (Figure 5-8) of all four types of AC exhibited a typical type IV isotherm and a hysteresis loop at relative pressure (P/P_o) equal to 0.45, characteristic of microporous materials with significant mesoporosity (Chen et al. 2010). AC-KB exhibited a sharp increase in the adsorption, indicating a more uniform pore size compared to other types of AC (Izquierdo-Barba et al. 2005), in line with the results from laser diffraction analysis. Specific surface area was determined from adsorption/desorption isotherms using the BET model, which revealed that AC-KB has the highest surface area of 1386.9 m^2/g, while AC-USP has the lowest surface area of 888.6 m^2/g, out of the four samples (Table 5-5). Pore volume and pore size results were determined using non-local density functional theory (NLDFT) model assuming slit-shaped pores and revealed that all the AC samples exhibited a broad distribution in the range of 2-14 nm, with AC-G60 and AC-USP showing very similar pore size distribution

(Figure 5-9) whereas AC-KB was found to have a broader pore size distribution compared to other types of AC since it was manufactured using chemical activation; Chemical activation was found to result in higher porosity compared to steam activation (Maciá-agulló & Linares-solano 2004).
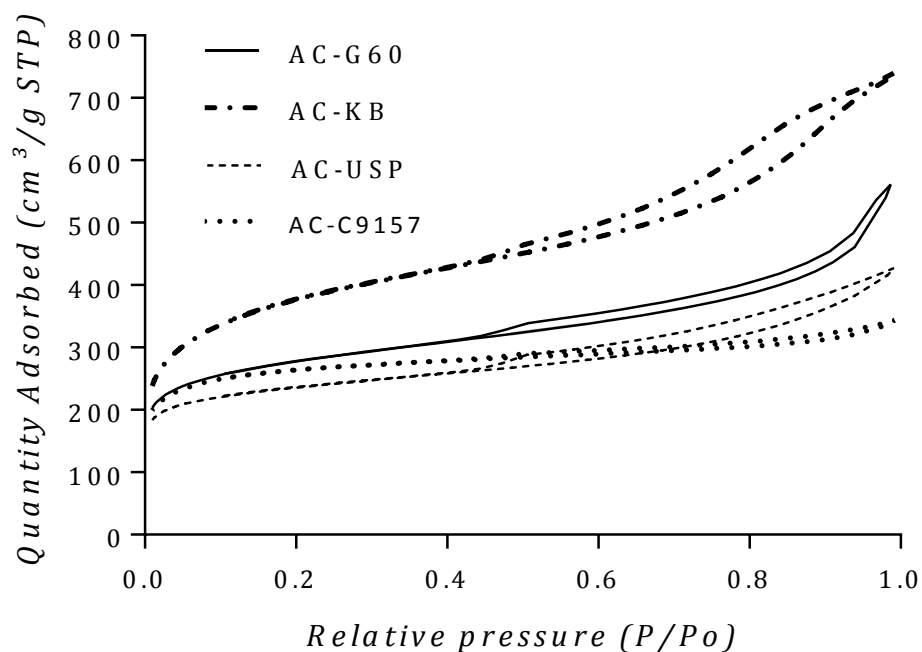
Figure 5-8: Nitrogen adsorption/desorption isotherms at 77 K of four types of activated carbon. All samples exhibited a typical type IV isotherm and a hysteresis loop at relative pressure (P/P$_o$) equal to 0.45, characteristic of microporous materials with significant mesoporosity.

Table 5-5: Surface areas and pore volumes of four different types of activated carbon

Sample	Specific surface area[a] (m²/g)	Total pore volume [b] (cm³/g)	Micropore volume [b] (cm³/g)	Micropore volume fraction
AC-G60	1027.4	0.81	0.33	0.407
AC-KB	1386.9	1.07	0.44	0.411
AC-USP	888.6	0.61	0.29	0.475
AC-C9157	1007.4	0.48	0.36	0.75

[a]Calculated using Brunauer-Emmett-Teller (BET) theory
[b]Determined by NLDFT theory assuming slit-shaped pores.
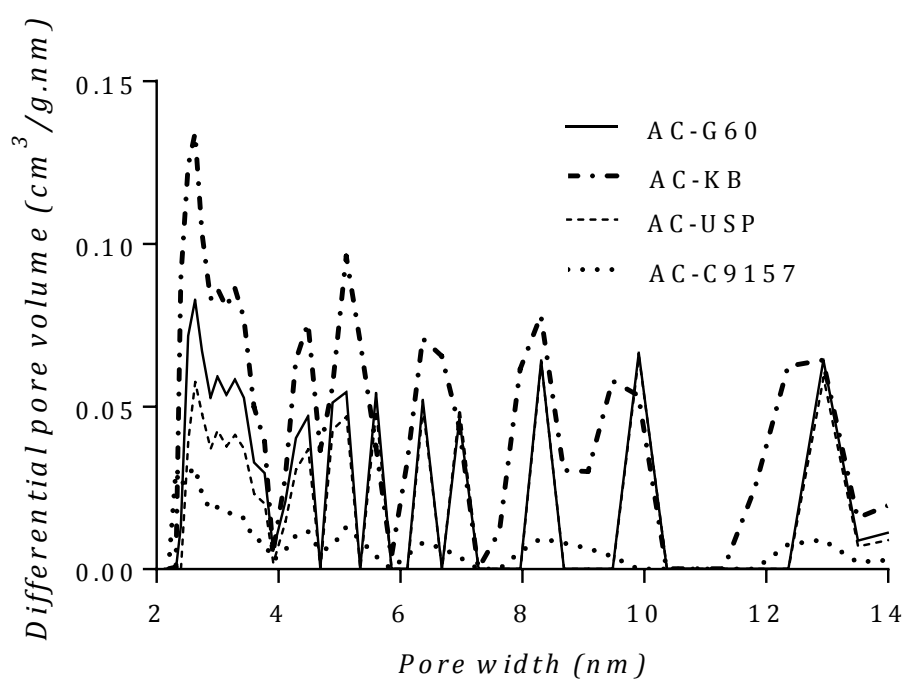
Figure 5-9: Pore size distribution (2-14nm) determined using NLDFT slit-shaped pore model, of four different types of activated carbon. AC-G60 and AC-USP have a very similar pore size distribution and AC-KB has a wider range of pores compared to other types of AC.

5.3.2.2. Drug Loading

To determine the effect of porosity on drug loading efficiency, PA was loaded into four different types of activated carbon (AC-G60, AC-KB, AC-USP, and AC-C9157) using solution adsorption-centrifugation method. 1000 mg of AC was added to 10 mL of saturated PA solution (150 mg/mL of ethanol) and was allowed to undergo stirring (100 rpm) at 20 $^{\circ}$C for 4 hours.

Drug loadings obtained for different ACs were compared with corresponding total pore volume (Figure 5-10). There was a statistically significant difference in the drug loading ($p<0.001$, one way ANOVA) between different types of AC. To assess the relationship between porosity (surface area, total pore volume and micropore volume) and drug loading, a Pearson's r test was used and there was a positive correlation (r $=0.96$, $p <0.05$) between total pore volume and % drug loading, indicating that carriers with high total pore volume could be advantageous to achieve high drug loading as seen in previous reports (Yu et al. 2014).
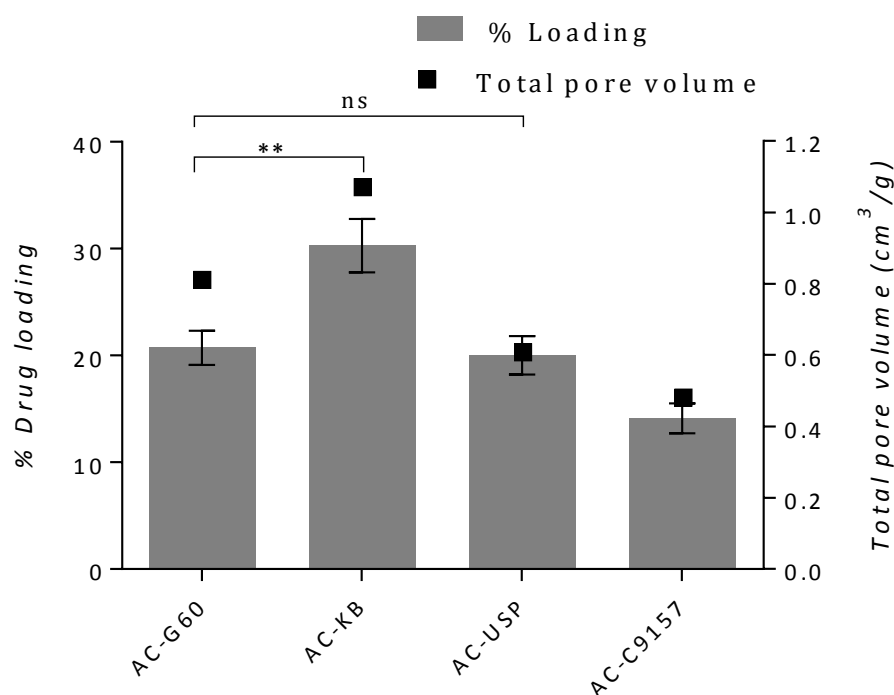
Figure 5-10: Drug loading efficiency of four different types of activated carbon. Drug loading was found to increase with increase in the total pore volume. Statistically significant differences are noted for $P < 0.05$ (** $p \leq 0.01$; one-way ANOVA and Tukey's multiple comparison test). Results are the mean of triplicate experiments $\pm$ SD

5.3.2.3. Drug Release

To investigate the effect of porosity on the drug release of drug/carrier complex, 50 mg of drug/carrier complex was added to 100 mL of phosphate buffer at pH 5.8 and was allowed to undergo stirring for 24 hours and the quantity of drug in the buffer was determined by UV analysis.

There was a statistically significant difference in the % drug release ($p < 0.001$, one way ANOVA) between different types of AC (Figure 5-11). To assess the relationship between porosity (surface area, total pore volume, and micropore volume) and drug release, a Pearson's r test was used. No correlation was found between surface area and total pore volume; however, there was a negative correlation ($r = -0.97$, $p < 0.05$) between micropore volume fraction and % drug release, indicating that application of carriers with

less microporosity could be advantageous in achieving complete drug release. Also, a post hoc test showed that there was no statistically significant difference ($p > 0.05$, Tukey's multiple comparison test) in the % drug release between AC-KB and AC-USP, even though there is a difference in the micropore volume fraction, indicating that there is an influence of some other factors, such as surface chemistry of carrier, on the drug release.
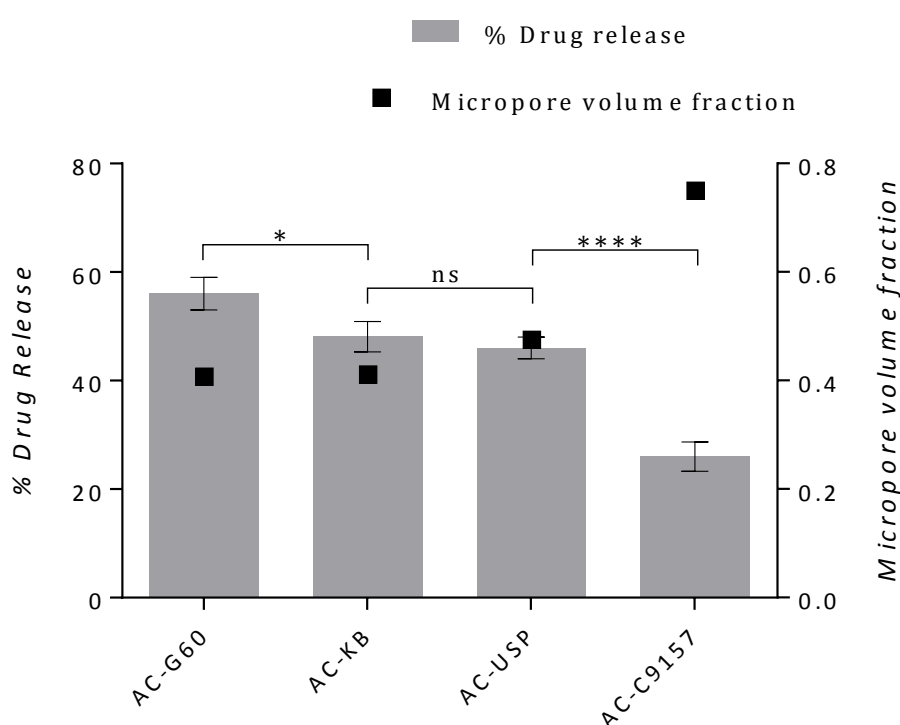
Figure 5-11: Drug release from four different types of activated carbon determined in phosphate buffer post stirring for 24 hours. Drug release was found to decrease with increase in the micropore volume fraction. Statistically significant differences are noted for $P < 0.05$ (* p < 0.05; **** p < 0.0001; one-way ANOVA and Tukey's multiple comparison test). Results are the mean of triplicate experiments $\pm$ SD

5.4. Conclusion

The work in this chapter showed that drug loading and release are affected by the characteristics of AC, such as porosity and surface chemistry. Drug release from AC was

incomplete (56%) in the absence of SDS and was attributed to the inaccessibility of dissolution to micropores, due to the poor wettability of AC. Therefore, to achieve complete drug release and to understand the effects of the surface chemistry of AC on drug loading and release, AC was subjected to three different surface modification techniques. High surface oxygen content was achieved when AC was treated with a mixture of H_2SO_4 and HNO_3 (AC-H_2SO_4/HNO_3); however, porosity was reduced significantly, leading to reduced PA loading (8%). Drug release studies indicated that percentage drug release increased with increase in the surface oxygen content and a complete drug release (93%) was achieved in AC-H_2SO_4/HNO_3. AC treated with HNO_3 (AC-HNO_3) and AC treated with NaOH (AC-NaOH) showed a drug release of 60 and 67%, respectively, indicating that treatment with NaOH and HNO_3 is ineffective to achieve complete drug release. Although AC-H_2SO_4/HNO_3 resulted in complete drug release, drug loading was reduced significantly, suggesting that an optimum surface treatment needs to be determined to achieve complete drug release without reducing the drug loading capacity.

In addition to surface chemistry, porosity was also found to affect the drug loading and release. Paracetamol was loaded into four different types of activated carbon with different porosity characteristics and drug loading was found to increase with an increase in the total pore volume. However, drug release was found to decrease with an increase in the micropore volume fraction, indicating that total drug release could be improved when AC with low microporosity is used.

Chapter 6 **-Synthesis of carbon onion for drug delivery applications**

Some of the results presented in this chapter have been presented in the paper:

6.1. Introduction

Carbon onion (OLC) has attracted great interest for various electronic, tribological and biological applications and can be produced via thermal annealing of ND under vacuum or inert gas atmosphere (Costa et al. 2014; Bartelmess & Giordani 2014).

ND used in the production of OLC are produced from detonation and consists of an sp^3 hybridised diamond core surrounded by sp^2 hybridised amorphous carbon fragments, stabilised by nitrogen and oxygen containing functional groups. The presence of functional groups and sp^2 carbon fragments in the ND structure results in the formation of tight aggregates reaching up to hundreds of nanometres in size which could only be disaggregated by functionalisation and this aggregation leads to the development of aggregate created porosity containing both open and closed pores. These primary aggregates form agglomerates up to several micrometres in size due to the presence of van der Waals interactions and can be broken down mechanically (Shenderova et al. 2002). Thermal annealing of these agglomerates of ND results in the formation of aggregates of OLC of several micrometres in size.

The particle size of OLC depends on the particle size of the ND used for the synthesis; the typical particle size of ND used for the synthesis of OLC is less than 10 nm, since smaller size NDs enable the graphitisation at lower temperatures compared to larger crystals (Joly-Pottuz et al. 2008; Terrones & Terrones 2003; Qian et al. 2004).

The transformation of ND to OLC involves graphitisation from the surface to the core; as the temperature increases, the surface functional groups of ND decompose between 200 and 700ºC, undergoes a phase transformation from sp^3 to sp^2 hybridisation between 700 and 1100 ºC in order to reduce the surface energy and finally forms completely merged graphitised carbon shells between 1100 and 1300 ºC (Zeiger, Jackel, et al. 2015).

The merging of graphite shells causes a significant decrease in the surface energy for the graphitised particles, which could be the driving force for the formation of spherical OLC. Formation of OLC from ND varies depending on the annealing conditions, such as annealing time, temperature and atmosphere, as shown in Table 6-1.

Table 6-1: Synthesis of carbon onion from nanodiamond at different annealing conditions

Annealing temperature (°C)	Annealing time (Atmosphere)	Results	Reference
900-1400	1 hour (Argon)	Carbon onions begin to form in the range of 1100–1200 °C with a diamond core. Complete transformation occurs at 1400 °C.	(Qiao et al. 2006a)
1400	2 hours (Argon)	Carbon onions formed initially are converted into graphitic ribbons.	(Qiao et al. 2006b)
RT to 1150	1 hour (Argon)	Graphitisation starts at 670 °C and ends at 1100 °C.	(Xu et al. 2002)
1866	1 hour (Argon)	Graphitic ribbon structures are formed due to carbon redistribution.	(Kuznetsov et al. 2004)
700-1100	--(Vacuum)	ND surface reconstructs below 900 °C and is progressively graphitised after 900 °C.	(Petit et al. 2011)
800-1700	1, 3 or 10 hours (Argon)	At 1700 °C, polyhedral graphite crystals can be formed. Surface area increases until 1300 °C and then remains constant before decreasing.	(Zeiger, Jäckel, et al. 2015)
1600	13 minutes (Vacuum)	Carbon onion with graphitic shell and diamond core of 8 nm.	(Joly-Pottuz et al. 2008)

6.2. Aims and Objectives

The aim of this current chapter, therefore, is to perform thermal annealing of nanodiamonds at three different temperatures and study the effect of annealing temperature on the physicochemical characteristics. To achieve this, the main objectives of this study were to:

1. Perform thermal annealing of nanodiamonds at 900, 1000 and 1100 ℃, under flowing nitrogen atmosphere.

2. Investigate the effect of annealing temperature on the surface morphology, using SEM, and analyse the structural transformation, using Raman spectroscopy, XRD and TEM techniques.

3. Study the effect of annealing temperature on the surface chemistry, using XPS and FTIR techniques, and to study the porosity using nitrogen sorption analysis.

6.3. Results and discussion

6.3.1. Surface morphology

Pristine nanodiamonds appear to have a light greyish colour and with the increase in the annealing temperature from 900 to 1100 °C, ND powders transform from light grey to dark grey and finally to dark black at 1100 °C. SEM pictures also reveal a significant difference in the morphology of ND-1100 compared to pristine nanodiamonds, ND-900 and ND-1000, as shown in Figure 6-1. ND-1100 showed tightly bound aggregates reaching up to 2 µm in size compared to other samples showing loosely bound agglomerates. During annealing ND undergoes a process of agglomeration and forms microparticles since ND particles have high agglomerating character, due to the surface

functional groups (El-Say 2011) resulting in the formation of OLC aggregates thereby leading to aggregate created porosity.

Aston University

Illustration removed for copyright restrictions

Figure 6-1: Scanning electron microscope pictures showing the morphology of (A) pristine nanodiamond and nanodiamonds annealed at temperatures (B) 900, (C) 1000 and (D) 1100 °C.

6.3.2. Structural characterisation

Raman spectra of the nanodiamond samples before and after annealing are shown in Figure 6-2. The peak positions and peak full width at half maximum (FWHM) were determined by fitting spectra with a Gaussian line shape using Origin software and are shown in Table 6-2.

The spectrum of pristine nanodiamonds (ND) showed two dominant peaks: one at 1325 cm^{-1}, corresponding to the sp^3 diamond bonds (F^{2g}) with a small background of sp^2 disorder peak (D band), and the second at 1595 cm^{-1}, corresponding to sp^2 dimer bonds (G band), indicating the presence of amorphous carbon fragments characteristics of ND produced from detonation process (Qiao et al. 2006b; Xie et al. 2010).

150

Post annealing, spectra of samples consists of a broad D band in the region 1332-1350 cm^{-1}, attributed to increase in the sp^2 disorder with a background of sp^3 diamond. With the increase in temperature, the intensity of this D band increased, suggesting the transformation of sp^3 to sp^2 configuration (Chu & Li 2006).

Also, with an increase in the annealing temperature, G band shifts downwards from 1594 to 1568 cm^{-1} which could be due to the removal of functional groups and then shifts upwards to 1587 cm^{-1} which could be due to tensile strain induced from graphene planes becoming spherical. The FWHM of G band decreases after annealing to 1000 and 1100 ºC, suggesting the increase in the long-range order of graphitic carbon. The G band of ND-1100 has the lowest FWHM, suggesting the high quality of graphitic shells around the diamond core. (Roy et al. 2003; Wang et al. 2005; Mochalin et al. 2013). The relative intensity of D and G bands (I_D/I_G) gives the degree of graphitisation during annealing, which is seen to gradually increase from 900 to 1100°C, suggesting the transformation from sp^3 to sp^2 configuration (Zeiger, Jäckel, et al. 2015).
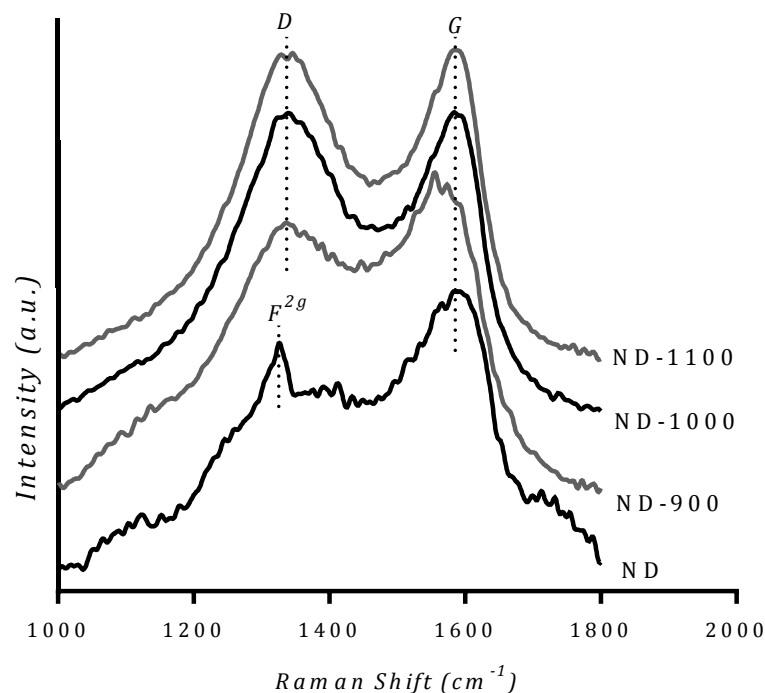
Figure 6-2: Raman spectra of ND, ND-900, ND-1000 and ND-1100 (bottom to top) showing the F^{2g} peak corresponding to the sp^3 diamond at 1325 cm^{-1}, D band and G band corresponding to sp^2 configuration at ~ 1330 cm^{-1} and ~1570 cm^{-1}, respectively. Note that the intensity scale is arbitrary.

Table 6-2: Raman shifts, areal intensities and peak widths obtained from the spectra of pristine nanodiamonds and nanodiamonds annealed at different temperatures determined by fitting spectra with a Gaussian line shape using Origin software.

Sample	Peak position (cm^{-1})	FWHM[a] (cm^{-1})	Peak Assignment	Areal intensity ratio[b] (I_D/I_G)
ND	1325	189.7	Diamond	-
	1594	116.4	G- sp^2 dimers	
ND-900	1343	215.85	D-sp^2 disorder	1.4
	1568	134.14	G-sp^2 clusters	
ND-1000	1345	175.6	D-Graphite	1.9
	1588	97.5	G-Graphite	
ND-1100	1343	204.7	D-Graphite	2.3
	1587	89	G Graphite	

[a] Peak Full width at half maximum
[b] Relative intensity of D and G bands

The peak corresponding to diamond should still be present in the Raman spectra of ND-1100, but could be masked by the intensive D peak. Hence, X-ray diffraction was used to investigate the presence of diamond core in ND-1100, using Miller indices {hkl} to identify different planes of atoms.

The XRD pattern of ND (Figure 6-3) shows three diffraction peaks at 2θ: 43° {111}, 75° {220}, and 91° {311}, corresponding to diamond, and a peak at 29° {002}, corresponding to the sp^2 carbon, (Tomita et al. 2002) suggesting the presence of amorphous carbon and supporting the results from the previous Raman data.

The lattice spacing of various planes and intensities of peaks were compared between ND and ND-1100; in ND-1100, the peak at 43° has lower intensity (Table 6-3) compared to unannealed ND, suggesting a decrease in the diamond carbon.

The FWHM of the diamond peak also increases after annealing, indicating the decrease in the crystallite size of ND (Xu et al. 2002). Since diffraction scattering corresponding to sp^3 diamond phase is more intense and can often mask the sp^2 signal, XRD data cannot be used to monitor the formation of sp^2 carbon but can only be used to monitor changes in the diamond phase.

Raman studies suggest that annealing of NDs resulted in the formation of sp^2 carbon from sp^3 carbon, whilst XRD studies suggest that sp^3 diamond phase was still present post annealing NDs to 1100 °C. The interpretation of these results is to assume that ND-1100 sample consists of particles with a diamond core surrounded by graphitic shells.
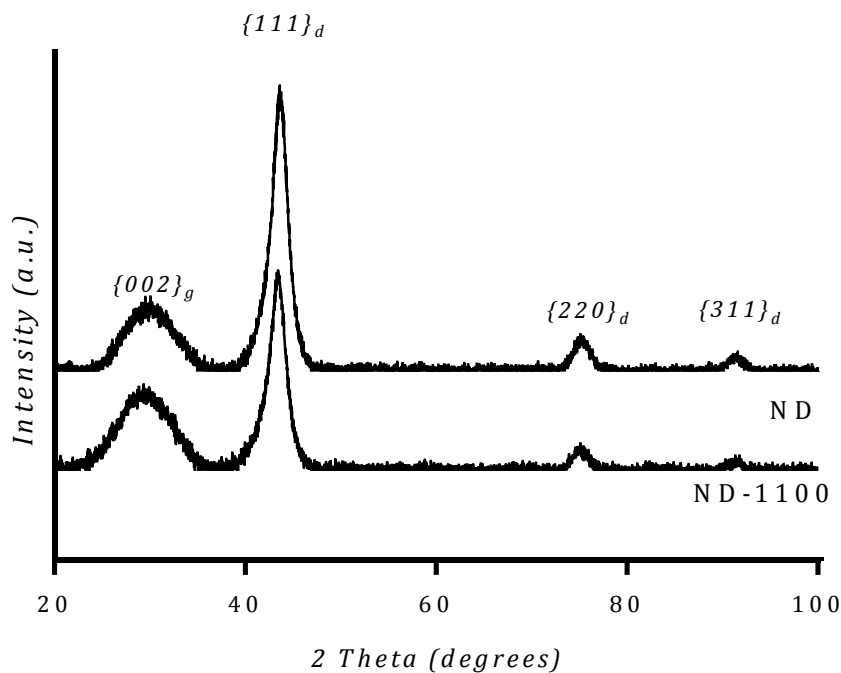
Figure 6-3: XRD patterns of ND and ND-1100 showing the diffractions of diamond and graphite planes showing peaks corresponding to diamond (d) planes at 2θ: 43° {111}, 75° {220} and 91° {311}, peaks corresponding to graphitic (g) planes at 29° {002}. Note that the intensity scale is arbitrary.

Table 6-3: Summary of results obtained from XRD analysis of ND and ND-1100.

Sample	Miller indices {hkl}	2θ (degrees)	d Value (Å)[a]	FWHM	% Relative intensity[b]
ND	002	29.87	2.99	5.66	12
	111	43.54	2.08	2.03	100
	220	75.17	1.26	2.02	13
	311	91.15	1.08	2.33	6
ND-1100	002	29.61	3.01	6.25	20.9
	111	43.4	2.08	2.06	51.6
	220	75.11	1.26	1.93	6.2
	311	91.37	1.08	1.79	2.8

[a]Lattice spacing
[b]Relative intensity is calculated by dividing the absolute intensity of each peak by absolute intensity of the most intense peak.

HRTEM was used to further confirm the presence of graphitic shells surrounding the diamond core in ND-1100. TEM images (Figure 6-4) of ND show a diamond core with a typical lattice spacing of ~ 2 Å {111} (Xiao et al. 2014), surrounded by amorphous carbon. TEM images of ND-1100 show diamond core surrounded by 3-5 graphitic shells, with a typical lattice spacing of ~ 3 Å {002} (Duffy et al. 2015) further supporting the data from Raman and XRD studies.
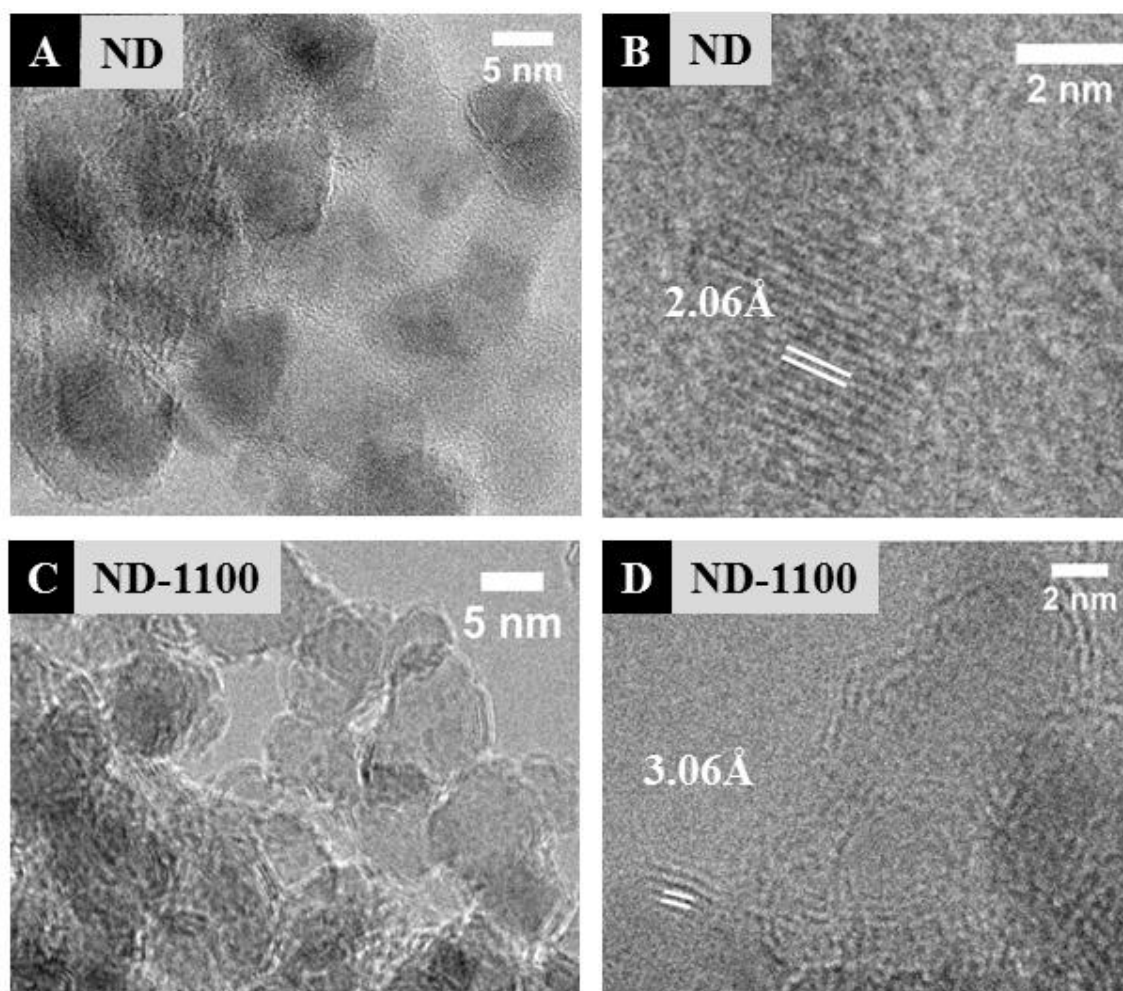
Figure 6-4: Transmission electron micrographs of pristine nanodiamond (A, B) showing the lattice spacing of 2.06 Å corresponding to the plane {111} and nanodiamond annealed at 1100 °C (C, D) showing the lattice spacing of 3.06 Å corresponding to the plane {002}.

6.3.3. Chemical characterisation

The surface chemistry of nanodiamonds before and after annealing was examined using XPS and FTIR techniques. XPS spectra (Figure 6-5) of ND contained an intense carbon (C 1s) peak and two weak peaks, corresponding to nitrogen (N 1s) and oxygen (O 1s), marked at 284, 400, and 532 eV, respectively. Also, a series of CKLL Auger peaks appear between 1200 and 1240 eV that can provide information about the chemical bonding (Wu & Pendleton 2001; Titantah & Lamoen 2005). The atomic percentage of carbon increased while the atomic percentage of nitrogen and oxygen decreased as the annealing temperature increases (Table 6-4), which could be due to the reduction in the surface dangling bonds, such as –C-H and –C-O- bonds, at high temperatures (Xie et al. 2010).
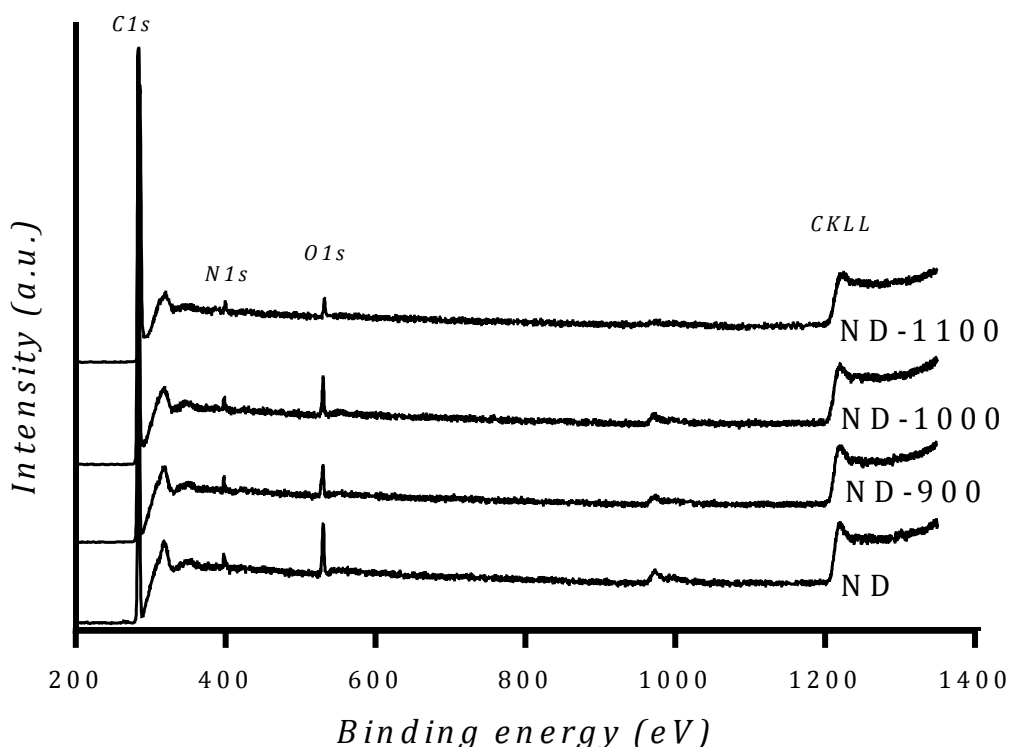
Figure 6-5: XPS spectra of pristine nanodiamonds (ND) and nanodiamonds annealed at different temperatures (ND-900, ND-1000 and ND-1100) . The major peaks are marked for Carbon (C 1s), Nitrogen (N 1s) and Oxygen (O 1s) present on the surface. Note that the intensity scale is arbitrary.

The relative contents of sp^3 and sp^2 carbon in the samples were determined by analysing the C-KLL X-ray excited Auger spectra (Table 6-4 and Figure 6-6) with the method used by Jones *et al*. (Jones & Ojeda 2012). The KLL spectrum was smoothened by Savitzy-Golay with 15 points and differentiated with 9 points (Kaciulis 2012). The distance (energy 'D') between the maximum of positive excursion and the minimum of negative excursion of the first differential was determined.

Post-annealing, D value was found to increase, indicating an increase in the content of sp^2 carbon (Xie et al. 2010), consistent with the results from Raman spectroscopy. Relative contents of sp^3 and sp^2 carbon were determined from the linear interpolation of D value of 13 eV for diamond (100%- sp^3) and 22 eV for graphite (100%- sp^2). D value of ND was found to be 13 eV despite the presence of sp^2 carbon as indicated from Raman and XRD data, and the exact reason for this is not clear. Sp^2 content was found to increase to 13% post annealing to 900 ºC. Annealing to 1000 ºC significantly increased the sp^2 content to 63% which was found nearly four times to that seen in ND-900. The rate of increase of sp^2 content decreased after 1000 ºC with ND-1100 showing sp^2 content of 68% indicating the successful conversion of sp^3 diamond to sp^2 graphite during annealing. ND-1100 sample also contains 32% of sp^3 carbon, indicating the presence of diamond core, consistent with the results from XRD and HRTEM analysis.
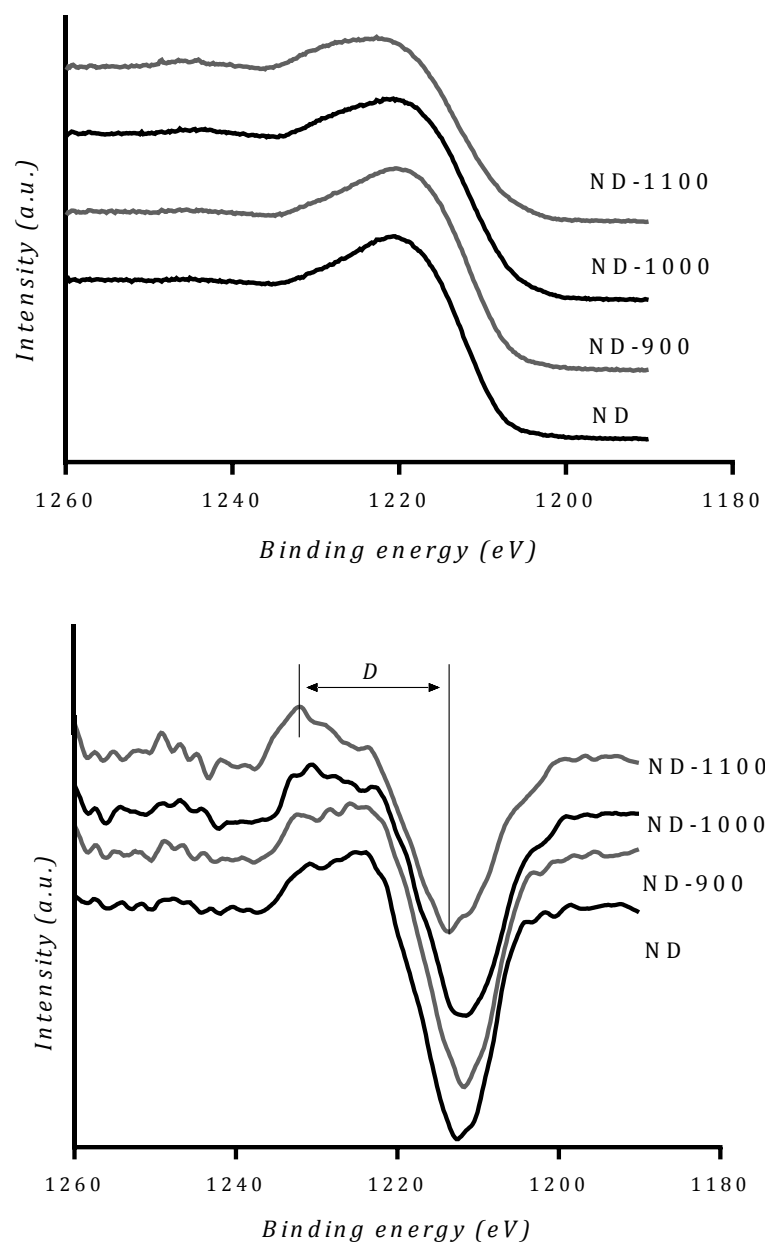
Figure 6-6: XPS C KLL Auger Spectra (Top) and their first derivatives (Bottom) as compared with pristine nanodiamonds (ND) and nanodiamonds annealed at different temperatures (ND-900, ND-1000 and ND-1100). D parameter represents the width between maximum and minimum excursions of the derivative of Auger spectra. Note that the intensity scale is arbitrary.

Table 6-4: The relative atomic contents of carbon, oxygen, and nitrogen, and the relative atomic contents of different chemical states of carbon determined from XPS analysis.

Sample	C (%)	O (%)	N (%)	C KLL Auger spectra		
				D^a (eV)	Sp^2 (%)	Sp^3 (%)
ND	93.8	3.9	1.9	13	0	100
ND-900	95.6	2.7	1.7	14.2	13	87
ND-1000	96.0	2.8	1.2	18.7	63	37
ND-1100	97.1	1.6	1.0	19.1	68	32

[a]D parameter represents the width between maximum and minimum excursions of the derivative of Auger spectra

FTIR spectra of nanodiamonds before and after annealing are shown in Figure 6-7. The broad band between 3000 and 3600 cm^{-1} can be attributed to O-H and N-H vibrations, indicating the presence of amino groups and acid groups or adsorbed water, and the intensity of this band has significantly reduced after thermal treatment since these groups are unstable at high temperatures. Peaks around 2900 cm^{-1} could be assigned to aliphatic –C-H- vibrations of amorphous carbon fragments and are present in all the samples and have reduced in intensity after thermal treatment and could be due to the graphitisation of carbon. The peak at 2300 cm^{-1} is assigned to the CO_2 from the ambient air (Jarre et al. 2014). The band at 1690 cm^{-1} can be assigned to C=O group, indicating the presence of acid groups, which reduced significantly after thermal annealing. The multiple peaks between 1100 and 1500 cm^{-1} can be attributed to C-N and C-O groups, which have also reduced in intensity post annealing.
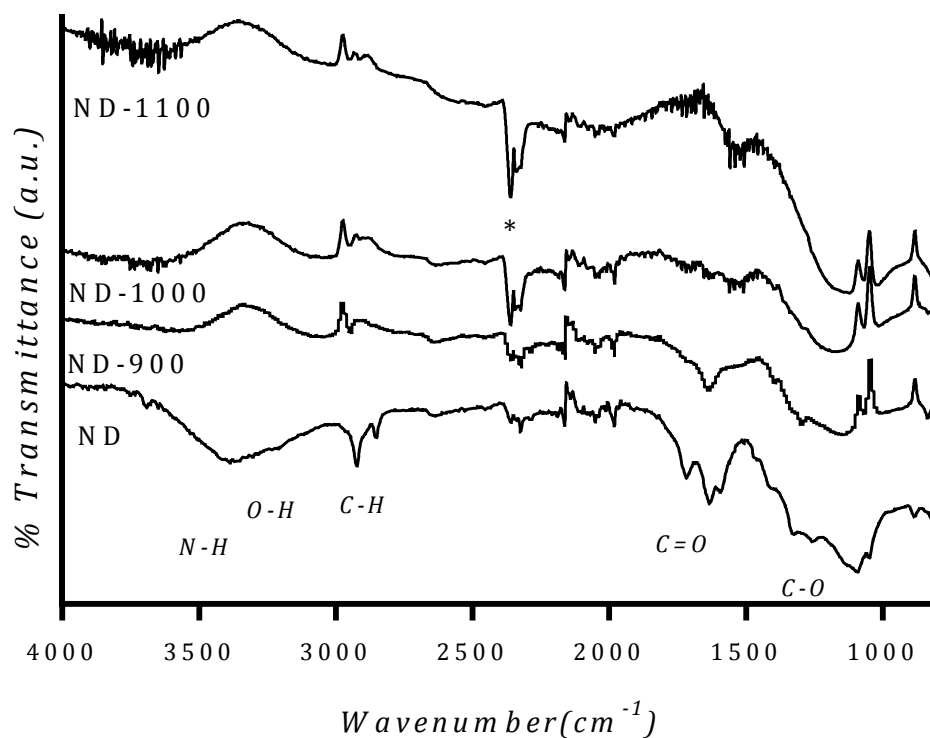
Figure 6-7: FTIR spectrum of pristine nanodiamonds and nanodiamonds annealed at different temperatures. Annealing nanodiamonds removed adsorbed water. *peak assigned to CO_2 from ambient air. Note that the transmittance scale is arbitrary.

The FTIR transmittance of various functional groups after thermal annealing is much smaller compared to pristine nanodiamonds, suggesting the reduction in surface dangling bonds, consistent with the results from XPS analysis. However, the functional groups were not completely removed and the presence of these functional groups on carbon onion surface results in higher stability and higher aggregation ability, due to intermolecular bonds between the functional groups, compared to carbon onions free of functional groups (Costa et al. 2014).

160

6.3.4. Porosity analysis

N_2 sorption analysis was performed to understand the changes in the porosity of ND before and after annealing since results from previous chapters indicated the infleunce of porosity on drug loading and release. N_2 isotherms of all samples showed a type II isotherm and H3 hysteresis loop (Figure 6-8), corresponding to particles with aggregate created porosity (Jackel et al. 2014). The presence of hysteresis loop indicates the presence of capillary condensation, due to mesopores characteristic of ND aggregates and OLC aggregates produced from thermal annealing. The lower closure point of the hysteresis loop at high pressure ($P/P_o \sim 0.75$) suggests that the mesopores were wide in size, since pore size affects the location of the capillary condensation (Monson 2012; Duffy et al. 2015).
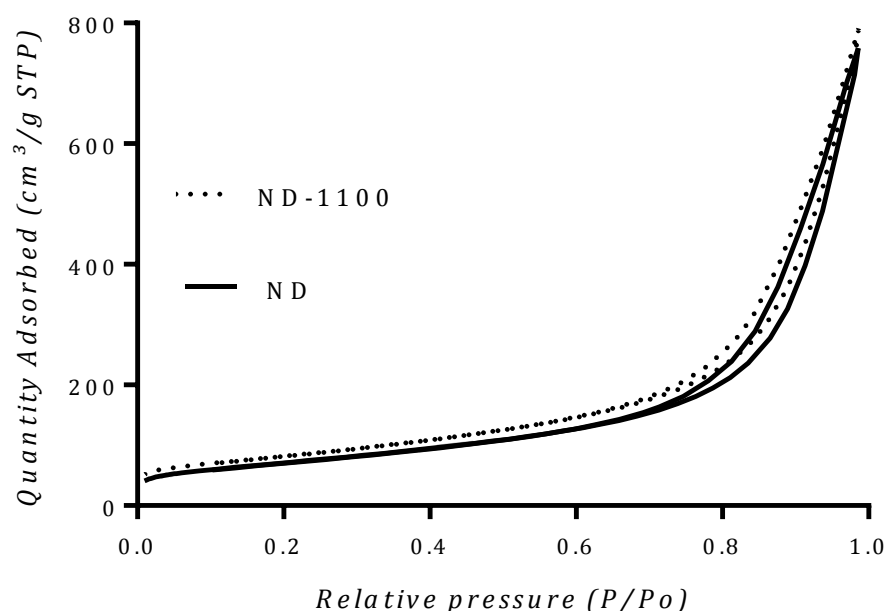
Figure 6-8: N_2 Sorption analysis as compared with ND and ND-1100. Nitrogen sorption isotherms showing Type II isotherm with a H3 hysteresis loop. Data for ND-900 and ND-1000 is not shown for clarity.

Pore size distribution curves (Figure 6-9) were determined using non-local density functional theory (NLDFT) model assuming slit-shaped pores. Pore size distribution curves of ND and ND-1100 samples in the diameter range of 3-30 nm are similar indicating that the agglomerate created porosity in the ND lead to the formation of intra aggregate porosity (Zeiger, Jäckel, et al. 2015).
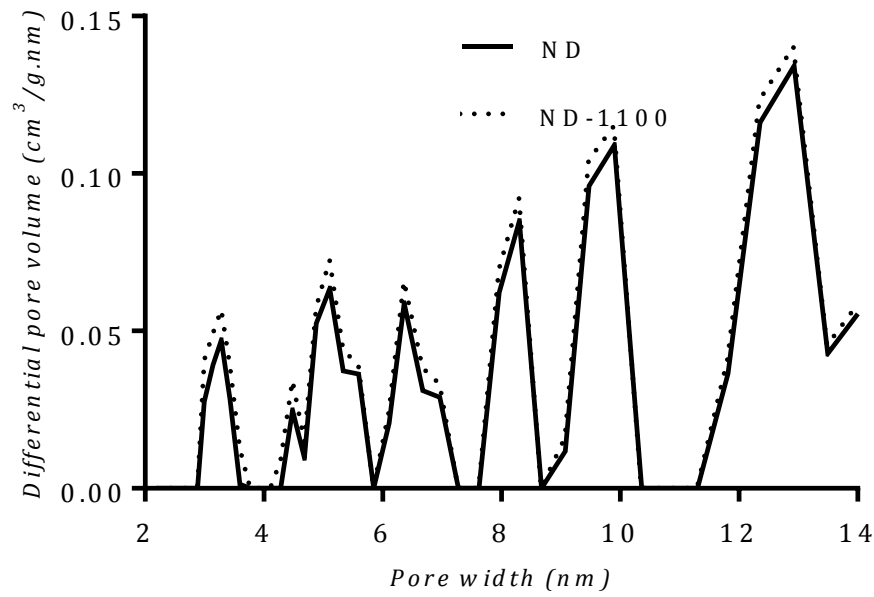
Figure 6-9: Pore size distribution in the range 2-14 nm for ND and ND-1100 determined using non-local density functional theory model. Data for ND-900 and ND-1000 is not shown for clarity.

BET surface area was determined from the nitrogen adsorption isotherm and surface area was found to increase with increase in the annealing temperature (Table 6-5) and could be due to the changes in the density due to loss of functional groups, transformation from sp^3 to sp^2 carbon and change in the particle size. The total pore volume and micropore volume in ND-1100 was also found to be slightly higher than ND and could be due to the opening of some closed pores (Zeiger, Jäckel, et al. 2015). The surface area of ND-1100 is significantly less than that of AC and could be due to the absence of significant microporosity in ND-1100, however, pore volume was found to be higher than and could be due to the higher amount of mesopores present in the aggregates of ND-1100.

Also when compared to the high surface area AC (1000 m^2/g), ND-1100 with a surface area of 293.3 m^2/g, could be disadvantageous as a carrier for drug loading, since drug loading capacity depends on the porosity of the carrier.

Table 6-5: Surface area and pore characteristics calculated from nitrogen sorption analysis.

Sample	Specific surface area [a] (m^2/g)	Total pore volume [b] (cm^3/g)	Micropore volume [b] (cm^3/g)
ND	256.7	1.16	0.018
ND-900	259.2	1.13	0.018
ND-1000	264.5	1.1	0.018
ND-1100	293.3	1.2	0.027

[a] BET specific surface area
[b] Total volume in pores determined by NLDFT theory assuming slit-shaped pores

6.4. Conclusion

In summary, nanodiamonds were annealed to three different temperatures (900, 1000 and 1100 °C). Results from Raman and XPS analysis indicated an increase in sp^2 carbon content with an increase in the annealing temperature. XRD and HRTEM studies suggested the presence of a diamond (sp^3) core surrounded by graphitic (sp^2) shells in nanodiamonds annealed at 1100 °C (ND-1100), suggesting that the transformation from sp^3 carbon to sp^2 carbon occurred in the direction of the outer layer to the core. XPS and FTIR studies also indicated the presence of various oxygen and nitrogen containing functional groups on the surface of ND before and after annealing. The number of functional groups decreased with an increase in the annealing temperature, however were still present even after annealing the ND to 1100 °C. N_2 sorption studies suggested a slight increase in the surface area after annealing to 1100 °C, which could be attributed to a change in the density, while the pore volume and pore size distribution remained almost constant. Post annealed ND-1100 will subsequently be referred to as carbon onion and its application in drug delivery will be investigated in chapter-7.

Chapter 7 **- Application of carbon onion aggregates as a carrier for amorphous drug delivery**

Some of the results presented in this chapter have been presented in the paper:

Miriyala, N., Kirby, D., Pazaras, I., Bo, Y., Ouyang, D., Ye, H (2017), "Synthesis and application of carbon onion for drug delivery" *(in preparation)*

7.1. Introduction

Recently, carbon based materials with aggregate created porosity such as nanodiamond (ND), fullerenes, and carbon nanotubes (CNT) have been studied as potential drug carriers via physical adsorption (Lim et al. 2016; Zhu et al. 2012; Cui et al. 2016); however, the application of these materials in drug delivery is often associated with limitations, such as: 1) requirement of incorporating functional groups in ND to improve the interaction between the drug and carrier (Lim et al. 2016; El-Say 2011; Shenderova et al. 2002), 2) complicated synthesis of fullerenes with very low purity and yield (Mojica et al. 2013; Kyesmen et al. 2016), and 3) toxicity concerns of CNT (Bergin & Witzmann 2013).

Carbon onion or onion-like carbon (OLC) can overcome the aforementioned limitations by its ability to facilitate stronger pi-pi interactions between the aromatic groups of the drug and the graphene rings of OLC (Bielicka et al. 2013; Terrones & Terrones 2003; Costa et al. 2014), without the need of functionalisation. In addition, OLC can be prepared in large quantities via annealing of nanodiamonds (ND) as described in chapter-6 and there are no reports indicating any significant toxicity of OLC (Zeiger, Jäckel, et al. 2015; Pakhira et al. 2016; Bartelmess & Giordani 2014). Also, OLC undergoes aggregation resulting in aggregate created mesoporosity with some microporosity, but compared to AC, OLC exhibits a relatively low surface area which could be disadvantageous since drug loading efficiency is proportional to the surface area of the carrier (Zeiger, Jäckel, et al. 2015). However, OLC can exhibit much stronger drug adsorption compared to AC due to the possible pi-pi interactions between the drug and spherical graphene layers of OLC (Bielicka et al. 2013).

The porosity of OLC aggregates and the possible pi-pi interactions can be advantageous for drug adsorption; therefore, exploring the potential of carbon onion in adsorption and release of drugs is of interest in this study.

Results in the previous chapter demonstrated that annealing of nanodiamonds at 1100 °C resulted in a sample (ND-1100) with the highest content of sp^2 carbon, with onion-like graphene shells surrounding a diamond core (Chapter 6); hence, this sample was studied for drug loading and is referred to as OLC in this chapter. Paracetamol and Ibuprofen were used as model drugs to investigate the adsorption of drugs onto OLC. Adsorption of the drug onto OLC and release of the drug is schematically represented in Figure 7-1.
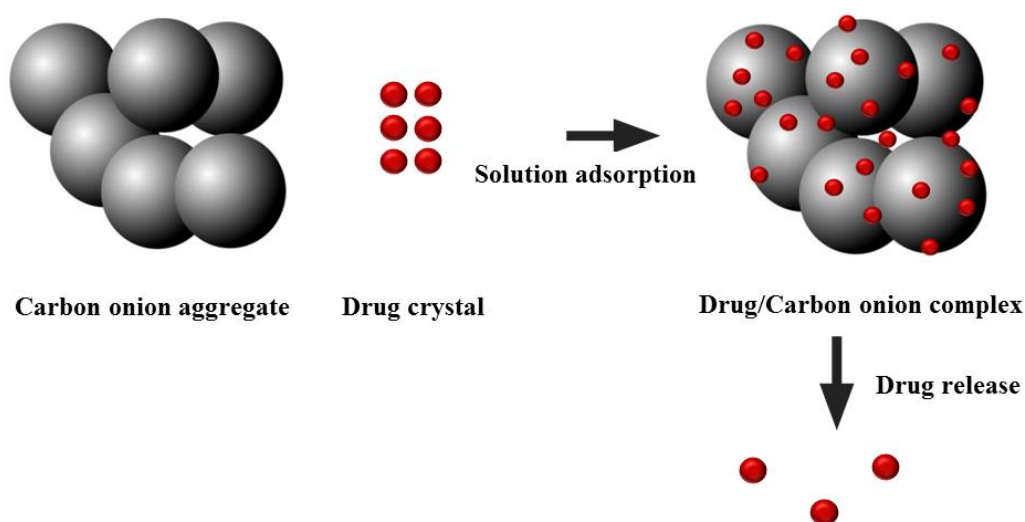
Figure 7-1: Schematic illustration of drug loading and release from carbon onion aggregates.

7.2. Aims and Objectives

The aim of this chapter is to investigate the application of carbon onion aggregates as a vehicle for drug delivery, using paracetamol and ibuprofen as model drugs. To achieve this, the main objectives were to:

1. Investigate the particle size of carbon onion or onion-like carbon (OLC) and study the cytotoxicity of OLC using Caco-2 cells.

2. Perform drug loading using solution adsorption method and study the effect of contact time on the drug loading efficiency.

3. Study the effect of drug characteristics (solubility and loading concentration) on the drug loading efficiency and solid state characteristics using DSC and XRD techniques.

4. Investigate the interactions between drugs and OLC and to understand if the drug loading was due to physical adsorption or chemical interaction using FTIR analysis.

5. To study the drug release from the drug/OLC complex and analyse the porosity of OLC before and after drug loading using nitrogen sorption analysis.

7.3. Results and Discussion

7.3.1. Characterisation of carbon onion

The primary particle size of OLC depends on the primary particle size of ND used; however, the aggregate size depends on various factors, such as annealing temperature and aggregate size of ND used for the synthesis (Moseenkov et al. 2014). Detonation ND usually has a primary particle size of less than 10 nm; however, to reduce the surface energy, these primary particles often form tight aggregates of size 20-30 nm, and these primary aggregates form secondary aggregates of 100 nm to a few micrometres in size. The functional groups that are present on the surface of each ND facilitate the formation of such aggregates. In addition, the presence of van der Waals interactions between these aggregates often leads to the formation of agglomerates (Shenderova et al. 2002). Application of these agglomerates of ND as a starting material in the synthesis of OLC results in the production of aggregates of OLC bonded by graphitic layers (Moseenkov et al. 2014).

OLC used in this study has an aggregate size in the range of 0.45- 21.5 µm (Figure 7-2 and Table 7-1), with nearly 90% of the particles ≤ 10 µm in size. Toxicity studies of these OLC aggregates were performed on Caco-2 cells to determine the feasibility of application of OLC in oral drug formulations. The efficiency of uptake of microparticles is much lower compared to nanoparticles, therefore the risk of toxicity associated with these OLC aggregates can be much lower. However, studies have shown uptake of microparticles of size up to 10 µm by intestinal epithelium, with particles of size < 5 µm transported through lymphatics and particles of size > 5 µm retained in the Peyer's patches (Desai et al. 1996), suggesting the importance of considering the toxicity of

microparticles. Hence, toxicity of OLC aggregates on Caco-2 cells was investigated by

MTT assay.
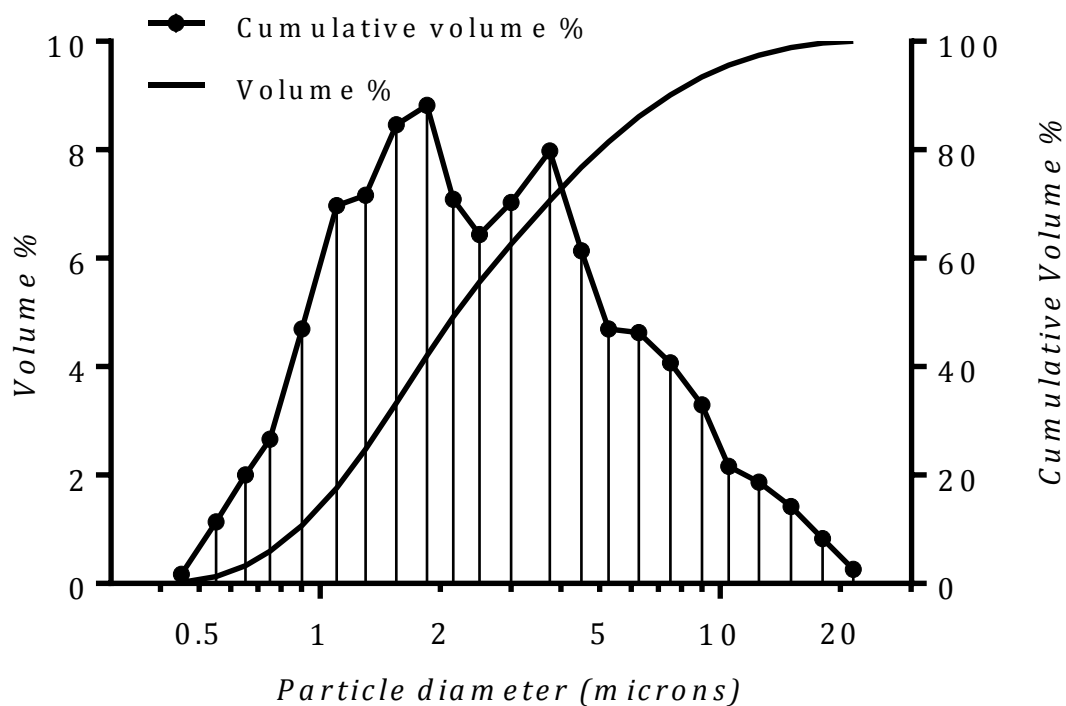
Figure 7-2: Particle volume size distribution of carbon onion obtained from laser diffraction analysis. All samples have a broad particle size distribution in the range of 0.5 to 21.5 µm.

Table 7-1: Particle size characteristics of four different types of carbon onion obtained from laser diffraction analysis.

Material	X10[a] (µm)	X50[b] (µm)	X90[c] (µm)	Volume mean diameter (µm)	Span
Carbon onion	0.88 ± 0.0	2.2 ± 0.0	7.45 ± 0.02	3.37 ± 0.01	2.99 ± 0.01

[a] Particle dimension corresponding to 10% of the cumulative undersize distribution
[b] Median particle dimension
[c] Particle dimension corresponding to 90% of the cumulative undersize distribution

OLC showed a significant effect (P<0.0001, one-way ANOVA) on the survival of Caco-

2 cells, with cell survival reduced when exposed to media containing OLC concentrations

170

≥ 400 µg/mL; however, the cell viability was still over 75% (Figure 7-3), suggesting OLC is a safe drug carrier for oral drug delivery. Cell uptake studies are necessary to determine the exact reasons behind the slight toxicity at high concentrations and also to investigate if the particles are being taken up by the cells. Also, producing OLC aggregates of particle size > 10 µm can eliminate the risk of internalisation by cells.

Additionally, 10% of the OLC used in this study exhibited particle size < 1 µm. Although the objective was to use OLC for oral drug delivery, it is also important to consider the toxicity of inhalation of these particles. Microparticles of size < 1 µm can deposit in the alveoli, where these particles can be taken by macrophages; however, most of the insoluble particles of this size are either exhaled or retained in the lungs (Luckey & Venugopal 1977). Since OLC aggregates are insoluble, the chance of internalisation is low, although synthesis conditions need to be optimised to eliminate the production of aggregates of size < 1 µm, to avoid the possibility of inhalation toxicity.
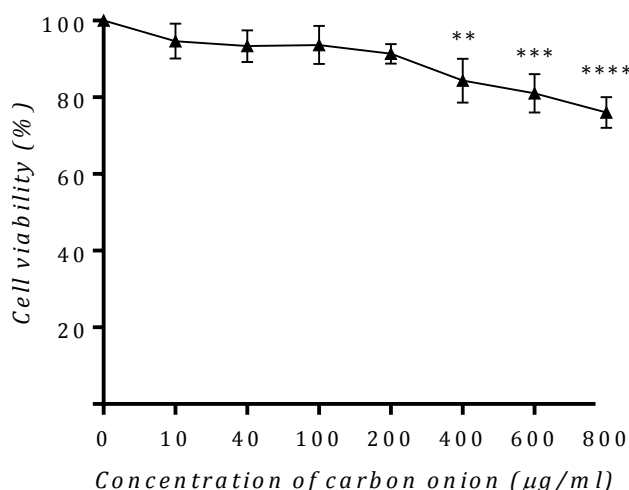
Figure 7-3: Cytotoxicity of carbon onion against Caco-2 cells. MTT assay was used to analyse the survival rate of Caco-2 cells incubated with different concentrations of carbon onion. Statistically significant differences compared to control (0 µg/mL) are noted for $P < 0.05$ (*$P \leq 0.05$; ** $P \leq 0.01$; *** $P \leq 0.001$; **** $P \leq 0.0001$, one-way ANOVA and Dunnett's multiple comparison test). Results are the mean of triplicate experiments ± SD.

7.3.2. Effect of contact time on adsorption of drugs onto carbon onion

Diffusion of drug molecules into the pores of the carrier depends on the contact time between the drug and the carrier (Thomas 1983), as evidenced in chapter-4; therefore, to determine the contact time required for maximum loading, drug loading was performed as described in section-2.7.1.

Results from both PA and IBU loading (Figure 7-4) showed a statistically significant difference in the drug loading of complexes obtained at different contact times ($p < 0.05$ for PA and $p < 0.001$ for IBU; one-way ANOVA). A post hoc test showed that loading increased significantly with an increase in contact time up to 1 hour ($p < 0.05$ for PA and $p < 0.001$ for IBU; one way ANOVA followed by Tukey's test) and there was no statistically significant difference ($p > 0.05$, Tukey's multiple comparison test) in the drug loading of complexes obtained at contact time of 1-4 hours, suggesting that equilibrium was reached at 1 hour and could be attributed to the saturation of adsorption sites after 1 hour of contact time. Therefore, all subsequent loadings were performed for 1 hour. The maximum drug loading efficiency was found to be 15.5% and 36.6% for PA and IBU, respectively. Higher drug loading of IBU is attributed to the higher concentration of IBU present in the loading solution similar to the results obtained with activated carbon (chapter 3) and the loadings achieved for OLC are only slightly less than AC (20.7% for PA and 44.4% for IBU) despite the huge difference in the surface area (surface area of OLC-293.3 and AC-1027.4 m^2/g) and it could be attributed to the higher pore volume of OLC compared to AC (Total pore volume of OLC and AC is 1.2 and 0.81 cm^3/g respectively).

Also, the time taken to reach equilibrium is faster for OLC (1 hour) compared to AC (4 hours) which could be attributed to the significant amount of micro porosity in AC

compared to OLC (micropore volume of AC and OLC is 0.33 and 0.03 cm^3/g respectively) requiring longer time for diffusion due to steric hindrance.
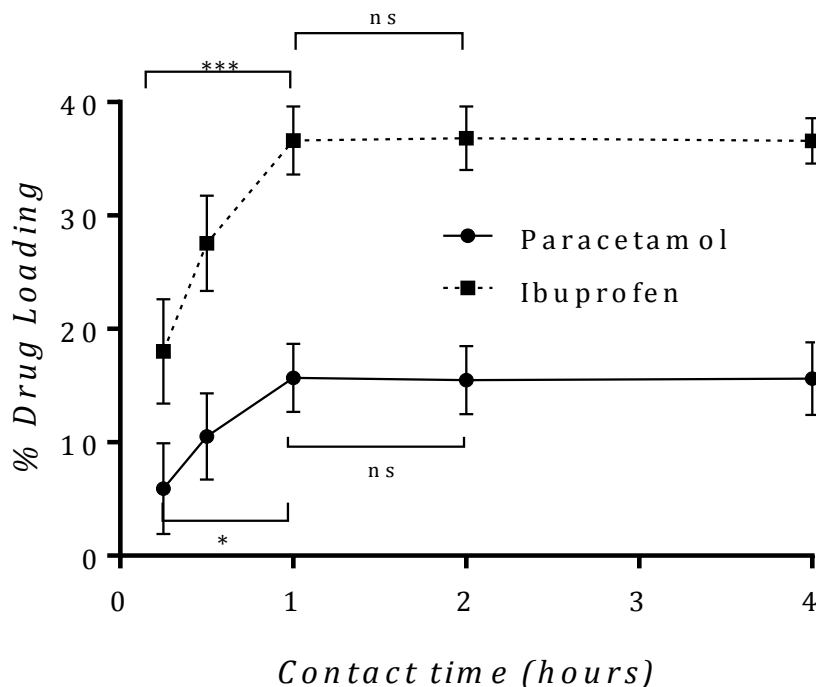
Figure 7-4: Effect of contact time on loading efficiency (stirring speed: 100 rpm; temperature: 20 °C; initial PA and IBU concentration: 150 and 698 mg/mL of ethanol respectively; solution volume: 5 mL; OLC dose: 500 mg). Results are the mean of triplicate experiments ± SD. Statistically significant differences are noted for $p < 0.05$ (*$p < 0.05$, *** $p < 0.001$; ns-no significance; one-way ANOVA and Tukey's multiple comparison test).

7.3.3. Effect of initial concentration of drug on loading efficiency and solid state properties

To determine the effect of concentration of drug in the loading solution on the loading efficiency, drug loading was performed as described in section-2.7.2. UV results indicated that, with the increase in the drug concentration, a statistically significant difference was found in the drug loading ($p < 0.05$ for PA and $p < 0.01$ for IBU; one-way ANOVA). Drug loading reached a maximum when the drug concentration in the loading solution reached the saturation point (Figure 7-5), indicating that drug loading can be

173

increased by increasing the initial concentration of drug in the loading solution similar to the results obtained with activated carbon (chapter-4).

Thermal analysis results of PA/OLC complex with different drug loadings were compared. In the case of PA/OLC complex, complex with a drug loading of 15.5% exhibited a melting peak at 169 °C, suggesting the presence of crystallinity; however, complex with drug loading $\leq$ 11.5% did not show any crystallinity (Figure 7-6), which could indicate that saturation has been reached and any loading higher than 11.5% results in crystallisation of paracetamol which is less than the drug loading achieved with AC (26.8%) without any crystallisation.
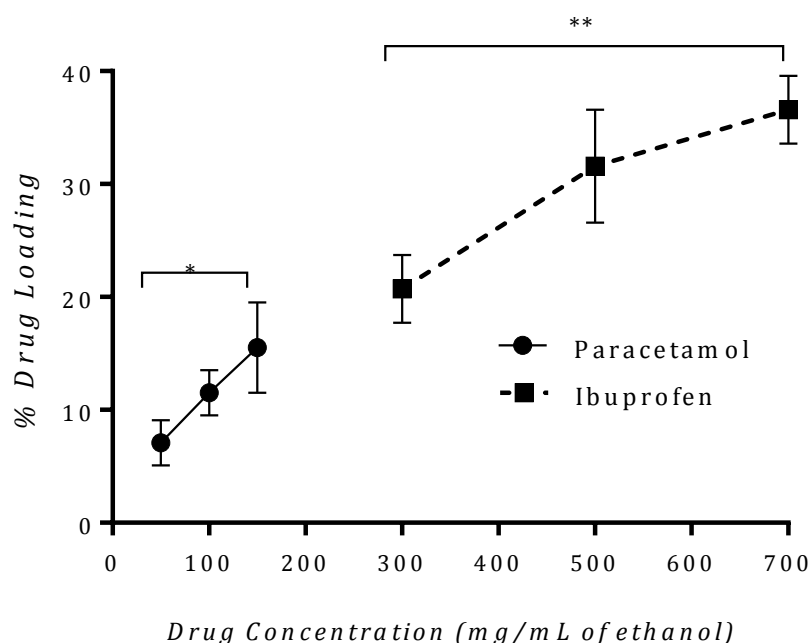
Figure 7-5: Effect of initial drug concentration on loading efficiency (stirring speed: 100 rpm; temperature: 20 °C; solution volume: 5 mL; OLC dose: 500 mg; contact time: 1 hour). Results are the mean of triplicate experiments $\pm$ SD. Statistically significant differences are noted for $p < 0.05$ (* $p < 0.05$, ** $p < 0.01$, one-way ANOVA and Tukey's multiple comparison test).

Solid state characteristics of IBU/OLC complex with different drug loadings were also compared and complex with a drug loading of 31.6% and 36.6% exhibited a melting peak

at 74.8 °C, suggesting the presence of crystallinity; however, complex with loading 20.7%, did not show any crystallinity (Figure 7-7), which could indicate that saturation has been reached and any loading higher than 20.7% results in crystallisation of ibuprofen, which is less than the drug loading achieved with AC (30.2%) without any crystallisation. The ability of AC to load more drug without crystallisation could be attributed to the higher fraction of microporosity in AC (40.7 %) compared to OLC (2.5%), since micropores can only accommodate a single layer of drug, unlike the mesopores that can allow multilayer drug adsorption thereby leading to crystallisation of the drug loaded.
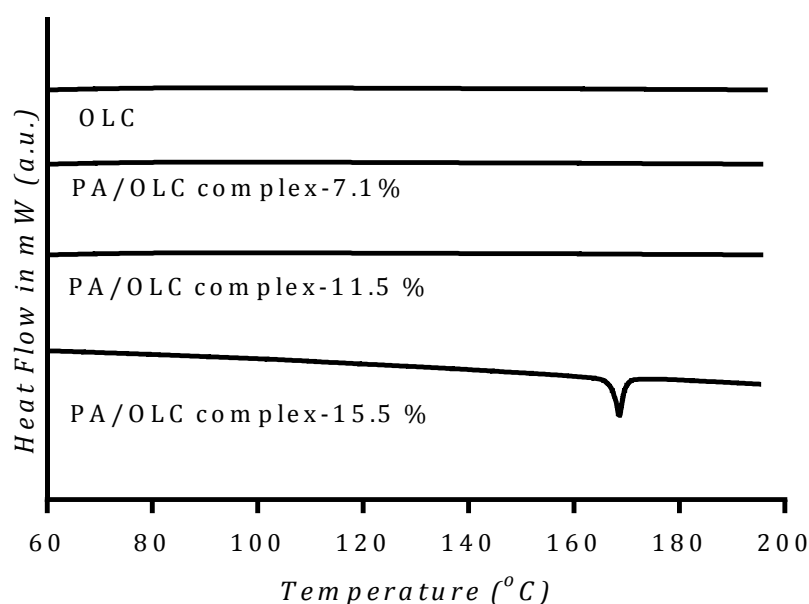
Figure 7-6: DSC curves of carbon onion (OLC) and paracetamol loaded carbon onion (PA/OLC complex) with different drug loadings. Complex with drug loading ≤ 11.5% did not exhibit a melting peak indicating that the drug loaded was completely amorphous. Note that the heat flow scale is arbitrary.
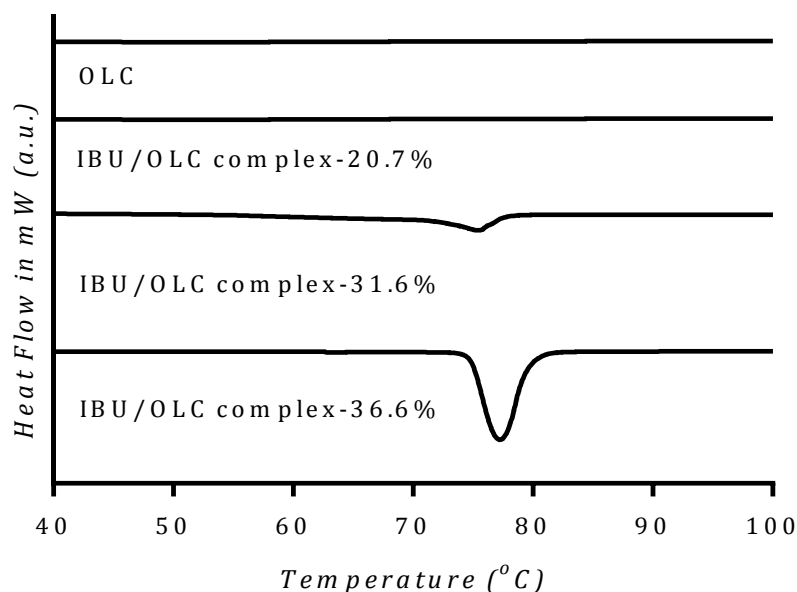
Figure 7-7: DSC curves of carbon onion (OLC) and ibuprofen-loaded carbon onion (IBU/OLC complex) with different drug loadings. Complex with drug loading of 20.7% did not exhibit a melting peak indicating that the drug loaded was completely amorphous. Note that the heat flow scale is arbitrary.

The results from DSC were confirmed by X-ray diffraction studies (Figure 7-8). XRD patterns of PA/OLC complex-11.5% did not show any peaks corresponding to crystalline PA, suggesting that the drug was completely present in an amorphous form. Similarly, IBU/OLC complex-20.7% did not show any diffraction pattern corresponding to crystalline IBU. Therefore, all subsequent studies were performed on PA/OLC complex-11.5% and IBU/OLC complex-20.7% only, which showed no crystallinity in the sample.

Results from DSC and XRD studies suggest that the optimum initial drug concentration to achieve drug/carrier complex without any crystallisation of drug is 100 mg/mL and 300 mg/mL, for PA and IBU, respectively, to achieve a drug loading of 11.5% and 20.7% respectively, indicating the effect of initial drug concentration on the loading efficiency and solid state characteristics.

Similar to AC, loading achieved in the case of OLC for PA is lower than that achieved for IBU and could be due to the higher melting point of PA compared to IBU since drugs with higher melting point readily undergo crystallisation (Brent 2015). Possible hydrophobic interactions between IBU and OLC could also be responsible for the higher stability of the loaded IBU compared to PA.
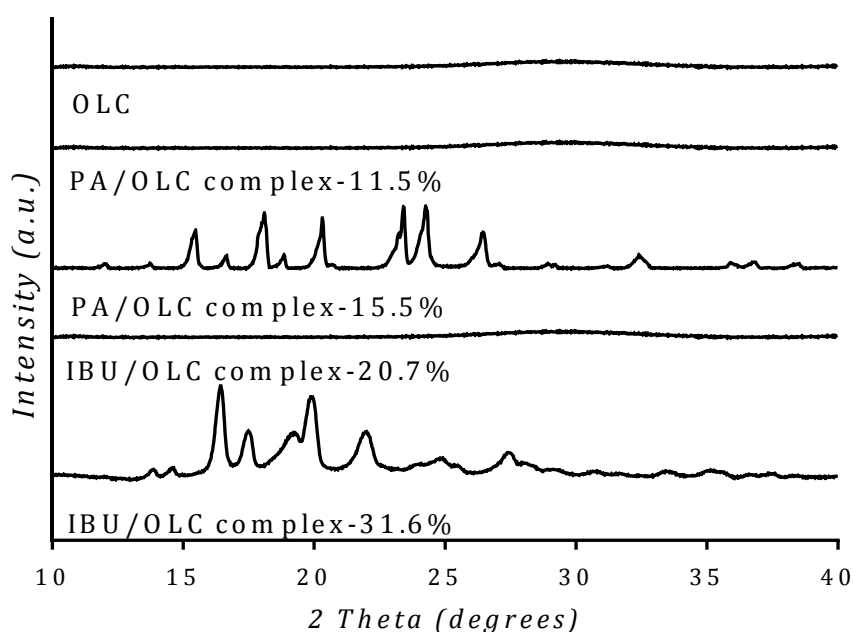
Figure 7-8: XRD patterns of carbon onion (OLC) paracetamol-loaded carbon onion (PA/OLC complex) and ibuprofen-loaded carbon onion (IBU/OLC complex) with different drug loadings. Note that the intensity cale is arbitrary.

7.3.4. Drug-carrier interactions

FTIR studies suggested that ND contained functional groups such as C=O, O-H, and N-H (Chapter-6). Post-annealing in OLC (ND-1100), these functional groups are still present, but have reduced in intensity. Therefore, it is important to consider possible chemical interactions between drugs and OLC, since these interactions can affect the chemical nature and stability of drugs. FTIR spectra of PA/OLC complex -11.5% and PA/OLC phy mix containing an equivalent amount of drug as that of the complex (Figure

7-9) showed peaks corresponding to an NH amide band stretch at 3320 cm^{-1} and a broad phenolic OH stretch at 3129 cm^{-1}, similar to that of Pure PA. Spectra of PA/OLC complex did not show any significant shift in the existing peaks or new peaks, confirming physical adsorption of PA. Also, spectra of IBU/OLC complex-20.7% and IBU/OLC phy mix containing an equivalent amount of drug as complex showed peaks corresponding to carbonyl CO stretch at 1694 cm^{-1}, similar to pure IBU, and no new peaks were found, indicating the absence of any chemical interactions (Figure 7-10).
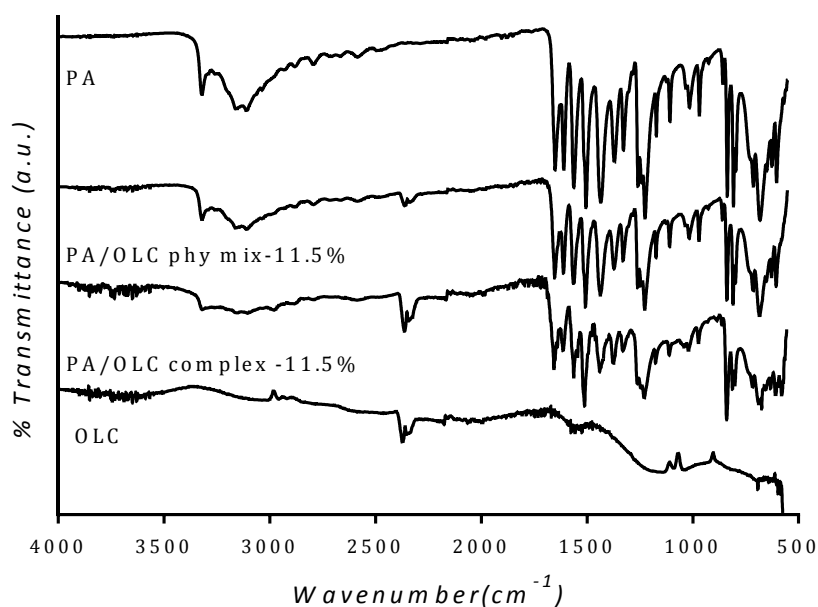
Figure 7-9: FTIR spectra of paracetamol (PA), carbon onion (OLC), paracetamol-loaded carbon onion (PA/OLC complex) and physical mixture of paracetamol and carbon onion (PA/AC phy mix). No chemical interactions could be detected between PA and OLC. Note that the transmittance scale is arbitrary.
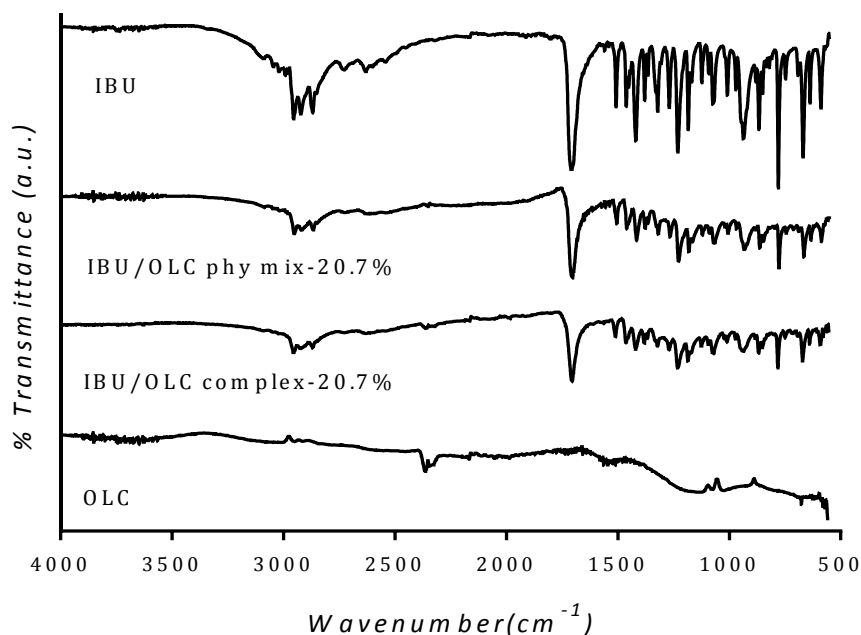
Figure 7-10: FTIR spectra of ibuprofen (IBU), carbon onion (OLC), ibuprofen-loaded carbon onion (IBU/OLC complex) and physical mixture of ibuprofen and carbon onion (IBU/OLC phy mix). No chemical interactions could be detected between IBU and OLC. Note that the transmittance scale is arbitrary.

7.3.5. *In vitro* drug release studies

Release profiles of pure drug and drug/OLC complex are shown in Figure 7-11 and Figure 7-12. Drug release from PA/OLC complex in the absence of SDS was incomplete, with only 11.4 % release in 10 min and could be due to poor wettability of carbon onion (particles were found to sticking to the surface of the vessel). Similar to PA/OLC complex, drug release from IBU/OLC complex in the absence of SDS was incomplete; however, this was slightly higher, with 17.4% release in 10 min and could be attributed to higher drug loading in IBU/OLC complex. In the presence of SDS, drug release from PA/OLC complex was complete in 15 min, and was significantly faster (p<0.0001, two-way ANOVA) compared to pure PA. Similarly, drug release of IBU/OLC complex was

179

complete in 30 min and significantly higher (p<0.0001) compared to pure crystalline IBU in the presence of SDS.

Compared to the pure drug, faster release in drug/OLC complex could be attributed to the amorphous nature of the drug loaded in complex and higher surface area that is in contact with the dissolution media, supporting the advantage of using OLC in amorphous drug delivery.

Drug release profiles obtained in the presence of SDS for PA and IBU were fitted with simplified Higuchi model based on Fick's law of diffusion which describes drug release from an insoluble matrix (Costa et al. 2001; Izquierdo-Barba et al. 2005).Higuchi square root of time plots for both drug loaded complexes in Figure 7-13, display a two-step release with an initial burst effect which could be attributed to the drug release from superficial pores followed by a slow release which could be attributed to the drug release from deeper micropores. Rate constants also suggest that drug release from OLC was slightly slower than that of AC and could be due to stronger adsorption between drug and OLC (Table 7-2).
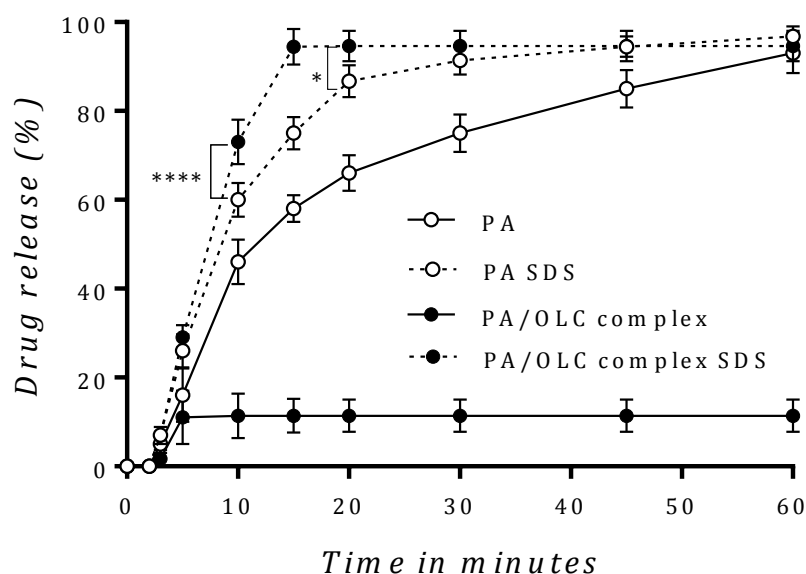
Figure 7-11: Dissolution profiles of paracetamol (PA) and paracetamol-loaded carbon onion (PA/OLC complex) determined at pH 5.8. Curves PA-SDS and PA/OLC complex-SDS represent dissolution profiles determined in media containing 1% SDS. Statistically significant differences are noted for P < 0.05 (*P < 0.05; **** P < 0.0001, two-way ANOVA and Bonferroni's multiple comparison test). Results are the mean of triplicate experiments ± SD.
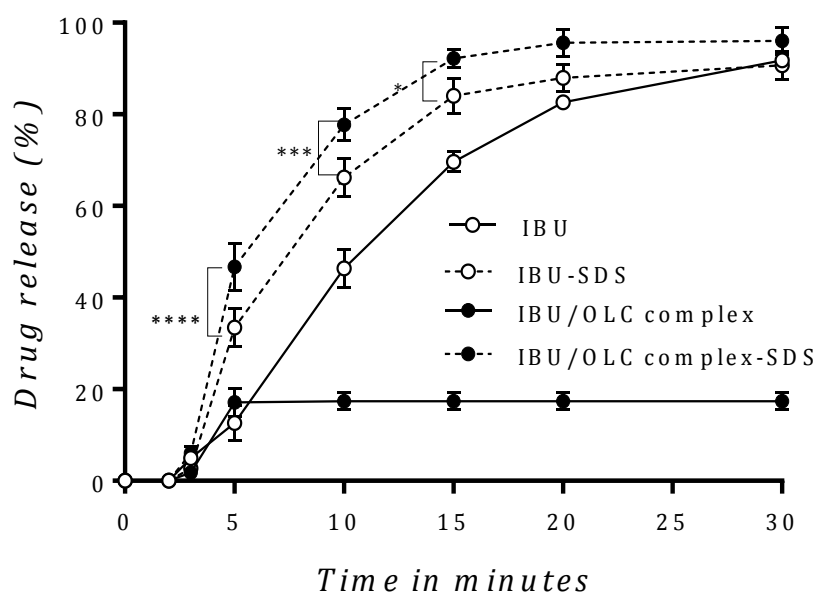
Figure 7-12: Dissolution profiles of ibuprofen (IBU) and ibuprofen-loaded carbon onion (IBU/OLC complex) determined at pH 5.5. Curves IBU-SDS and IBU/OLC complex-SDS represent dissolution profiles determined in media containing 1% SDS. Statistically significant differences are noted for P < 0.05 (*P < 0.05; *** P < 0.001; **** P < 0.0001, two-way ANOVA and Bonferroni's multiple comparison test). Results are the mean of triplicate experiments ± SD.

181
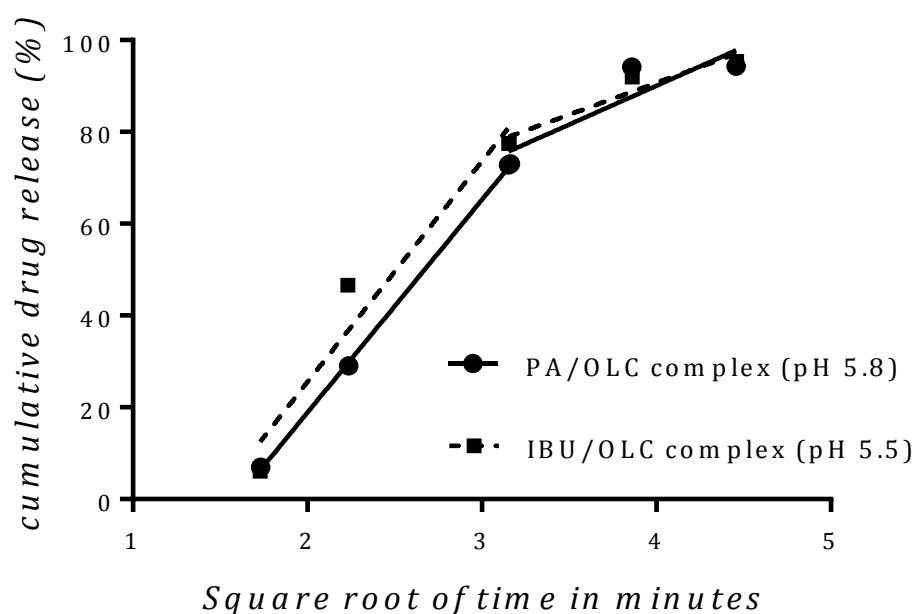
Figure 7-13: Two step regression linear utilising Higuchi's square root of time plot for drug release from complex in the presence of SDS. In brackets pH of the dissolution medium. Each point represents the mean of n=3 determinations.

Table 7-2: Kinetic parameters of drug release from paracetamol and ibuprofen loaded carbon onion

Sample	Higuchi diffusion two step		
	Duration	Rate constant	Linear regression coefficient
PA/OLC complex at pH 5.8	3-10 min	46.34	0.999
	10-20 min	16.91	0.797
IBU/OLC complex at pH 5.5	3-10 min	48.07	0.94
	10-20 min	13.87	0.916

7.3.6. Porosity analysis of carrier before and after drug loading

Adsorption isotherms and pore size distribution curves of OLC before and after drug

loading are shown in Figure 7-14 and Figure 7-15, with the data from N_2 sorption studies

summarised in Table 7-3. The adsorption/desorption isotherm of OLC exhibited a typical

type II isotherm and H3 hysteresis loop, corresponding to aggregate created porosity. The pore size distribution of pure OLC shows the presence of pores in the range of 2-14 nm. For PA/OLC physical mixture, a reduction in surface area and pore volume was observed, but the pore size distribution was similar to that of OLC, indicating that there was no drug present in the pores of OLC. However, for IBU/OLC physical mixture, pores in the range of 2-5 nm completely disappeared and the exact reason is not clear but could be due to the adsorption of IBU on OLC due to hydrophobic interactions resulting in some pores being blocked. Post loading, in PA/OLC complex, a reduction in the pore size was observed in pores in the range of 10-14 nm and the pore size distribution broadens in the range of 7.5-10.5 nm, suggesting the adsorption of PA into the pores of OLC. In the case of IBU/OLC complex, pores in the range of 2-5 nm completely disappeared and the pore size distribution broadens for pores in the range of 5-14 nm, which could be due to the reduction of pore size from drug loading. Also, the reduction in pore volume and surface area from IBU loading is much higher than that for PA loading indicating the higher affinity of IBU towards AC possibly due to hydrophobic interactions.

Table 7-3: Surface areas and pore volumes obtained from Nitrogen sorption of carbon onion (OLC), ibuprofen-loaded carbon onion (IBU/OLC complex) and paracetamol loaded carbon onion (PA/OLC complex)

Sample	Specific surface area[a] (m^2/g)	Total pore volume (cm^3/g)	Micro pore volume[b] (cm^3/g)
OLC	293.3	1.2	0.03
PA/OLC complex-11.5%	138.4	0.73	0.002
PA/OLC phy mix-11.5%	210.1	0.86	0.015
IBU/OLC complex-20.7%	46.1	0.27	0
IBU/OLC phy mix-20.7%	65.4	0.38	0

[a] Calculated by BET method
[b] Calculated by NLDFT method
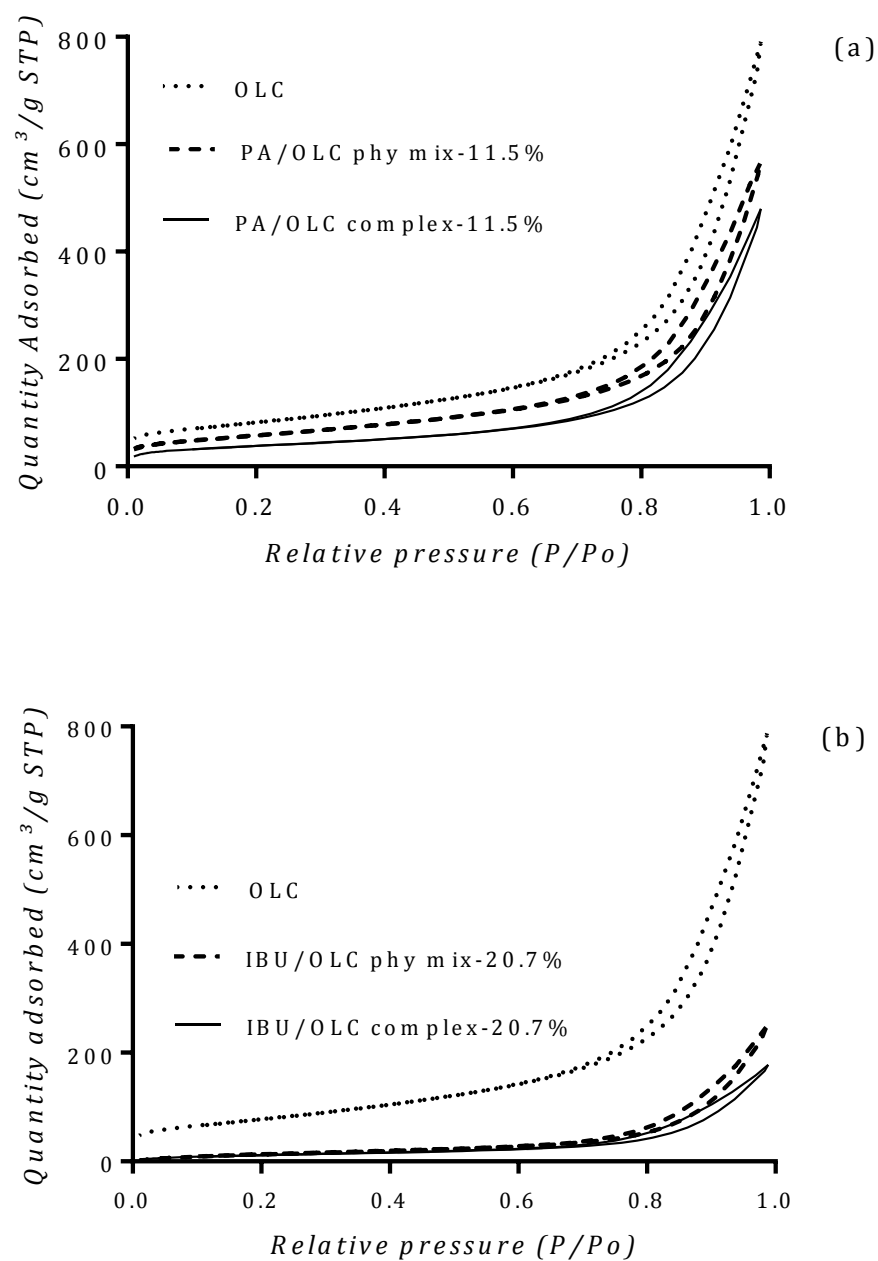
Figure 7-14: Nitrogen adsorption/desorption isotherms at 77 K of carbon onion (OLC) before and after drug loading showing, (a) paracetamol loaded carbon onion (PA/OLC complex) and physical mixture of paracetamol and carbon onion (PA/OLC phy mix); (b) ibuprofen-loaded carbon onion (IBU/OLC complex) and physical mixture of ibuprofen and carbon onion (IBU/OLC phy mix).
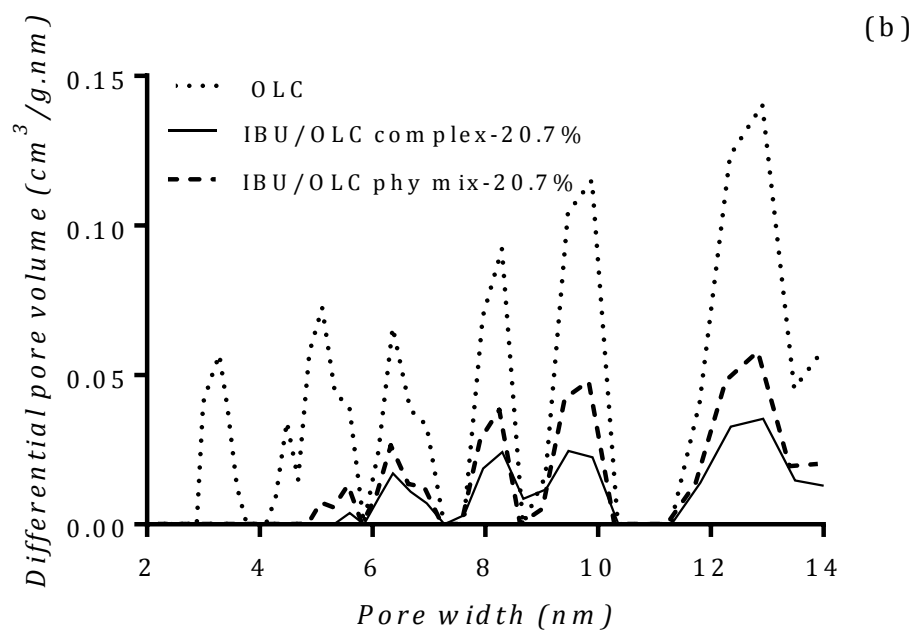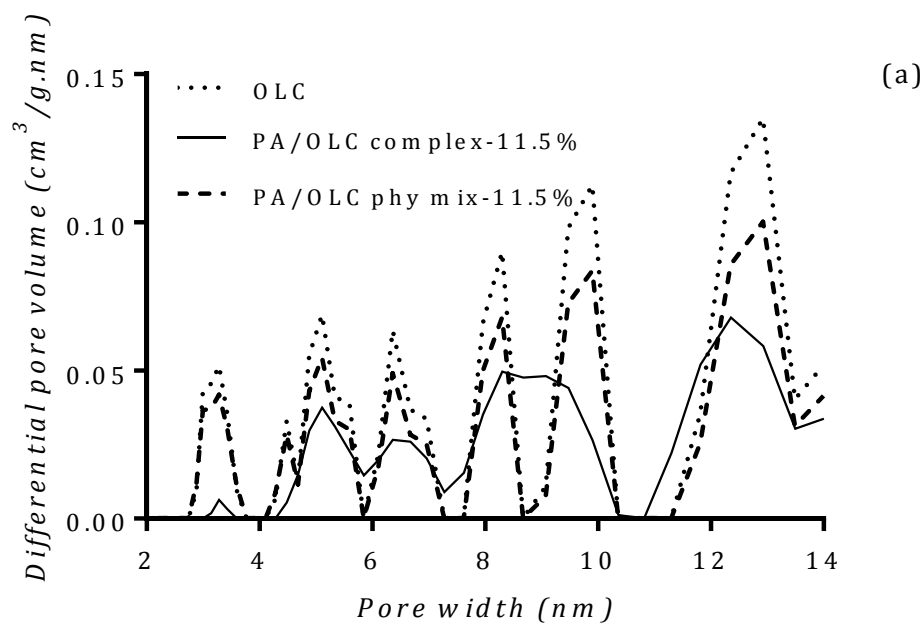
Figure 7-15: Pore size distribution (2-14nm) calculated using NLDFT slit-shaped pore model of carbon onion (OLC) before and after drug loading showing- (a) paracetamol-loaded carbon onion (PA/OLC complex) and physical mixture of paracetamol and carbon onion (PA/OLC phy mix); (b) ibuprofen-loaded carbon onion (IBU/OLC complex) and physical mixture of ibuprofen and carbon onion (IBU/OLC phy mix).

7.4. Conclusions

The current study investigated the application of carbon onion (OLC) aggregates as drug carriers using paracetamol and ibuprofen as model drugs. OLC aggregate microparticles exhibited very low cytotoxicity on Caco-2 cells with cell viability over 80% at all the concentrations tested (10–800 µg/mL). The solution adsorption method was employed for drug loading, as with activated carbon in previous chapters, and the results demonstrated that loading efficiency increased with an increase in the contact time, reaching a maximum loading (15.5% for PA and 36.6% for IBU) after one hour for both drugs and no further increase could be observed even after 4 hours, suggesting that equilibrium has been achieved after one hour.

To understand the effect of initial drug concentration on the loading efficiency, drug solutions of varying concentrations were used for loading at a constant temperature. These studies have shown, that with an increase in initial drug concentration, loading efficiency increased reaching maximum when the initial drug concentration reached the saturation point.

Results from thermal analysis and diffraction studies suggested that both PA/OLC complex and IBU/OLC complex with the highest loading showed crystallinity. The drug was found to be completely amorphous in PA/OLC complex and IBU/OLC complex with the loading of 11.5% and 20.7%, respectively, indicating that the concentration of drug in the loading solution needs to be optimised, to achieve complex without any crystalline drug. Furthermore, these maximum levels for amorphous drug loading were less than those seen with AC (26.8% and 30.2% for PA and IBU respectively) and could be due to lower surface area of OLC compared to AC, however the drug loading achieved for OLC were relatively high and could be due to higher pore volume of OLC compared to AC.

Drug release kinetics were studied using USP II dissolution method in sodium phosphate buffer with and without SDS. About 11.4% and 17.1% of the total loaded PA and IBU, respectively, was released; however, this was incomplete due to poor wettability of OLC in the absence of SDS. Complete drug release was achieved in the presence of SDS and dissolution rate was higher than that of the pure crystalline drug, establishing that drug loading was reversible and also faster due to amorphous nature of the drug loaded into OLC, suggesting that these results are promising for the development of carbon onion based drug delivery systems.

Chapter 8 **-General discussion and conclusions**

Drug solubility and dissolution play a crucial role in the development of drug delivery systems in order to achieve optimum bioavailability. Conversion of crystalline forms of drugs to the amorphous form has previously been found to improve the solubility and dissolution profile of drugs, due to the structural disorder and higher internal energy of amorphous forms. However, amorphous forms have poor stability and tend to convert into crystalline forms (Fasinu et al. 2011; Hancock & Parks 2000). Drug loading into porous materials has shown great potential in stabilising the amorphous form of drugs due to the restricted pore space and drug-carrier interactions; however, porous materials that have been investigated so far are associated with limitations, such as high cost of production, poor stability, high toxicity, and low loading capacity (Salonen, Laitinen, et al. 2005; Heikkilä et al. 2010; Ng et al. 2013). Therefore, it is important to explore porous materials that can overcome the aforementioned limitations.

Recently, several porous carbon materials have been studied as carriers for drug delivery applications due to their high surface area, chemical inertness, and high chemical and thermal stability (X. Wang et al. 2011; Chen et al. 2016). Amongst those carbon materials, activated carbon (AC) was found to be inexpensive, commercially available with high surface area to volume ratio and with clinical applications as an antidote, which can favour the development of an efficient, cost-effective and safe carrier for oral drug delivery. AC has been previously investigated as a drug carrier for lymphatic targeting (Guo et al. 2011); however, there is no information on the drug loading efficiency, drug release kinetics, and application for amorphous drug delivery.

In addition, carbon onion (OLC) is a novel carbon material that consists of several spherical graphene shells, which can result in possible pi-pi interactions with aromatic molecules, and also exhibits aggregate created pores, which can be potential adsorption

sites for drug molecules (Zeiger, Jäckel, et al. 2015; Reinert et al. 2015). OLC has been studied for its ability to cross the blood brain barrier and for application in cellular imaging, due to their ability to undergo cellular internalisation (Bartelmess & Giordani 2014; Pakhira et al. 2016). However, there is no specific research on the application of OLC as a drug carrier.

Therefore, investigating the potential of activated carbon and carbon onion as amorphous drug carriers for oral delivery formed the basis of this thesis.

8.1. Activated carbon: Optimisation of drug loading method and factors affecting drug loading and release

Activated carbon exhibited low toxicity on Caco-2 cells, indicating its safety for application in drug delivery. Paracetamol (PA) and Ibuprofen (IBU) were used as model drugs to investigate drug loading using solution adsorption method. Saturated drug ethanol solution was used as loading solution; the drug loading achieved and solid state characteristics of the drug in the complexes were different for PA and IBU, which was attributed to the difference in the initial concentration of drug in the loading solution indicating that application of saturated drug solution is not an ideal method to achieve completely amorphous drug loading. Also, *in vitro* release revealed that drug release was incomplete, which is attributed to the poor wettability of AC resulting in inaccessibility of the dissolution medium to the deeper pores. However, drug release was complete in the presence of sodium dodecyl sulphate (SDS) in the dissolution medium for both PA/AC and IBU/AC complexes, and is attributed to the reduction in surface tension between AC and dissolution medium. SDS molecules in the dissolution media could also be displacing the adsorbed drug molecules resulting in complete drug release since studies have reported that small molecules are displaced by larger molecules due to

competitive and displacement adsorption (Kawaguchi et al. 1986). Also, the release was faster compared to the pure crystalline drug and is attributed to the amorphous nature of the drug loaded and a higher surface that is in contact with the dissolution media.

To achieve completely amorphous loading and to improve the drug release from AC, factors affecting drug loading and release were subsequently studied. Results revealed that drug loading is influenced by a range of factors, such as the loading method, initial concentration of drug in the loading solution, temperature, contact time and carrier dose, indicating that these factors need to be taken into consideration to achieve reproducibility. Solution adsorption followed by centrifugation was found to be the optimum method to achieve a complex with the least drug crystallinity compared to rotary evaporation and solution adsorption-filtration methods. Also, drug loading without any drug crystallinity was achieved when the initial concentration of the drug in the loading solution was optimised. However, the optimum concentration was different for PA and IBU, indicating the influence of the chemical nature of the drug and the requirement of optimisation of loading method for different drugs. Also, no chemical interactions could be detected between the drug and AC even at higher drug loading, supporting the physical adsorption of the drug.

To improve the drug release, AC was surface treated and drug release was found to increase with an increase in the surface oxygen content, indicating that modification of surface chemistry improved the wettability thereby, improving the drug release. However, an increase in the surface oxygen content also resulted in the decrease in porosity, thereby leading to reduced drug loading, indicating that the surface treatment needs to be optimised to achieve improved wettability without reducing the drug loading capacity.

In addition to surface chemistry, porosity was also found to affect the drug loading and release. PA loading into four different types of AC with different porosity characteristics revealed that drug loading increased with an increase in the total pore volume, whilst drug release decreased with an increase in the micropore volume fraction, indicating that total drug release could be improved when AC with low microporosity is used.

8.2. Carbon onion: synthesis and application as carrier for amorphous drug delivery

To synthesise carbon onion for application in drug delivery, nanodiamonds were annealed to three different temperatures and results showed the presence of a diamond core surrounded by graphitic shells when annealed at 1100 °C; this was, therefore, referred to as carbon onion (OLC), and its application in drug delivery was investigated.

OLC exhibited low toxicity on Caco-2 cells, indicating its safety for application in drug delivery. Drug loading studies indicated the ability of OLC to achieve complete amorphous loading; however, drug release was incomplete in the absence of SDS, similar to that of AC, due to the poor wettability of OLC. Drug release was complete in the presence of SDS and was faster compared to the pure crystalline drug, indicating the potential of OLC as an amorphous drug carrier. Also, no chemical interactions could be detected between the drug and OLC, indicating the safety of loading into OLC without changing the chemical nature of the drug.

8.3. Activated carbon vs Carbon onion as a drug carrier

Drug loading was found to reach an equilibrium faster in the case of OLC compared to AC and could be due to the significant amount of micro porosity in AC, requiring a longertime for diffusion due to steric hindrance.

Furthermore, when drug loading was performed using saturated drug solution, drug loadings achieved in OLC were less than those seen with AC and could be due to the lower surface area of OLC compared to AC; however, the drug loadings achieved for OLC were relatively high, despite the huge difference in the surface area, and could be due to the higher pore volume of OLC compared to AC.

Post optimisation of drug loading method, the maximum drug loading achieved without any crystallinity was higher in AC compared to OLC, and this ability of AC to load more drug without crystallisation could be attributed to the higher fraction of microporosity in AC compared to OLC, since micropores can only accommodate a single layer of drug, unlike the mesopores that can allow multilayer drug adsorption resulting in crystallisation of the drug loaded. However, if the microporosity of the carrier is responsible for the higher capacity of stabilisation of amorphous drug, reducing the microporosity of AC to improve drug release could be disadvantageous, indicating that modifying the surface chemistry of AC is the ideal method to achieve complete drug release.

Also, drug release in the absence of SDS was much lower in the case of OLC compared to AC, indicating the more hydrophobic nature of OLC. However, in the presence of SDS, drug release from both AC and OLC was very similar and faster compared to the pure crystalline drug.

Nevertheless, both AC and OLC were found to be promising materials for application as amorphous drug carriers, especially AC, with its loading capacity and ability to stabilise amorphous drug similar to that of ordered mesoporous materials such as silica despite the disordered porous structure of the former. Additionally, AC is inexpensive, non-toxic, commercially available and is clinically used indicating the feasibility for commercial development of porous carrier based formulations.

8.4. Final conclusions

To summarise, in relation to the thesis aims and objectives, these studies have shown that:

1. Activated carbon and carbon onion exhibited low cytotoxicity in Caco-2 cells, indicating their safety for application in oral drug delivery.

2. PA and IBU were loaded successfully into AC and OLC using solution adsorption followed by centrifugation method.

3. Maximum loadings of 26.8% (PA) and 30.2% (IBU) without any drug crystallinity were achieved for AC, whilst for OLC the loadings were 11.5% (PA) and 20.7% (IBU).

4. Drug loading efficiency and solid state characteristics of the drug loaded in both carriers were influenced significantly by the initial concentration of drug in the loading solution and the chemical nature of the drug.

5. Drug release from both activated carbon and carbon was completely reversible and faster compared to the pure crystalline drug, indicating the potential of activated carbon and carbon onion as porous carriers for amorphous drug delivery.

8.5. Future work

The wettability of AC and OLC needs to be improved to further optimise the drug release. Surface treatment of activated carbon with nitric acid and sulphuric acid mixture resulted in loss of porosity, whereas treatment with nitric acid alone at room temperature did not show significant difference in the drug release; boiling with nitric acid under reflux for

different durations could be attempted to increase the surface oxygen content, without resulting in loss of porosity. Also, to improve the drug loading capacity of OLC, chemical activation to create porosity in the shells of OLC could be performed to increase the porosity, which can result in an increase in the drug loading. Residual solvent content in the carriers, post loading needs to be determined and other non-solvent drug loading methods can be investigated. Also, atomic force microscopy and polarised light microscopy could be employed to visually identify sites of drug adsorption. Long term stability studies need to be performed to understand the ability of these carriers to maintain the amorphous nature of the drug on storage. In order to further understand the toxicity of AC and OLC, cell internalisation studies need to be employed.

References

Ahern, R.J. et al., 2013. Comparison of fenofibrate mesoporous silica drug-loading processes for enhanced drug delivery. *European Journal of Pharmaceutical Sciences*, 50(34), pp.400–409. Available at: http://dx.doi.org/10.1016/j.ejps.2013.08.026.

Ahnert H. A.; Pinto, N. G., F.. A., 2009. A study of the influence of hydrophobicity of activated carbon on the adsorption equilibrium of aromatics in non-aqueous media. *Adsorption*, 43(10), pp.3421–3429.

Andersson, J. et al., 2004. Influences of material characteristics on ibuprofen drug loading and release profiles from ordered micro- and mesoporous silica matrices. *Chemistry of Materials*, 16(21), pp.4160–4167.

Andersson, J. & Rosenholm, J., 2008. Mesoporous Silica : An Alternative Diffusion Controlled Drug Delivery System. *Topics in Tissue Engineering*, pp.1–19.

Arce, F.T. et al., 2008. Chapter Twenty - Self-Assembled Monolayers on C(0001). In E. J. Bottani & J. M. D. Tascón, eds. *Adsorption by Carbons*. Amsterdam: Elsevier, pp. 513–529. Available at: http://www.sciencedirect.com.openathensproxy.aston.ac.uk/science/article/pii/B97800804 44642500249.

Atieh, M.A. et al., 2010. Effect of carboxylic functional group functionalized on carbon nanotubes surface on the removal of lead from water. *Bioinorganic Chemistry and Applications*, 2010.

Baeza-Squiban, A., Lacroix, G. & Bois, F.Y., 2011. Experimental Models in Nanotoxicology. In P. Houdy, M. Lahmani, & F. Marano, eds. *Nanoethics and Nanotoxicology*. Berlin, Heidelberg: Springer Berlin Heidelberg, pp. 63–86. Available at: http://dx.doi.org/10.1007/978-3-642-20177-6_3.

Banker, G.S., Siepmann, J. & Rhodes, C., 2002. *Modern Pharmaceutics, Fourth Edition*, CRC Press. Available at: https://books.google.co.uk/books?id=s1-BerNQAtsC.

Bartelmess, J. & Giordani, S., 2014. Carbon nano-onions (multi-layer fullerenes): Chemistry and applications. *Beilstein Journal of Nanotechnology*, 5(1), pp.1980–1998.

Bergin, I.L. & Witzmann, F.A., 2013. Nanoparticle toxicity by the gastrointestinal route: evidence and knowledge gaps. *International journal of biomedical nanoscience and nanotechnology*, 3(1–2), p.10.1504/IJBNN.2013.054515. Available at: http://www.ncbi.nlm.nih.gov/pmc/articles/PMC3822607/.

Bhatnagar, A. et al., 2013. An overview of the modification methods of activated carbon for its water treatment applications. *Chemical Engineering Journal*, 219, pp.499–511. Available at: http://www.sciencedirect.com/science/article/pii/S1385894712016786.

Bielicka, A. et al., 2013. Carbon materials as new nanovehicles in hot-melt drug deposition. *Journal of Physics Condensed Matter*, 25(35). Available at: http://www.scopus.com/inward/record.url?eid=2-s2.0-84881530950&partnerID=40&md5=baf40bd00643399c2124b7d10577abfb.

Biswas, S. et al., 2013. Polymeric Micelles for the Delivery of Poorly Soluble Drugs. In *Drug Delivery Strategies for Poorly Water-Soluble Drugs*.

Blazkova, I. et al., 2014. Fullerene as a transporter for doxorubicin investigated by analytical methods and in vivo imaging. *Electrophoresis*, 35(7), pp.1040–1049.

196

Boehm, H.-P., 2008. Chapter Thirteen - Surface Chemical Characterization of Carbons from Adsorption Studies. In E. J. Bottani & J. M. D. Tascón, eds. *Adsorption by Carbons*. Amsterdam: Elsevier, pp. 301–327. Available at: http://www.sciencedirect.com.openathensproxy.aston.ac.uk/science/article/pii/B97800804 44642500171.

Brent, R., 2015. Investigating Differences in Solubilility Between Crystalline and Amorphous Forms of Pharmaceuticals. In *Astrazeneca*. Available at: https://docs.google.com/viewer?url=http://www.mmsconferencing.com/pdf/eyp/r.brent.pdf.

Bruce, D.W., Walton, R.I. & Hare, D.O., 2010. *Porous Materials* D. O. H. Duncan W Bruce Richard I Walton, ed., Hoboken, NJ, USA: John Wiley & Sons. Available at: http://site.ebrary.com/lib/aston/docDetail.action?docID=10469667.

Burguete, P. et al., 2012. Pore Length Effect on Drug Uptake and Delivery by Mesoporous Silicas. *ChemPlusChem*, 77(9), pp.817–831. Available at: http://dx.doi.org/10.1002/cplu.201200099.

Cano, H., Gabas, N. & Canselier, J.P., 2001. Experimental study on the ibuprofen crystal growth morphology in solution. *Journal of Crystal Growth*, 224(3–4), pp.335–341. Available at: http://www.sciencedirect.com/science/article/pii/S0022024801009691.

Cauda, V. et al., 2008. Large antibiotic molecule diffusion in confined mesoporous silica with controlled morphology. *Journal of Materials Chemistry*, 18(48), pp.5888–5899. Available at: http://www.scopus.com/inward/record.url?eid=2-s2.0-57349102539&partnerID=40&md5=4a0cce8be04b52732c09bae2635927ad.

Cebik, J. et al., 2013. Raman spectroscopy study of the nanodiamond-to-carbon onion transformation. *Nanotechnology*, 24(20), p.205703. Available at: http://stacks.iop.org/0957-4484/24/i=20/a=205703.

Chen, L. et al., 2012. Electro- and Photodriven Phase Change Composites Based on Wax-Infiltrated Carbon Nanotube Sponges. *ACS Nano*, 6(12), pp.10884–10892. Available at: http://dx.doi.org/10.1021/nn304310n.

Chen, M. et al., 2016. Nanodiamond-Mediated Delivery of. *ACS Nano*, 3(7), pp.2016–2022.

Chen, S. et al., 2010. Equilibrium and kinetic studies of methyl orange and methyl violet adsorption on activated carbon derived from Phragmites australis. *Desalination*, 252(1–3), pp.149–156. Available at: http://www.sciencedirect.com/science/article/pii/S0011916409012193.

Chen, S., Jin, L. & Chen, X., 2011. Procedia Engineering The effect and prediction of temperature on adsorption capability of coal / CH 4. *Procedia Engineering*, 26, pp.126–131. Available at: http://dx.doi.org/10.1016/j.proeng.2011.11.2149.

Chiang, H.-L.L., Huang, C.P.P. & Chiang, P.C.C., 2002. The surface characteristics of activated carbon as affected by ozone and alkaline treatment. *Chemosphere*, 47(3), pp.257–265. Available at: http://www.sciencedirect.com/science/article/pii/S0045653501002156 [Accessed June 1, 2017].

Choucair, M. & Stride, J.A., 2012. The gram-scale synthesis of carbon onions. *Carbon*, 50(3), pp.1109–1115. Available at: http://dx.doi.org/10.1016/j.carbon.2011.10.023.

Choudhari, Y. et al., 2014. Mesoporous Silica Drug Delivery Systems. In N. Shah et al., eds. *Amorphous Solid Dispersions: Theory and Practice*. New York, NY: Springer New York,

pp. 665–693. Available at: http://dx.doi.org/10.1007/978-1-4939-1598-9_23.

Chu, M. et al., 2013. Laser light triggered-activated carbon nanosystem for cancer therapy. *Biomaterials*, 34(7), pp.1820–1832. Available at: http://www.sciencedirect.com/science/article/pii/S0142961212012860.

Chu, P.K. & Li, L., 2006. Characterization of amorphous and nanocrystalline carbon films. *Materials Chemistry and Physics*, 96(2), pp.253–277.

Costa, G.C.C. et al., 2014. Thermochemistry of onion-like carbons. *Carbon*, 69(0), pp.490–494. Available at: http://dx.doi.org/10.1016/j.carbon.2013.12.053.

Costa, P. et al., 2001. Modeling and comparison of dissolution profiles. *European Journal of Pharmaceutical Sciences*, 13(2), pp.123–133. Available at: http://www.sciencedirect.com/science/article/pii/S0928098701000951.

Craig, D.Q.M. et al., 1999. The relevance of the amorphous state to pharmaceutical dosage forms: Glassy drugs and freeze dried systems. *International Journal of Pharmaceutics*, 179(2), pp.179–207.

Cui, Z. et al., 2016. Sodium alginate-functionalized nanodiamonds as sustained chemotherapeutic drug-release vectors. *Carbon*, 97, pp.78–86. Available at: http://www.sciencedirect.com/science/article/pii/S0008622315300890.

Dąbrowski, A., 2001. Adsorption - From theory to practice. *Advances in Colloid and Interface Science*, 93(1–3), pp.135–224. Available at: http://www.scopus.com/inward/record.url?eid=2-s2.0-0035828566&partnerID=40&md5=14f23beb05353e2e923272a2e2578522.

Dahan, A. et al., 2013. Purely in Silico BCS Classification: Science Based Quality Standards for the World's Drugs. *Molecular Pharmaceutics*, 10(11), pp.4378–4390. Available at: http://dx.doi.org/10.1021/mp400485k.

Daniel, L.S. et al., 2013. Photocatalytic Activity of Vis-Responsive Ag-Nanoparticles/TiO2 Composite Thin Films Fabricated by Molecular Precursor Method (MPM). *Catalysts*, 3(3), pp.625–645. Available at: http://www.mdpi.com/2073-4344/3/3/625.

Darmstadt, H., Ryong, R. & Ryoo, R., 2008. ADSORPTION ON ORDERED POROUS CARBONS. In E. J. Bottani & J. M. D. Tascón, eds. *Adsorption by Carbons*. Amsterdam: Elsevier, pp. 455–477. Available at: http://www.sciencedirect.com.openathensproxy.aston.ac.uk/science/article/pii/B9780080444642500225.

Desai, M.P. et al., 1996. Gastrointestinal uptake of biodegradable microparticles: Effect of particle size. *Pharmaceutical Research*, 13(12), pp.1838–1845. Available at: https://www.scopus.com/inward/record.uri?eid=2-s2.0-0030471901&doi=10.1023%2FA%3A1016085108889&partnerID=40&md5=1364ef13d886caa680e67113e30eda26.

Desai, M.P. et al., 1997. The Mechanism of Uptake of Biodegradable Microparticles in Caco-2 Cells Is Size Dependent. *Pharmaceutical Research*, 14(11), pp.1568–1573. Available at: http://dx.doi.org/10.1023/A:1012126301290.

Doadrio, A. et al., 2015. Drug release from ordered mesoporous silicas. *Current Pharmaceutical Design*, 21(42), pp.6213–6819. Available at: http://www.eurekaselect.com/openurl/content.php?genre=article&issn=1381-6128&volume=21&issue=42&spage=6213.

Doadrio, J.C. et al., 2006. Functionalization of mesoporous materials with long alkyl chains as a strategy for controlling drug delivery pattern. *Journal of Materials Chemistry*, 16(5), pp.462–466. Available at: http://dx.doi.org/10.1039/B510101H.

Domańska, U. et al., 2009. pKa and Solubility of Drugs in Water, Ethanol, and 1-Octanol. *The Journal of Physical Chemistry B*, 113(26), pp.8941–8947. Available at: http://dx.doi.org/10.1021/jp900468w.

Douroumis, D. & Fahrenkamp, A., 2012. *Drug Delivery Strategies for Poorly Water-Soluble Drugs*, Somerset, NJ, USA: John Wiley & Sons. Available at: http://site.ebrary.com/lib/aston/docDetail.action?docID=10650976.

Dudognon, E. et al., 2008. Evidence for a new crystalline phase of racemic Ibuprofen. *Pharmaceutical research*, 25(12), pp.2853–2858.

Duffy, E. et al., 2015. Thermally controlled growth of carbon onions within porous graphitic carbon-detonation nanodiamond monolithic composites. *RSC Adv.*, 5(29), pp.22906–22915. Available at: http://dx.doi.org/10.1039/C5RA00258C.

Ehrhardt, C. & Kim, K.J., 2007. *Drug Absorption Studies: In Situ, In Vitro and In Silico Models*, Springer US. Available at: https://books.google.co.uk/books?id=3geWUtmDPxwC.

El-Say, K.M., 2011. Nanodiamond as a drug delivery system: Applications and prospective. *Journal of Applied Pharmaceutical Science*, 1(6), pp.29–39. Available at: http://www.scopus.com/inward/record.url?eid=2-s2.0-84875830783&partnerID=40&md5=e57a33e27e031fddb22579422e1b35f8.

Enoki, T. & Kobayashi, Y., 2005. Magnetic nanographite: an approach to molecular magnetism. *Journal of Materials Chemistry*, 15(37), pp.3999–4002. Available at: http://dx.doi.org/10.1039/B500274P.

Fasinu, P. et al., 2011. Diverse approaches for the enhancement of oral drug bioavailability. *Biopharmaceutics and Drug Disposition*, 32(4), pp.185–209. Available at: http://www.scopus.com/inward/record.url?eid=2-s2.0-79955051472&partnerID=40&md5=4d8e61d50d714a0d6ea83a547a85e786.

Fröhlich, E., 2012. The role of surface charge in cellular uptake and cytotoxicity of medical nanoparticles. *International Journal of Nanomedicine*, 7, pp.5577–5591. Available at: http://www.ncbi.nlm.nih.gov/pmc/articles/PMC3493258/.

Garzón, L.C. et al., 2004. Temperature Dependence of Solubility for Ibuprofen in Some Organic and Aqueous Solvents. *Journal of Solution Chemistry*, 33(11), pp.1379–1395. Available at: http://dx.doi.org/10.1007/s10953-004-1051-2.

Gracin, S. & Rasmuson, Å.C., 2002. Solubility of Phenylacetic Acid, p-Hydroxyphenylacetic Acid, p-Aminophenylacetic Acid, p-Hydroxybenzoic Acid, and Ibuprofen in Pure Solvents. *Journal of Chemical & Engineering Data*, 47(6), pp.1379–1383. Available at: http://dx.doi.org/10.1021/je0255170.

Granberg, R.A. & Rasmuson, Å.C., 1999. Solubility of Paracetamol in Pure Solvents. *Journal of Chemical & Engineering Data*, 44(6), pp.1391–1395. Available at: http://dx.doi.org/10.1021/je990124v.

Gubarevich, A.V. et al., 2003. Onion-like carbon deposition by plasma spraying of nanodiamonds. *Carbon*, 41(13), pp.2601–2606. Available at: http://www.sciencedirect.com/science/article/pii/S0008622303003385.

Guo, F. et al., 2011. Gemcitabine adsorbed onto carbon particles increases drug concentrations at

the injection site and in the regional lymph nodes in an animal experiment and a clinical study. *Journal of International Medical Research*, 39(6), pp.2119–2127. Available at: http://www.scopus.com/inward/record.url?eid=2-s2.0-84555208728&partnerID=40&md5=3f7129f8ddfff6638667358b8d7592c1.

Guo, X. et al., 2013. Drug-nanocarrier interaction-tracking the local structure of calcium silicate upon ibuprofen loading with X-ray absorption near edge structure (XANES). *Phys. Chem. Chem. Phys.*, 15(36), pp.15033–15040. Available at: http://dx.doi.org/10.1039/C3CP50699A.

Haghseresht, F. et al., 2002. Adsorption of Aromatic Compounds onto Activated Carbons: Effects of the Orientation of the Adsorbates. *Langmuir*, 18(16), pp.6193–6200. Available at: http://dx.doi.org/10.1021/la025541b.

Hagiwara, A. & Takahashi, T., 1987. A new drug-delivery-system of anticancer agents: activated carbon particles adsorbing anticancer agents. *In Vivo*, 1(4), pp.241–252.

Hancock, B.C. & Parks, M., 2000. What is the true solubility advantage for amorphous pharmaceuticals? *Pharmaceutical Research*, 17(4), pp.397–404.

Hancock, B.C. & Zografi, G., 1997. Characteristics and significance of the amorphous state in pharmaceutical systems. *Journal of Pharmaceutical Sciences*, 86(1), pp.1–12. Available at: http://www.sciencedirect.com/science/article/pii/S002235491550227X.

Harris, P.J.F., Liu, Z. & Suenaga, K., 2008. Imaging the atomic structure of activated carbon. *Journal of physics: Condensed matter*, 20(36), p.362201.

Hayati, B. & Mahmoodi, N.M., 2012. Modification of activated carbon by the alkaline treatment to remove the dyes from wastewater: mechanism, isotherm and kinetic. *Desalination and Water Treatment*, 47(1–3), pp.322–333. Available at: http://dx.doi.org/10.1080/19443994.2012.696429.

He, C.X., He, Z.G. & Gao, J.Q., 2010. Microemulsions as drug delivery systems to improve the solubility and the bioavailability of poorly water-soluble drugs. *Expert Opin Drug Deliv*, 7(4), pp.445–460.

He, H. et al., 2013. Carbon Nanotubes: Applications in Pharmacy and Medicine. *BioMed Research International*, 2013, p.12. Available at: http://dx.doi.org/10.1155/2013/578290.

He, Y. & Park, K., 2016. Effects of the microparticle shape on cellular uptake. *Molecular Pharmaceutics*, 13(7), pp.2164–2171.

Hecini, M. et al., 2013. Study of formation, stabilization and properties of porous silicon and porous silica. *Journal of Physics and Chemistry of Solids*, 74(9), pp.1227–1234. Available at: http://www.sciencedirect.com/science/article/pii/S0022369713001285.

Heikkilä, T. et al., 2010. Cytotoxicity study of ordered mesoporous silica MCM-41 and SBA-15 microparticles on Caco-2 cells. *European Journal of Pharmaceutics and Biopharmaceutics*, 74(3), pp.483–494. Available at: http://dx.doi.org/10.1016/j.ejpb.2009.12.006.

Ho, D. et al., 2010. Nanodiamond particle complexes. Available at: http://www.google.com/patents/US20100305309.

Horcajada, P. et al., 2004. Influence of pore size of MCM-41 matrices on drug delivery rate. *Microporous and Mesoporous Materials*, 68(1–3), pp.105–109. Available at: http://www.sciencedirect.com/science/article/pii/S1387181103007054.

Hughey, J.R. & Williams, R.O., 2012. Solid-State Techniques for Improving Solubility. In R. O.

Williams III, A. B. Watts, & D. A. Miller, eds. *Formulating Poorly Water Soluble Drugs*. New York, NY: Springer New York, pp. 95–131. Available at: http://dx.doi.org/10.1007/978-1-4614-1144-4_3.

Inagaki, M., 2009. Pores in carbon materials-importance of their control. *New Carbon Materials*, 24(3), pp.193–232.

Izquierdo-Barba, I. et al., 2005. Release evaluation of drugs from ordered three-dimensional silica structures. *European Journal of Pharmaceutical Sciences*, 26(5), pp.365–373. Available at: http://www.scopus.com/inward/record.url?eid=2-s2.0-27644598988&partnerID=40&md5=7ac7f9d110e444cecaea569f2ec0128a.

Jackel, N. et al., 2014. Comparison of carbon onions and carbon blacks as conductive additives for carbon supercapacitors in organic electrolytes. *Journal of Power Sources*, 272, pp.1122–1133. Available at: http://www.sciencedirect.com/science/article/pii/S037877531401355X.

Jaganathan, H. & Godin, B., 2012. Biocompatibility assessment of Si-based nano- and micro-particles. *Advanced Drug Delivery Reviews*, 64(15), pp.1800–1819. Available at: http://www.sciencedirect.com/science/article/pii/S0169409X12001895.

Jaramillo, J. et al., 2010. Oxidation of activated carbon by dry and wet methods surface chemistry and textural modifications. *Fuel Processing Technology*, 91(11), pp.1768–1775. Available at: http://www.sciencedirect.com/science/article/pii/S0378382010002523.

Jarre, G. et al., 2014. Synthesis of nanodiamond derivatives carrying amino functions and quantification by a modified Kaiser test P. J. Skabara, ed. *Beilstein Journal of Organic Chemistry*, 10, pp.2729–2737. Available at: http://www.ncbi.nlm.nih.gov/pmc/articles/PMC4273261/.

Jarvis, K.L., Barnes, T.J. & Prestidge, C.A., 2012. Surface chemistry of porous silicon and implications for drug encapsulation and delivery applications. *Advances in Colloid and Interface Science*, 175(0), pp.25–38. Available at: http://dx.doi.org/10.1016/j.cis.2012.03.006.

Joly-Pottuz, L. et al., 2008. Diamond-derived carbon onions as lubricant additives. *Tribology International*, 41(2), pp.69–78. Available at: http://www.scopus.com/inward/record.url?eid=2-s2.0-34848820629&partnerID=40&md5=fb9e6e10f010b930d4dd55dfbca119c7.

Jones, B.J. & Ojeda, J.J., 2012. Substrate and material transfer effects on the surface chemistry and texture of diamond-like carbon deposited by plasma-enhanced chemical vapour deposition. *Surface and Interface Analysis*, 44(8), pp.1187–1192. Available at: http://dx.doi.org/10.1002/sia.4871.

Juurlink, D.N., 2016. Activated charcoal for acute overdose: A reappraisal. *British Journal of Clinical Pharmacology*, 81(3), pp.482–487.

Kaciulis, S., 2012. Spectroscopy of carbon: from diamond to nitride films. *Surface and Interface Analysis*, 44(8), pp.1155–1161. Available at: http://dx.doi.org/10.1002/sia.4892.

Kalantzi, L. et al., 2006. Biowaiver monographs for immediate release solid oral dosage forms: Acetaminophen (paracetamol). *Journal of Pharmaceutical Sciences*, 95(1), pp.4–14. Available at: http://dx.doi.org/10.1002/jps.20477.

Kalia, A. & Poddar, M., 2011. Solid dispersions: an approach towards enhancing dissolution rate. *Int. J. Pharm. Pharm. Sci*, 3(4), pp.9–19.

Kamarudin, N.H.N. et al., 2015. Elucidation of acid strength effect on ibuprofen adsorption and

release by aluminated mesoporous silica nanoparticles. *RSC Adv.*, 5(38), pp.30023–30031. Available at: http://dx.doi.org/10.1039/C4RA16761A.

Kaplan, I.G., 2006. *Intermolecular Interactions: Physical Picture, Computational Methods and Model Potentials*, Wiley. Available at: https://books.google.co.uk/books?id=UX-cKCgYlW4C.

Kawaguchi, M., Sakai, A. & Takahashi, A., 1986. Competitive and displacement adsorption of polystyrene and poly(ethylene oxide). *Macromolecules*, 19(12), pp.2952–2955. Available at: http://dx.doi.org/10.1021/ma00166a012.

Kazarian, S.G. & Chan, K.L.A., 2013. ATR-FTIR spectroscopic imaging: recent advances and applications to biological systems. *The Analyst*, 138(7), pp.1940–51. Available at: http://www.ncbi.nlm.nih.gov/pubmed/23400222.

Khadka, P. et al., 2014. Pharmaceutical particle technologies: An approach to improve drug solubility, dissolution and bioavailability. *Asian Journal of Pharmaceutical Sciences*, 9(6), pp.304–316. Available at: http://www.sciencedirect.com/science/article/pii/S1818087614000348.

Kinnari, P. et al., 2011. Comparison of mesoporous silicon and non-ordered mesoporous silica materials as drug carriers for itraconazole. *International Journal of Pharmaceutics*, 414(1–2), pp.148–156.

Knappe, D.R.U. et al., 2004. *Effects of Activated Carbon Characteristics on Organic Contaminant Removal*, IWA Publishing. Available at: https://books.google.co.uk/books?id=syOixS78P70C.

Kolosnjaj-Tabi, J. et al., 2012. Toxicity Studies of [60]Fullerene and Carbon Nanotubes: State of the Art. In *Handbook of Carbon Nano Materials*. pp. 49–81. Available at: http://www.worldscientific.com/doi/abs/10.1142/9789814401449_0002.

Kong, Y. & Hay, J.N., 2002. The measurement of the crystallinity of polymers by DSC. *Polymer*, 43(14), pp.3873–3878. Available at: http://www.sciencedirect.com/science/article/pii/S0032386102002355.

Konno, T., Kinuno, K. & Kataoka, K., 1986. Physical and Chemical Changes of Medicinals in Mixtures with Adsorbents in the Solid State. I. : Effect of Vapor Pressure of the Medicinals on Changes in Crystalline Properties. *CHEMICAL & PHARMACEUTICAL BULLETIN*, 34(1), pp.301–307.

Kuznetsov, V.L. et al., 2004. Carbon redistribution processes in nanocarbons. *Carbon*, 42(5–6), pp.1057–1061. Available at: http://www.sciencedirect.com/science/article/pii/S0008622303006213.

Kwon, S. et al., 2013. Silica-based mesoporous nanoparticles for controlled drug delivery. *Journal of tissue engineering*, 4, p.2041731413503357. Available at: http://www.pubmedcentral.nih.gov/articlerender.fcgi?artid=3764983&tool=pmcentrez&rendertype=abstract.

Kyesmen, P.I., Onoja, A. & Amah, A.N., 2016. Fullerenes synthesis by combined resistive heating and arc discharge techniques. *SpringerPlus*, 5(1), p.1323. Available at: http://springerplus.springeropen.com/articles/10.1186/s40064-016-2994-7.

Lai, J. et al., 2017. Investigating the Effects of Loading Factors on the In Vitro Pharmaceutical Performance of Mesoporous Materials as Drug Carriers for Ibuprofen. *Materials* , 10(2).

Laitinen, R. et al., 2013. Emerging trends in the stabilization of amorphous drugs. *International*

Journal of Pharmaceutics, 453(1), pp.65–79. Available at: http://www.sciencedirect.com/science/article/pii/S0378517312004127.

Lawrence, M. & Jiang, Y., 2017. *Bio-aggregates Based Building Materials*, Available at: http://link.springer.com/10.1007/978-94-024-1031-0.

Lee, M. et al., 2007. Control of Crystal Density of E -Hexanitrohexaazaisowurzitane in Evaporation Crystallization. , pp.1500–1504.

Lehto, V.P. et al., 2013. Nanostructured Silicon-Based Materials as a Drug Delivery System for Water-Insoluble Drugs. *Drug Delivery Strategies for Poorly Water-Soluble Drugs*, pp.477–508.

Leuner, C. & Dressman, J., 2000. Improving drug solubility for oral delivery using solid dispersions. *European journal of pharmaceutics and biopharmaceutics : official journal of Arbeitsgemeinschaft für Pharmazeutische Verfahrenstechnik e.V*, 50(1), pp.47–60. Available at: http://www.ncbi.nlm.nih.gov/pubmed/10840192.

Li-hong, W. et al., 2013. A novel strategy to design sustained-release poorly water-soluble drug mesoporous silica microparticles based on supercritical fluid technique. *International Journal of Pharmaceutics*, 454(1), pp.135–142. Available at: http://www.sciencedirect.com.openathensproxy.aston.ac.uk/science/article/pii/S0378517313006327.

Li, G.Y., Wang, P.M. & Zhao, X., 2005. Mechanical behavior and microstructure of cement composites incorporating surface-treated multi-walled carbon nanotubes. *Carbon*, 43(6), pp.1239–1245. Available at: http://www.sciencedirect.com/science/article/pii/S0008622305000199.

Li, L., Quinlivan, P.A. & Knappe, D.R.U.U., 2002. Effects of activated carbon surface chemistry and pore structure on the adsorption of organic contaminants from aqueous solution. *Carbon*, 40(12), pp.2085–2100. Available at: http://www.sciencedirect.com/science/article/pii/S0008622302000696.

Li, Y.H., Lee, C.W. & Gullett, B.K., 2003. Importance of activated carbon's oxygen surface functional groups on elemental mercury adsorption☆. *Fuel*, 82(4), pp.451–457. Available at: http://www.sciencedirect.com/science/article/pii/S0016236102003071.

Liang, P. et al., 2013. Coupling ion-exchangers with inexpensive activated carbon fiber electrodes to enhance the performance of capacitive deionization cells for domestic wastewater desalination. *Water Research*, 47(7), pp.2523–2530. Available at: http://www.sciencedirect.com/science/article/pii/S0043135413001413.

Lim, D.G. et al., 2016. Combinatorial nanodiamond in pharmaceutical and biomedical applications. *International Journal of Pharmaceutics*, 514(1), pp.41–51. Available at: //www.sciencedirect.com/science/article/pii/S037851731630480X.

Limnell, T., 2011. *Mesoporous silica- and silicon-based materials as carriers for poorly water soluble drugs*. University of Helsinki.

Limnell, T. et al., 2007. Surface chemistry and pore size affect carrier properties of mesoporous silicon microparticles. *International Journal of Pharmaceutics*, 343(1–2), pp.141–147. Available at: http://www.sciencedirect.com/science/article/pii/S0378517307004243.

Linares, C.F. et al., 2007. A new antacid drug from activated carbon modified with calcium carbonate. *Materials Letters*, 61(11–12), pp.2362–2364.

Linares, C.F. et al., 2006. Study of activated carbon modified with sodium carbonate as a possible antacid drug. *Materials Letters*, 60(4), pp.439–441.

Liu, C. et al., 2008. Wettability modification of pitch-based spherical activated carbon by air oxidation and its effects on phenol adsorption. *Applied Surface Science*, 254(9), pp.2659–2665.

Liu, J., Cui, L. & Losic, D., 2013. Graphene and graphene oxide as new nanocarriers for drug delivery applications. *Acta Biomaterialia*, 9(12), pp.9243–9257. Available at: http://www.sciencedirect.com/science/article/pii/S174270611300408X.

Liu, Y. et al., 2014. Electrical Signal Guided Ibuprofen Release from Electrodeposited Chitosan Hydrogel. *International Journal of Polymer Science*, 2014, p.8. Available at: http://dx.doi.org/10.1155/2014/736898.

Liu, Z. et al., 2011. Carbon materials for drug delivery & cancer therapy. *Materials Today*, 14(7–8), pp.316–323. Available at: http://www.sciencedirect.com/science/article/pii/S1369702111701614.

Löbmann, K. et al., 2012. Co-amorphous simvastatin and glipizide combinations show improved physical stability without evidence of intermolecular interactions. *European Journal of Pharmaceutics and Biopharmaceutics*, 81(1), pp.159–169.

Loftsson, T. & Brewster, M.E., 2013. Drug Solubilization and Stabilization by Cyclodextrin Drug Carriers. In *Drug Delivery Strategies for Poorly Water-Soluble Drugs*. pp. 67–101.

Luckey, T.D. & Venugopal, B., 1977. Modes of Intake and Absorption. In *Physiologic and Chemical Basis for Metal Toxicity*. Boston, MA: Springer US, pp. 39–91. Available at: http://dx.doi.org/10.1007/978-1-4684-2952-7_2.

Luo, Y. et al., 2015. Solid lipid nanoparticles for oral drug delivery: Chitosan coating improves stability, controlled delivery, mucoadhesion and cellular uptake. *Carbohydrate Polymers*, 122, pp.221–229. Available at: http://dx.doi.org/10.1016/j.carbpol.2014.12.084.

Maciá-agulló, J.A. & Linares-solano, A., 2004. Activation of Coal Tar Pitch Carbon Fibres : Physical Activation vs . Chemical Activation Activation of coal tar pitch carbon fibres : Physical activation. *Carbon*, 42(December), pp.1367–1370.

Mamaeva, V., Sahlgren, C. & Lindén, M., 2013. Mesoporous silica nanoparticles in medicine-Recent advances. *Advanced Drug Delivery Reviews*, 65(5), pp.689–702. Available at: http://dx.doi.org/10.1016/j.addr.2012.07.018.

Manzano, M. et al., 2008. Studies on MCM-41 mesoporous silica for drug delivery: Effect of particle morphology and amine functionalization. *Chemical Engineering Journal*, 137(1), pp.30–37.

Mao, Z., Zhou, X. & Gao, C., 2013. Influence of structure and properties of colloidal biomaterials on cellular uptake and cell functions. *Biomater. Sci.*, 1(9), pp.896–911. Available at: http://dx.doi.org/10.1039/C3BM00137G.

Marsh, H. & Rodriguez-reinoso, F., 2006. Activated Carbon. *Technology*, 94(4), p.536. Available at: http://dx.doi.org/10.1016/B978-008044463-5/50017-0.

Martín, Á. et al., 2009. Production of Polymorphs of Ibuprofen Sodium by Supercritical Antisolvent (SAS) Precipitation. *Crystal Growth & Design*, 9(5), pp.2504–2511. Available at: http://dx.doi.org/10.1021/cg900003m.

Martinez, C.R. & Iverson, B.L., 2012. Rethinking the term "pi-stacking." *Chemical Science*, 3(7),

p.2191. Available at: http://xlink.rsc.org/?DOI=c2sc20045g.

Matthews, R.P., Welton, T. & Hunt, P.A., 2014. Competitive pi interactions and hydrogen bonding within imidazolium ionic liquids †. *Phys. Chem. Chem. Phys.*, 16, pp.3238–3253.

McDonough, J.J.K. & Gogotsi, Y., 2013. Carbon onions: synthesis and electrochemical applications. *Electrochem. Soc. Interface*, 22(3), pp.61–65. Available at: https://www.electrochem.org/dl/interface/fal/fal13/fal13_p61_66.pdf.

McDonough, J.K. et al., 2012. Influence of the structure of carbon onions on their electrochemical performance in supercapacitor electrodes. *Carbon*, 50(9), pp.3298–3309. Available at: http://dx.doi.org/10.1016/j.carbon.2011.12.022.

Mellaerts, R. et al., 2010. Aging behavior of pharmaceutical formulations of itraconazole on SBA-15 ordered mesoporous silica carrier material. *Microporous and Mesoporous Materials*, 130(13), pp.154–161. Available at: http://www.sciencedirect.com/science/article/pii/S1387181109004934.

Mellaerts, R. et al., 2008. Increasing the oral bioavailability of the poorly water soluble drug itraconazole with ordered mesoporous silica. *European Journal of Pharmaceutics and Biopharmaceutics*, 69(1), pp.223–230. Available at: http://www.scopus.com/inward/record.url?eid=2-s2.0-41549142680&partnerID=40&md5=2eac7e411170281e087385435c4afac2.

Mochalin, V.N. et al., 2013. Adsorption of Drugs on Nanodiamond: Toward Development of a Drug Delivery Platform. *Molecular Pharmaceutics*, 10(10), pp.3728–3735. Available at: http://dx.doi.org/10.1021/mp400213z.

Mochida, I. et al., 2000. Removal of SOx and NOx over activated carbon fibers. *Carbon*, 38(2), pp.227–239. Available at: http://www.sciencedirect.com/science/article/pii/S0008622399001797.

Mochida, I., Yoon, S.-H. & Qiao, W., 2006. Catalysts in syntheses of carbon and carbon precursors. *Journal of the Brazilian Chemical Society*, 17, pp.1059–1073. Available at: http://www.scielo.br/scielo.php?script=sci_arttext&pid=S0103-50532006000600002&nrm=iso.

Mojica, M., Alonso, J.A. & Méndez, F., 2013. Synthesis of fullerenes. *Journal of Physical Organic Chemistry*, 26(7), pp.526–539. Available at: http://dx.doi.org/10.1002/poc.3121.

Monson, P.A., 2012. Understanding adsorption/desorption hysteresis for fluids in mesoporous materials using simple molecular models and classical density functional theory. *Microporous and Mesoporous Materials*, 160, pp.47–66. Available at: //www.sciencedirect.com/science/article/pii/S1387181112002569.

Montellano, A. et al., 2011. Fullerene C60 as a multifunctional system for drug and gene delivery. *Nanoscale*, 3(10), pp.4035–4041. Available at: http://dx.doi.org/10.1039/C1NR10783F.

Morishita, M. & Peppas, N.A., 2012. Advances in oral drug delivery: Improved bioavailability of poorly absorbed drugs by tissue and cellular optimization. *Advanced Drug Delivery Reviews*, 64(6), p.479. Available at: http://dx.doi.org/10.1016/j.addr.2012.02.008.

Moseenkov, S.I., Kuznetsov, V.L. & Ishchenko, A. V., 2014. Change in sizes of carbon aggregates and primary particles of the onion-like carbon synthesized by high-temperature annealing of nanodiamond. *Russian Chemical Bulletin*, 63(3), pp.599–604. Available at: http://dx.doi.org/10.1007/s11172-014-0479-9.

Nakase, Y. et al., 2004. Intratumoral administration of methotrexate bound to activated carbon

particles: Antitumor effectiveness against human colon carcinoma xenografts and acute toxicity in mice. *Journal of Pharmacology and Experimental Therapeutics*, 311(1), pp.382–387. Available at: http://www.scopus.com/inward/record.url?eid=2-s2.0-4644276698&partnerID=40&md5=98333dc292fd95fa41d4398704ed11cb.

Newcombe, G., 2008. Chapter Twentysix - Adsorption from Aqueous Solutions: Water Purification. In E. J. Bottani & J. M. D. Tascón, eds. *Adsorption by Carbons*. Amsterdam: Elsevier, pp. 679–709. Available at: http://www.sciencedirect.com/science/article/pii/B9780080444642500304.

Ng, E.-P. et al., 2013. Eco-friendly synthesis for MCM-41 nanoporous materials using the non-reacted reagents in mother liquor. *Nanoscale research letters*, 8(1), p.120. Available at: http://www.pubmedcentral.nih.gov/articlerender.fcgi?artid=3599658&tool=pmcentrez&rendertype=abstract.

Nikonova, R.M. et al., 2016. Changes of the structure of fullerite and graphite during their mechanical activation. *Journal of Alloys and Compounds*, 682, pp.61–69. Available at: http://www.sciencedirect.com/science/article/pii/S0925838816312701.

Niu, X. et al., 2013. Mesoporous carbon as a novel drug carrier of fenofibrate for enhancement of the dissolution and oral bioavailability. *International Journal of Pharmaceutics*, 452(1–2), pp.382–389. Available at: http://dx.doi.org/10.1016/j.ijpharm.2013.05.016.

Oelichmann, J., 1989. Surface and depth-profile analysis using FTIR spectroscopy. *Fresenius' Zeitschrift f{ü}r analytische Chemie*, 333(4), pp.353–359. Available at: http://dx.doi.org/10.1007/BF00572327.

Olivier, J.P., 2008. The surface heterogeneity of carbon and its assessment. *Adsorption by Carbons*, pp.147–166.

Olson, K.R., 2010. Activated Charcoal for Acute Poisoning: One Toxicologist's Journey. *Journal of Medical Toxicology*, 6(2), pp.190–198. Available at: https://www.scopus.com/inward/record.uri?eid=2-s2.0-77956192107&partnerID=40&md5=8af2206a026c3122e8bbf51898498d64.

Pakhira, B. et al., 2016. Carbon nano onions cross the blood brain barrier. *RSC Advances*, 6(35), pp.29779–29782. Available at: http://dx.doi.org/10.1039/C5RA23534K.

Pan, L. et al., 2010. Conducting polymer nanostructures: template synthesis and applications in energy storage. *International journal of molecular sciences*, 11(7), pp.2636–2657.

Park, S.-J. & Jang, Y.-S., 2002. Pore Structure and Surface Properties of Chemically Modified Activated Carbons for Adsorption Mechanism and Rate of Cr(VI). *Journal of Colloid and Interface Science*, 249(2), pp.458–463. Available at: http://www.sciencedirect.com/science/article/pii/S002197970298269X.

Peter, J.F.H., Zheng, L. & Kazu, S., 2008. Imaging the atomic structure of activated carbon. *Journal of physics: Condensed matter*, 20(36), p.362201. Available at: http://stacks.iop.org/0953-8984/20/i=36/a=362201.

Petit, T. et al., 2011. Early stages of surface graphitization on nanodiamond probed by x-ray photoelectron spectroscopy. *Physical Review B*, 84(23), p.233407. Available at: http://link.aps.org/doi/10.1103/PhysRevB.84.233407.

Pharmacopoeia, B., 2016. *British Pharmacopoeia*,

Piotto, C. & Bettotti, P., 2017. Porous Silicon: From Optical Sensor to Drug Delivery System. In P. Bettotti, ed. *Submicron Porous Materials*. Cham: Springer International Publishing, pp.

217–252. Available at: http://dx.doi.org/10.1007/978-3-319-53035-2_8.

Plonska-Brzezinska, M.E. et al., 2011. Electrochemical properties of oxidized carbon nano-onions: DRIFTS-FTIR and raman spectroscopic analyses. *ChemPhysChem*, 12(14), pp.2659–2668.

Popov, I.A., Bozhenko, K. V & Boldyrev, A.I., 2012. Is graphene aromatic? *Nano Research*, 5(2), pp.117–123. Available at: http://dx.doi.org/10.1007/s12274-011-0192-z.

Pouton, C.W., 2006. Formulation of poorly water-soluble drugs for oral administration : Physicochemical and physiological issues and the lipid formulation classification system ℅. *Journal of Pharmaceutical Sciences*, 9(June 2005), pp.278–287.

Preisig, D. et al., 2014. Drug loading into porous calcium carbonate microparticles by solvent evaporation. *European Journal of Pharmaceutics and Biopharmaceutics*, 87(3), pp.548–558. Available at: http://dx.doi.org/10.1016/j.ejpb.2014.02.009.

Presser, V., Heon, M. & Gogotsi, Y., 2011. Carbide-Derived Carbons – From Porous Networks to Nanotubes and Graphene. *Advanced Functional Materials*, 21(5), pp.810–833. Available at: http://dx.doi.org/10.1002/adfm.201002094.

Qi, S. et al., 2008. An investigation into the effects of thermal history on the crystallisation behaviour of amorphous paracetamol. *European Journal of Pharmaceutics and Biopharmaceutics*, 69(1), pp.364–371. Available at: http://www.sciencedirect.com/science/article/pii/S0939641107003505.

Qian, J. et al., 2004. Graphitization of diamond powders of different sizes at high pressure–high temperature. *Carbon*, 42(12–13), pp.2691–2697. Available at: http://www.sciencedirect.com/science/article/pii/S000862230400404X.

Qiao, Z. et al., 2006a. Graphitization and microstructure transformation of nanodiamond to onion-like carbon. *Scripta Materialia*, 54(2), pp.225–229. Available at: http://www.sciencedirect.com/science/article/pii/S1359646205005919.

Qiao, Z. et al., 2006b. Structural evolution and Raman study of nanocarbons from diamond nanoparticles. *Chemical Physics Letters*, 429(4–6), pp.479–482. Available at: http://www.sciencedirect.com/science/article/pii/S0009261406011651.

Qu, F., Zhu, G., et al., 2006. A controlled release of ibuprofen by systematically tailoring the morphology of mesoporous silica materials. *Journal of Solid State Chemistry*, 179(7), pp.2027–2035. Available at: http://www.sciencedirect.com.openathensproxy.aston.ac.uk/science/article/pii/S00224596 06002052.

Qu, F., Zhu, G., et al., 2006. Controlled release of Captopril by regulating the pore size and morphology of ordered mesoporous silica. *Microporous and Mesoporous Materials*, 92(1–3), pp.1–9. Available at: http://www.scopus.com/inward/record.url?eid=2-s2.0-33646879801&partnerID=40&md5=cce215f6d9f2d3f4d697fda2bc62772b.

Radke, C.J. & Prausnitz, J.M., 1972. Adsorption of Organic Solutes from Dilute Aqueous Solution of Activated Carbon. *Industrial & Engineering Chemistry Fundamentals*, 11(4), pp.445–451. Available at: http://pubs.acs.org/doi/abs/10.1021/i160044a003.

Reinert, L., Zeiger, M. & Presser, V., 2015. Dispersion analysis of carbon nanotubes, carbon onions , and nanodiamonds for their application as reinforcement phase in nickel metal matrix composites. *RSC Adv.*, 5, pp.95149–95159.

Rios, R.R.A. et al., 2003. Tailoring activated carbon by surface chemical modification with O, S, and N containing molecules. *Materials Research*, 6(2), pp.129–135. Available at: http://www.scielo.br/scielo.php?script=sci_arttext&pid=S1516-14392003000200004&lng=en&nrm=iso&tlng=en.

Rivera-Leyva, J.C. et al., 2012. Comparative Studies on the Dissolution Profiles of Oral Ibuprofen Suspension and Commercial Tablets using Biopharmaceutical Classification System Criteria. *Indian Journal of Pharmaceutical Sciences*, 74(4), pp.312–318. Available at: http://www.ncbi.nlm.nih.gov/pmc/articles/PMC3630726/.

Rodriguez-Reinso, F., 2007. *EFFECT OF POROSITY AND FUNCTIONALITY OF ACTIVATED CARBON IN ADSORPTION* Adsorption. L. Zhou, ed., River Edge, UNITED STATES: World Scientific Publishing Company. Available at: http://ebookcentral.proquest.com/lib/aston/detail.action?docID=1681410.

Roy, D. et al., 2003. Characterisation of carbon nano-onions using Raman spectroscopy. *Chemical Physics Letters*, 373(1), pp.52–56.

Runt, J. & Rim, P.B., 1982. Effect of preparation conditions on the development of crystallinity in compatible polymer blends: poly(styrene-co-acrylonitrile)/poly(iε-caprolactone). *Macromolecules*, 15(4), pp.1018–1023. Available at: http://dx.doi.org/10.1021/ma00232a013.

Salonen, J., Paski, J., et al., 2005. Determination of drug load in porous silicon microparticles by calorimetry. *physica status solidi (a)*, 202(8), pp.1629–1633. Available at: http://dx.doi.org/10.1002/pssa.200461204.

Salonen, J. et al., 2008. Mesoporous silicon in drug delivery applications. *Journal of Pharmaceutical Sciences*, 97(2), pp.632–653. Available at: http://www.scopus.com/inward/record.url?eid=2-s2.0-39749159993&partnerID=40&md5=3c875c4d32a70e9c488dd06decc6f912.

Salonen, J., Laitinen, L., et al., 2005. Mesoporous silicon microparticles for oral drug delivery: Loading and release of five model drugs. *Journal of Controlled Release*, 108(2–3), pp.362–374. Available at: http://www.sciencedirect.com/science/article/pii/S0168365905003974.

Sano, N. et al., 2002. Properties of carbon onions produced by an arc discharge in water. *Journal of Applied Physics*, 92(5), pp.2783–2788.

Serajuddin, A.T.M., 2007. Salt formation to improve drug solubility. *Advanced Drug Delivery Reviews*, 59(7), pp.603–616.

Shah, I.A., Lindup, W.E. & McCulloch, P.G., 1998. Variability of Mitomycin C Adsorption by Activated Charcoal. *Journal of Pharmacy and Pharmacology*, 50(3), pp.251–256. Available at: http://dx.doi.org/10.1111/j.2042-7158.1998.tb06857.x.

Shenderova, O.A., Zhirnov, V. V & Brenner, D.W., 2002. Carbon Nanostructures. *Critical Reviews in Solid State and Materials Sciences*, 27(3–4), pp.227–356. Available at: http://dx.doi.org/10.1080/10408430208500497.

Shin, Y.-R.R. et al., 2013. The oxidation mechanism of highly ordered pyrolytic graphite in a nitric acid/sulfuric acid mixture. *Carbon*, 52, pp.493–498. Available at: http://www.sciencedirect.com/science/article/pii/S0008622312008147.

Sibik, J. et al., 2014. Crystallization and phase changes in paracetamol from the amorphous solid to the liquid phase. *Molecular Pharmaceutics*, 11(4), pp.1326–1334.

Singhal, D. & Curatolo, W., 2004. Drug polymorphism and dosage form design: A practical

perspective. *Advanced Drug Delivery Reviews*, 56(3), pp.335–347.

Slowing, I., Trewyn, B.G. & Lin, V.S.Y., 2006. Effect of Surface Functionalization of MCM-41-Type Mesoporous Silica Nanoparticles on the Endocytosis by Human Cancer Cells. *Journal of the American Chemical Society*, 128(46), pp.14792–14793. Available at: http://dx.doi.org/10.1021/ja0645943.

Smith, B.T., 2016. *Physical pharmacy* Remington., Pharmaceutical Press.

Song, S.-W., Hidajat, K. & Kawi, S., 2005. Functionalized SBA-15 materials as carriers for controlled drug delivery: influence of surface properties on matrix-drug interactions. *Langmuir : the ACS journal of surfaces and colloids*, 21(21), pp.9568–9575.

Sonja, J. & Bunjes, H., 2013. Solid Lipid Nanoparticles for Drug Delivery. In *Drug Delivery Strategies for Poorly Water-Soluble Drugs*. pp. 103–149.

Stella, V.J. & Nti-Addae, K.W., 2007. Prodrug strategies to overcome poor water solubility. *Advanced Drug Delivery Reviews*, 59(7), pp.677–694.

Strelko, V. & Malik, D.J., 2002. Characterization and metal sorptive properties of oxidized active carbon. *Journal of colloid and interface science*, 250(1), pp.213–220.

Suárez-García, F., Martínez-Alonso, A. & Tascón, J.M.D., 2008. Chapter Fourteen - Adsorption on Fullerenes. In E. J. Bottani & J. M. D. Tascón, eds. *Adsorption by Carbons*. Amsterdam: Elsevier, pp. 329–367. Available at: http://www.sciencedirect.com.openathensproxy.aston.ac.uk/science/article/pii/B9780080444642500183.

Taylor, M.J., Tanna, S. & Sahota, T., 2010. In vivo study of a polymeric glucose-sensitive insulin delivery system using a rat model. *Journal of pharmaceutical sciences*, 99(10), pp.4215–4227.

Terrones, H. & Terrones, M., 2003. Curved nanostructured materials. *New Journal of Physics*, 5(1), p.126. Available at: http://stacks.iop.org/1367-2630/5/i=1/a=126.

Terzyk, A.P. et al., 2012. Enhanced adsorption of paracetamol on closed carbon nanotubes by formation of nanoaggregates: Carbon nanotubes as potential materials in hot-melt drug deposition-experiment and simulation. *Journal of Colloid and Interface Science*, 376(1), pp.209–216. Available at: http://www.sciencedirect.com/science/article/pii/S0021979712002469.

Terzyk, A.P., 2001. The influence of activated carbon surface chemical composition on the adsorption of acetaminophen (paracetamol) in vitro. Part II. TG, FTIR, and XPS analysis of carbons and the temperature dependence of adsorption kinetics at the neutral pH. *Colloids and Surfaces A: Physicochemical and Engineering Aspects*, 177(1), pp.23–45. Available at: http://www.sciencedirect.com/science/article/pii/S092777570000594X.

Terzyk, A.P. & Rychlicki, G., 2000. The influence of activated carbon surface chemical composition on the adsorption of acetaminophen (paracetamol) in vitro: The temperature dependence of adsorption at the neutral pH. *Colloids and Surfaces A: Physicochemical and Engineering Aspects*, 163(2–3), pp.135–150.

Thomas, F.G., 1983. *Adsorption from aqueous solutions*,

Thommes, M., 2010. Physical adsorption characterization of nanoporous materials. *Chem. Ing. Tech*, 82(7), pp.1059–1073.

Titantah, J.T. & Lamoen, D., 2005. sp3/sp2 characterization of carbon materials from first-

principles calculations: X-ray photoelectron versus high energy electron energy-loss spectroscopy techniques. *Carbon*, 43(6), pp.1311–1316. Available at: http://www.sciencedirect.com/science/article/pii/S0008622305000059.

Tomita, S. et al., 2002. Diamond nanoparticles to carbon onions transformation: X-ray diffraction studies. *Carbon*, 40(9), pp.1469–1474.

Ukmar, T. et al., 2011. Understanding controlled drug release from mesoporous silicates: Theory and experiment. *Journal of Controlled Release*, 155(3), pp.409–417. Available at: http://www.sciencedirect.com/science/article/pii/S0168365911004731.

Vallet-Regi, M. et al., 2001. A new property of MCM-41: Drug delivery system. *Chemistry of Materials*, 13(2), pp.308–311. Available at: http://dx.doi.org/10.1021/cm0011559.

Vallet-Regi-, M. et al., 2007. Mesoporous materials for drug delivery. *Angewandte Chemie - International Edition*, 46(40), pp.7548–7558. Available at: http://www.scopus.com/inward/record.url?eid=2-s2.0-35048818437&partnerID=40&md5=ac62fa7cda67f7b30e4cffb90b73ea6d.

Viseras, C. et al., 1995. The effect of recrystallization on the crystal growth, melting point and solubility of ketoconazole. *Thermochimica Acta*, 268, pp.143–151. Available at: http://www.sciencedirect.com/science/article/pii/0040603195023194.

Wang, C. et al., 2012. Graphene oxide stabilized polyethylene glycol for heat storage. *Phys. Chem. Chem. Phys.*, 14(38), pp.13233–13238. Available at: http://dx.doi.org/10.1039/C2CP41988B.

Wang, I.-C. et al., 2011. Polymorph Transformation in Paracetamol Monitored by In-line NIR Spectroscopy During a Cooling Crystallization Process. *AAPS PharmSciTech*, 12(2), pp.764–770. Available at: http://www.ncbi.nlm.nih.gov/pmc/articles/PMC3134639/.

Wang, S., 2009. Ordered mesoporous materials for drug delivery. *Microporous and Mesoporous Materials*, 117(1), pp.1–9. Available at: http://www.sciencedirect.com/science/article/pii/S1387181108003302.

Wang, S. et al., 2010. Solubilities of Ibuprofen in Different Pure Solvents. *Journal of Chemical & Engineering Data*, 55(11), pp.5283–5285. Available at: http://dx.doi.org/10.1021/je100255z.

Wang, X. et al., 2005. The Raman spectrum of nano-structured onion-like fullerenes. *Physica B: Condensed Matter*, 357(3–4), pp.277–281. Available at: http://www.sciencedirect.com/science/article/pii/S0921452604012256.

Wang, X., Liu, P. & Tian, Y., 2011. Ordered mesoporous carbons for ibuprofen drug loading and release behavior. *Microporous and Mesoporous Materials*, 142(1), pp.334–340. Available at: http://dx.doi.org/10.1016/j.micromeso.2010.12.018.

Wang, X.Q. & Zhang, Q., 2013. Microemulsions for Drug Solubilization and Delivery. In *Drug Delivery Strategies for Poorly Water-Soluble Drugs*. pp. 287–323.

White, R.J., 2015. The Search for Functional Porous Carbons from Sustainable Precursors. In *Porous Carbon Materials from Sustainable Precursors*. The Royal Society of Chemistry, pp. 3–49. Available at: http://dx.doi.org/10.1039/9781782622277-00003.

Wilhelm, P., 1996. Applications of FT-IR microscopy with materials analyses. *Micron*, 27(5), pp.341–344.

Wong, B.S. et al., 2013. Carbon nanotubes for delivery of small molecule drugs. *Advanced Drug*

Delivery Reviews, 65(15), pp.1964–2015. Available at: http://www.scopus.com/inward/record.url?eid=2-s2.0-84888865277&partnerID=40&md5=1bcc79efc2dd9fabde7a56551ee8e5db.

Wu, E.C. et al., 2008. Oxidation-triggered release of fluorescent molecules or drugs from mesoporous Si microparticles. *ACS Nano*, 2(11), pp.2401–2409.

Wu, S.H. & Pendleton, P., 2001. Adsorption of Anionic Surfactant by Activated Carbon: Effect of Surface Chemistry, Ionic Strength, and Hydrophobicity. *Journal of Colloid and Interface Science*, 243(2), pp.306–315. Available at: http://www.sciencedirect.com/science/article/pii/S0021979701979056.

Wu, W. et al., 2016. Hierarchical mesoporous silica nanoparticles for tailorable drug release. *International Journal of Pharmaceutics*, 511(1), pp.65–72. Available at: http://linkinghub.elsevier.com/retrieve/pii/S0378517316306238.

Xia, Y., Yang, Z. & Mokaya, R., 2010. *Templated Porous Carbon Materials: Recent Developments*,

Xiao, J. et al., 2014. Reversible nanodiamond-carbon onion phase transformations. *Nano Letters*, 14(6), pp.3645–3652.

Xie, F.Y. et al., 2010. Surface characterization on graphitization of nanodiamond powder annealed in nitrogen ambient. *Surface and Interface Analysis*, 42(9), pp.1514–1518. Available at: http://dx.doi.org/10.1002/sia.3350.

Xu, F. et al., 2004. Thermodynamic study of ibuprofen by adiabatic calorimetry and thermal analysis. *Thermochimica Acta*, 412(1–2), pp.33–57. Available at: http://www.sciencedirect.com/science/article/pii/S0040603103004404.

Xu, N.S., Chen, J. & Deng, S.Z., 2002. Effect of heat treatment on the properties of nano-diamond under oxygen and argon ambient. *Diamond and Related Materials*, 11(2), pp.249–256. Available at: http://www.sciencedirect.com/science/article/pii/S092596350100680X.

Xu, W., Riikonen, J. & Lehto, V.-P.P., 2013. Mesoporous systems for poorly soluble drugs. *International Journal of Pharmaceutics*, 453(1), pp.181–197. Available at: http://www.sciencedirect.com/science/article/pii/S0378517312008733.

Yi, Z. et al., 2016. Kinetics, equilibrium, and thermodynamics investigation on the adsorption of lead(II) by coal-based activated carbon. *SpringerPlus*, 5(1), p.1160. Available at: http://www.ncbi.nlm.nih.gov/pmc/articles/PMC4958095/.

Yin, C.Y., Aroua, M.K. & Daud, W.M.A.W., 2007. Review of modifications of activated carbon for enhancing contaminant uptakes from aqueous solutions. *Separation and Purification Technology*, 52(3), pp.403–415.

Yokota, T. et al., 2000. Lymph-node staining with activated carbon CH40: A new method for axillary lymph-node dissection in breast cancer. *Canadian Journal of Surgery*, 43(3), pp.191–196. Available at: https://www.scopus.com/inward/record.uri?eid=2-s2.0-0034121759&partnerID=40&md5=bc26703328c5631cfcc16e8e97fbc6f8.

Yu, L., 2001. Amorphous pharmaceutical solids: preparation, characterization and stabilization. *Advanced Drug Delivery Reviews*, 48(1), pp.27–42. Available at: http://www.sciencedirect.com/science/article/pii/S0169409X01000989.

Yu, M. et al., 2014. Porous HA microspheres as drug delivery: Effects of porosity and pore structure on drug loading and in vitro release. *Ceramics International*, 40(8 PART A), pp.12617–12621. Available at: http://dx.doi.org/10.1016/j.ceramint.2014.04.100.

Yuan, X. et al., 2009. Preparation and application of mesoporous Fe/carbon composites as a drug carrier. *Microporous and Mesoporous Materials*, 117(3), pp.678–684. Available at: http://www.sciencedirect.com/science/article/pii/S1387181108003570.

Yun, J. et al., 2008. Controlled release behavior of temperature responsive composite hydrogel containing activated carbon. *Carbon Lett*, 9(4), pp.283–288.

Zeiger, M., Jäckel, N., et al., 2015. Understanding structure and porosity of nanodiamond-derived carbon onions. *Carbon*, 84(1), pp.584–598.

Zeiger, M., Jackel, N., et al., 2015. Vacuum or flowing argon: What is the best synthesis atmosphere for nanodiamond-derived carbon onions for supercapacitor electrodes? *Carbon*, 94, pp.507–517. Available at: http://www.sciencedirect.com/science/article/pii/S0008622315300518.

Zhang, C.-Y. et al., 2015. An investigation on the effect of evaporation rate on protein crystallization. *Journal of Crystal Growth*, 418, pp.45–51. Available at: http://www.sciencedirect.com/science/article/pii/S0022024815000561.

Zhang, Q. et al., 2014. Functionalized Mesoporous Silica Nanoparticles with Mucoadhesive and Sustained Drug Release Properties for Potential Bladder Cancer Therapy. *Langmuir*, 30(21), pp.6151–6161. Available at: http://dx.doi.org/10.1021/la500746e.

Zhang, X. & Cresswell, M., 2016. Chapter 4 - Silica-Based Amorphous Drug Delivery Systems. In X. Zhang & M. Cresswell, eds. *Inorganic Controlled Release Technology*. Boston: Butterworth-Heinemann, pp. 93–137. Available at: http://www.sciencedirect.com/science/article/pii/B9780080999913000041.

Zhang, Y., Wang, H., et al., 2014. A novel three-dimensional large-pore mesoporous carbon matrix as a potential nanovehicle for the fast release of the poorly water-soluble drug, celecoxib. *Pharmaceutical Research*, 31(4), pp.1059–1070.

Zhang, Y., Zhi, Z., et al., 2013. Carboxylated mesoporous carbon microparticles as new approach to improve the oral bioavailability of poorly water-soluble carvedilol. *International Journal of Pharmaceutics*, 454(1), pp.403–411. Available at: http://dx.doi.org/10.1016/j.ijpharm.2013.07.009.

Zhang, Y., Wang, H., et al., 2013. Highly ordered mesoporous carbon nanomatrix as a new approach to improve the oral absorption of the water-insoluble drug, simvastatin. *European Journal of Pharmaceutical Sciences*, 49(5), pp.864–872.

Zhang, Y., Che, E., et al., 2014. Increasing the dissolution rate and oral bioavailability of the poorly water-soluble drug valsartan using novel hierarchical porous carbon monoliths. *International Journal of Pharmaceutics*, 473(1–2), pp.375–383. Available at: http://www.scopus.com/inward/record.url?eid=2-s2.0-84905054831&partnerID=40&md5=0d52bf693f4f0f5e04f7bedbbdcdc1c6.

Zhang, Y. et al., 2010. Spherical mesoporous silica nanoparticles for loading and release of the poorly water-soluble drug telmisartan. *Journal of Controlled Release*, 145(3), pp.257–263. Available at: http://dx.doi.org/10.1016/j.jconrel.2010.04.029.

Zhao, F. et al., 2004. Effect of Sodium Lauryl Sulfate in Dissolution Media on Dissolution of Hard Gelatin Capsule Shells. *Pharmaceutical Research*, 21(1), pp.144–148. Available at: http://dx.doi.org/10.1023/B:PHAM.0000012162.52419.b3.

Zhao, P. et al., 2012. Uniform mesoporous carbon as a carrier for poorly water soluble drug and its cytotoxicity study. *European Journal of Pharmaceutics and Biopharmaceutics*, 80(3),

pp.535–543. Available at: http://dx.doi.org/10.1016/j.ejpb.2011.12.002.

Zhu, S. et al., 2011. Thermo-responsive polymer-functionalized mesoporous carbon for controlled drug release. *Materials Chemistry and Physics*, 126(1–2), pp.357–363. Available at: http://www.sciencedirect.com/science/article/pii/S025405841000903X.

Zhu, W. et al., 2014. Mesoporous carbon as a carrier for celecoxib: The improved inhibition effect on MDA-MB-231 cells migration and invasion. *Asian Journal of Pharmaceutical Sciences*, 9(2), pp.82–91. Available at: http://www.sciencedirect.com/science/article/pii/S1818087614000099.

Zhu, Y. et al., 2012. The biocompatibility of nanodiamonds and their application in drug delivery systems. *Theranostics*, 2(3), pp.302–312.